THESIS

Presented at:

FACULTY OF SCIENCES – PHYSICS DEPARTMENT

To obtain the degree of:

DOCTOR OF SCIENCES

Specialty: Physics

Option: Condensed Matter Physics and Semiconductors

By:

Mr ALKAHTANI Esam Ahmed Abdulla

Theme

Density Functional Theory investigation of structural, electronic and optical properties of Erbium Zinc Oxide alloys

---

Publicly defended at November 2016 in Tlemcen front of the jury composed of:

Mme OULD KADDOUR Fouzia	Professor	Tlemcen University	Chairman
Mr MERAD Abdelkrim	Professor	Tlemcen University	Thesis Advisor
Mr BENOSMAN Abdelhakim	Associate Professor	Tlemcen University	Thesis Co-Advisor
Mr HOUARI Ahmed	Professor	Tlemcen University	Examiner
Mme RAHAL Madjda	Professor	SBA University	Examiner
Mr BENZAIR Abdenour	Professor	SBA University	Examiner

Theoretical Physics Laboratory (LPT)

BP 119, 13000 Tlemcen - Algeria

ACKNOWLEDGMENTS

DEDICATIONS

I dedicate this thesis to:

My lovely parents

My life partner, my lovely wife

My children (Mohammad, Shahd and Ala'a), my life

light

My brothers Yassin, Anwer, Ashraf and Gaiss

My sisters Norah and Thekra

CONTENTS

CHAPITER III: METHODOLOGY

CHAPITER IV: STRUCTURAL AND ELECTRONIC PROPERTIES OF $Zn_{1-x}Er_xO$ ALLOYS

CHAPITER V: ELECTRONIC AND OPTICAL PROPERTIES OF ZnO AND Er DOPED ZnO

LIST OF FIGURES

LIST OF TABLES

GENERAL INTRODUCTION

GENERAL INTRODUCTION

More efforts have been advanced on wide-band gap semiconductors because of the intense interest in technologic indusrerial as ultraviolet light emitters and detectors [1]. Among them, ZnO is one of the potential candidates in several technological applications such as, optoelectronic, solar cells, and photocatalyst [2-3] due to its high exciton binding energy (60 meV) and its wide band gap (~3.3 eV) [3]. It is known as an n-type semiconductor material. Further, ZnO is a commercially available material having the advantages of low cost, non-toxicity and high chemical stability [4]. It is a key technological and a versatile functional material.

In the past decade, ZnO has been explored for new device applications when extra functionalities are intentionally introduced through proper doping or alloying with impurity ions despite the considerable challenges.

Recently, the ZnO presented an interesting subject for doping with various elements such as transition and noble metals. This is of course very suitable to improve the optoelectronic and photocatalytic properties because the incorporation of dopants generates lattice defects and changes consequently the band gap energy [5].

In particular, the doping with rare-earth elements has been extensively investigated, experimentally as well as theoretically.

ZnO is worth noting that much effort has also been made through doping rare earth (RE) ions into the ZnO host, which undergoes up conversion (UC) luminescence and energy transfer, in realizing new optoelectronic and photonic device applications such as solid-state full-colour displays, infrared detectors, solar cells, biological fluorescent labels, and all-solid compact lasers [6].

There have been many recent studies reported the electronic and optical properties of rare earth elements doped ZnO such as Poongodi et al (2015) [7] deposited nanostructured Nd doped ZnO thin films on glass substrate by a sol–gel spin coating technique, Honglin et al (2014) [8] prepared the ZnO nanopowders doped with (La,Er,Nd) rare-earth by chemical method and Zhang et al (2014) [9] studied the electronic structure and magnetism of RE (RE = La, Ce, Pr, Nd and Eu) doped ZnO using generalized gradient approximation (GGA) and GGA+U.

In particular, the attractive interest of Erbium (Er)-doped semiconductors in optical applications such as light-emitting and laser diodes, is because of the sharp photoluminescence (PL) at 1.54 μm from the intra-4f shell transition in Er^{3+} ions [10]. Wherefore, many investigations are done for optical properties of Er doped ZnO, and some of them specifically, the photocatalysis of Er-doped ZnO [11-15]. Likewise the Er-doped ZnO films have been fabricated using many techniques, including sintering [16], wet processing [17], ion implantation [18, 19], textured spraying [20], electron-beam evaporation [21], and pulsed-laser deposition (PLD) [22, 23].

The majority of works carried out the above properties at low temperature (77 K) precluding their use at room temperature [24]. However, few reports for Er doped ZnO in thin film or wurtzite phases have been experimentally investigated showing the PL spectra at room temperature, as given in the work of Honglin [8]. Consequently, no further theoretical understanding on the correlation between their properties is clarified. Therefore, it is still important to present a theoretical investigation of structural, electronic and optical properties of such material in order to enlighten the correlation between them.

Erbium can be found in three magnetic phases: ferromagnetic below 19 K, antiferromagnetic between 19 and 80 K and paramagnetic above 80 K [8]. In this work,

we aimed to study the structural and electronic properties of $Zn_{1-x}Er_xO$ for (x= 0, 0.25, 0.50, 0.75, 1) by density functional theory (DFT) with generalized gradient approximation (GGA) and studying the effect of Er doped ZnO in comparison with pure ZnO in paramagnetic phase that is observed at high temperature using modified Becke-Johnson exchange potential (mBJ).

 In this case, electronic and optical properties are obtained for 25% of Er doped ZnO in zinc blend structure by caring out a first principles calculations based on density functional theory (DFT). In general, it is shown that this structure is similar to wurtzite one in electronic and optical band structure [25]. This work is considered as an extension of our recent studies realized on ZnO-ZB [25]. Our results were discussed qualitatively as well as quantitatively in comparison with few experimental available results.

The present thesis is divided into five chapters. In Chapter I, we introduce the domain of the II-VI semiconductors, rare earth elements and REE doping II-VI semiconductors and their technological applications.

Chapter II resumes the basic ideas behind the DFT, while Chapter III contains a brief description of the methodology of calculations.

In chapter IV, we report the numerical investigations of the structural, and electronic properties of $Zn_{1-x}Er_xO$ for (x= 0, 0.25, 0.50, 0.75, 1) carried out by density functional theory (DFT) with generalized gradient approximation (GGA).

Fifth chapter discusses the results of the electronic and optical properties of pure ZnO and Er-doped ZnO executed by modified Becke-Johnson exchange potential (mBJ).

Finally, a general conclusion is presented for each of the investigated class of systems.

REFERENCES

[1] Y.S. Lee, S. N. Lee, I. K. Park, Growth of ZnO hemi spheres on silicon by a hydrothermal method, Ceramics International 39(2013)3043–3048.

[2] C. Klingshirn, Phys. Stat. Sol. (b) 244 (2007) 3027.

[3] D. K. Kim, and H. B. Kim, J. Alloys Compd. 509 (2011) 421.

[4] Li, Gang, et al. "Doping and annealing effects on ZnO: Cd thin films by sol–gel method." Journal of Alloys and Compounds 509.14 (2011): 4816-4823.

[5] D. Li, J. F. Huang, L. Y. Cao, L. I. Jia-Yin, H. B. OuYang and C. Y. Yao, Ceramics International, 40 (2014) 2647.

[6] X.Wang, X. Kong, G. Shan et al., "Luminescence spectroscopy and visible upconversion properties of Er^{3+} in ZnO nanocrystals," Journal of Physical Chemistry B, vol. 108, no. 48, pp. 18408–18413, 2004.

[7] G Poongodi, R. M. Kumar and R. Jayavel. Ceramics International 41 (2015) 4169.

[8] L. Honglin, L. Yingbo, L. Jinzhu and Y. Ke, J. Alloys Compd 617 (2014) 102.

[9] X. J. Zhang, W. B. Mi, X. C. Wang and H. L. Bai, J Alloys Compd 617 (2014) 828.

[10] T. Gregorkiewicz and J. M. Langer, MRS Bull. 24 (1999) 27.

[11] V. Kumari, V. Kumar, B. P. Malik, R. M. Mehra, and D. Mohan, "Nonlinear optical properties of erbium doped zinc oxide (EZO) thin films," Optics Communications, vol. 285, no. 8, pp. 2182–2188, 2012.

[12] J. C. Sin, S. M. Lam, K. T. Lee, and A. R.Mohamed, "Fabrication of erbium-doped spherical-like ZnO hierarchical nanostructures with enhanced visible light-driven photocatalytic activity," Materials Letters, vol. 91, pp. 1–4, 2013.

[13] J. Rita and R. Rajaram, "Synthesis and characterization of rare earth ion doped Nano ZnO," Nano-Micro Letters, vol. 4, no. 2, pp. 65–72, 2012.

[14] W. C. Yang, C. W. Wang, J. C.Wang et al., "Aligned Er-doped ZnOnanorod arrays with enhanced 1.54 μminfrared emission," Journal of Nanoscience and Nanotechnology, vol. 8, no. 7, pp. 3363–3368, 2008.

[15] J. Ebothe, W. Gruhn, A. Elhichou, I. V. Kityk, R. Dounia, and M. Addou, "Giant piezooptics effect in the ZnO-Er3+ crystalline films deposited on the glasses," Optics and Laser Technology, vol. 36, no. 3, pp. 173–180, 2004.

[16] Park Y K, Han J I, Kwak M G, Yang H, Ju S H and ChoW S 1998 Appl. Phys. Lett. 72 668

[17] Mais N, Reithmaier J P, Forchel A, Kohls M, Spanhel L and M¨uller G 1999 Appl. Phys. Lett. 75 2005

[18] Wahl U, Rita E, Correia J G, Alves E, Ara´ujo J P and The ISOLDE Collaboration 2003 Appl. Phys. Lett. 82 1173

[19] Alves E, Rita E, Wahl U, Correia J G, Monteiro T, Soares J and Boemare C 2003 Nucl. Instrum. Methods B206 1047

[20] Bubendorff J L, Ebothe J, El Hichou A, Dounia R and Addou M 2006 J. Appl. Phys. 100 014505

[21] Zhang X T, Liu Y C, Ma J G, Lu Y M, Shen D Z, Xu W, Zhong G Z and Fan X W 2002 Thin Film 413 257

[22] Komuro S, Katsumata T, Morikawa T, Zhao X, Isshiki H and Aoyagi Y 2000 J. Appl. Phys. 88 7129

[23] P´erez-Casero R, Gutierr´ez-Llorente A, Pons-Y-Moll O, Seiler W, Defourneau R M, Defourneau D, Millon E, Perri´ere J, Goldner P and Viana B 2005 J. Appl. Phys. 97 054905.

[24] G. Murtaza, I. Ahmad, B. Amin, A. Afaq, F. Ghafoor and A. Benamrani, Physica B: Condensed Matter 406 (2011) 2632.

[25] M. R. Boufatah and A. E. Merad. Mater. Sci. Semicon. Process. 19 (2014) 179.

CHAPTER I

1.1 INTRODUCTION

Semiconductors are the materials, which play an important role in the development in the field of science and technology. The two most important semiconductors are Silicon (Si) and Germanium (Ge). Since last three decades, various groups of semiconductors have come up to play the role in various terrestrial as well as extraterrestrial applications. Some important semiconducting materials that compete with Ge and Si belong to II-VI, III-V etc. group of materials.

The group II-VI compounds like ZnS, ZnSe, ZnO and ZnTe have been successfully used as a detector, sensors, modulators and many more scientific applications. Besides, rare earth elements occupy a very special position in solid-state physics because of their unique outer electron configuration including two unfilled shells. This chapter deals II-VI semiconductors, as especially Zinc Oxide in addition to Rare Earth Elements doped ZnO.

1.2 II-VI SEMICONDUCTORS COMPOUNDS

II-VI semiconductor compounds are combinations of two atoms, one of the alkaline earth metals (group 2 of the Periodic table) or one of the group 12 elements (group 12 of the periodic table) and one atom of the Chalcogens (group 16 of the periodic table). The II–VI semiconductors have been extensively studied due to their effective use in optoelectronic industry. These compounds are commonly used in many established commercial electronic and optoelectronic devices operating in blue to ultraviolet spectral regions such as visual displays, high-density optical memories, transparent conductors, solid-state laser devices, photodetectors, solar cells etc.

In recent years, II-VI compound semiconductors have attracted considerable technological and scientific interest due to the large range of electronic energy band gaps, which they exhibit. The direct band gaps of these alloys cover the entire spectral region from near infrared to ultra violet. The wide band gap materials consist of the chalcogen compounds of Zn and Cd such as ZnTe, ZnS and CdTe. The largest band gap is 3.4eV for ZnS. The range of technical applications of these compounds extends beyond those of the more established semiconductors such as Si, Ge and some of the III-V compounds, primarily because they offer this wider range of band gap values. In addition, when the ternary II-VI compounds such as CdHgTe are included, the range of band gaps available becomes continuous. Some of the devices for which these materials are important and in which they are commonly used are solar cells, infrared detectors, electroluminescent diodes, lasers, phosphors, switches, passivation layers and radiation detectors.

The electronic and optical properties of these semiconductors can be controlled by concentration of impurities in the materials as well as growth and operating conditions.

1.2.1 CRYSTAL STRUCTURE OF II-VI COMPOUNDS

The compounds belonging to group II-VI consist of equal number of atoms of an element from the II b column of periodic table and of an element from the VI column. They are related in crystallography and physical properties to the semiconducing III-V compounds and the IV b elements Ge and Si. Almost all the compounds of group II-VI crystallize in such a manner that each atom of one element is located at the centre of a regular tetrahedron, the apices of which are occupied by atoms of other elements. Two possible structures can be formed from such tetrahedral zinc blende (cubic) phase and the wurtzite (hexagonal) phase. In the sphalerite structure, the atoms of one element are located at the sites of an fcc lattice, while the atoms of the second element occupy centers of four (out of total of eight) small cubes as shown in figure 1.1. The space group is *F43m ($T_d{}^2$)*. The coordination is 4 for atoms of both elements. Similarly, the other possible structure observed in group II-VI compounds is wurtzite as shown in figure 1.2. Its space group is *P6$_3$mc (C$_{6v}{}^4$)*. Here again the coordination number is 4 for atoms of both elements. The zinc blende and wurtzite structures are almost similar. The main reason for such a similarity is the number of atoms in the first and second coordination spheres are the same. The basic difference between the two structures arises due to the position of atoms in the third coordination sphere. The distance from a given atom to its neighbours in that sphere is shorter in wurtizite structure than in the sphalerite structure. In the majority of II-VI compounds, the interatomic distances in the tetrahedral of both modifications are very similar. Moreover, the distance from a given atom to its neighbours in the first and second coordination spheres are also very similar for both structures.
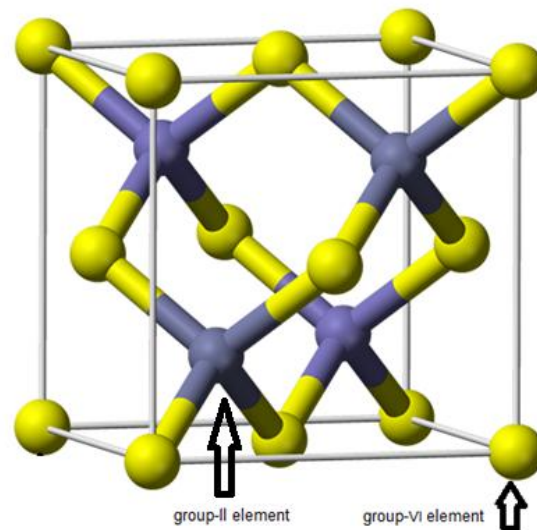
Figure 1.1 The zinc blende structure of ZnO.
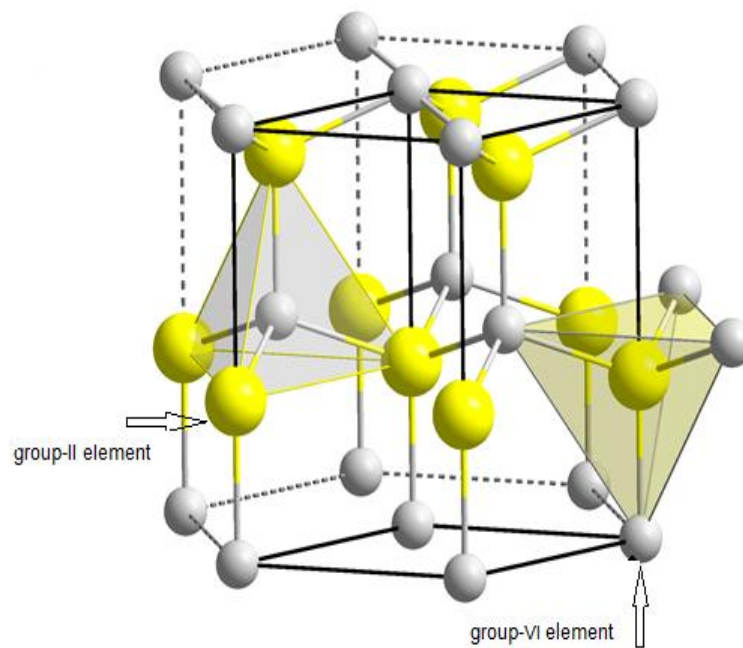
Figure 1.2 The wurtzite structure of ZnO.

Table 1.1 Physical Properties of some II–VI compound semiconductors.

Material property	ZnS	ZnO	ZnSe	ZnTe	CdS	CdSe
Melting point(K)	2038 (WZ,150 atm)	2248	1797	1513	2023 (WZ,100 atm)	1623
Energy gap E_g at 300K(ev)(ZB/WZ)	3.68/3.911	-/3.4	2.71/-	2.394	2.50/2.50	-/1.751
dE_g/dT (x 10^{-4} ev /K) ZB/W	4.6/8.5	–/9.5	4.0/–	5.5/–	–/5.2	–/4.6
Structure	ZB/WZ	WZ	ZB/WZ	ZB	WZ	WZ
Bond length (µm)	2.342 (WZ)	1.977 (WZ)	2.454 (ZB)	2.636 (ZB)	2.530 (ZB)	2.630 (ZB)
Lattice constant (ZB) a at 300K (Å)	5.41	–	5.67	6.10	5.82	6.08
ZB nearest-neighbor dist.at 300K (nm)	0.234	–	0.246	0.264	0.252	0.263
ZB density at 300K (g/cm³)	4.11	–	5.26	5.65	4.87	5.655
Lattice constant (WZ) at 300K (nm)						
$a= b$	3.811	3.2495	3.98	4.27	4.135	4.30
c	6.234	5.2069	6.53	6.99	6.749	7.02
c/a	1.636	1.602	1.641	1.637	1.632	1.633
WZ density at 300K (g/cm³)	3.98	5.606	–	–	4.82	5.81
Symmetry ZB/WZ	C6me/F43m	–/C6me	–/F43m	–/F43m	C6me/F43m	C6me/F43m
Exciton binding energy(meV)	36	60	21	10	30.5	15
Absorption coeff. (including two surfaces) (cm^{-1})	≤ 0.15	–	1-2×10⁻³	–	≤ 0.007	0.0015≤

1.3 ZINC OXIDE (ZnO)

Zinc Oxide is a semiconducting compound of the group-II b element Zn and the group VI element O. The zinc atoms locate almost in the position of hexagonal close packing. Every oxygen atom places within a tetrahedral group of four zinc atoms. Zinc Oxide is an inorganic compound with the formula of ZnO. It is a II–VI compound semiconductor whose ionicity resides at the borderline between the covalent and ionic semiconductors. It occurs in nature as the mineral zincite. It is a key technological material. It belongs to the family of II–VI compound wide-gap semiconductor with a room temperature direct band gap of 3.37 eV and a large exciton binding energy of about 60 meV, which makes it a very attractive material for the applications to the advanced optoelectronic devices [1, 2]. Zinc oxide has attracted significant attention as a material for ultraviolet (UV) light-emitters, varistors, transparent high power electronics, surface acoustic wave devices, piezoelectric transducers and gas sensors and also as a window material for displays and solar cells[3,4].

1.3.1 STRUCTURAL PROPERTIES OF ZnO

Table 1.2 shows a compilation of basic physical parameters for ZnO [7, 8]. It should be noted that there still exists uncertainty in some of these values. For example, there have few reports of p-type ZnO and therefore the hole mobility and effective mass are still in debate. Similarly, the values for thermal conductivity show some spread in values and this may be a result of the influence of defects such as dislocations [9], as was the case for GaN. The values for carrier mobility will undoubtedly increase as more control is gained over compensation and defects in the material.

Table 1.2 Physical parameters of ZnO

Physical parameters	Values
Lattice parameters at 300 K *a* *c* **u**	3.2495 Å 5.2069 Å 0.345
Density	5.606 g/cm^3
Stable phase at 300 K	Wurtzite
Melting point	1975 C^0
Thermal conductivity	0.6, 1–1.2
Linear expansion	a_0: 6.5 $\times 10^{-6}$
coefficient(/C^0)	c_0: 3.0 $\times 10^{-6}$
Static dielectric constant	8.656
Refractive index (ZB,WZ)	2.008, 2.029
Energy gap	3.37 eV, direct
Intrinsic carrier **Concentration**	$<10^6$ cm^{-3} (max n-type doping$>10^{20}$ cm^{-3} electrons; max p-type doping$<10^{17}$ cm^{-3} holes)
Exciton binding energy	60 meV
Electron effective mass	0.24
Electron Hall mobility at 300 K for low n-type conductivity	200 cm^2/V s
Hole effective mass	0.59
Hole Hall mobility at 300 K for low p-type conductivity	5–50 cm^2/V s

ZnO belongs to the group of II-VI binary compound semiconductors which crystallize

in either a cubic (zinc blende) or hexagonal (wurtzite) structure where each anion is

surrounded by four cations at the corners of a tetrahedron, and vice versa. The bonding

of this tetrahedral coordination is characteristic of sp3 covalent bonding, but these

materials also have substantial ionic character. Therefore, as shown in Figure 1.3, the

crystal structures of ZnO are wurtzite (B4), zinc blende (B3), and rock-salt (B1). Under

ambient conditions, the thermodynamically stable phase is wurtzite, while the ZB ZnO

structure is only revealed by growth on cubic substrates; moreover, the RS (NaCl)

structure probably grows at relatively high pressure.

Rocksalt (B1)   Zinc blende (B3)   Wurtzite (B4)

(a)   (b)   (c)
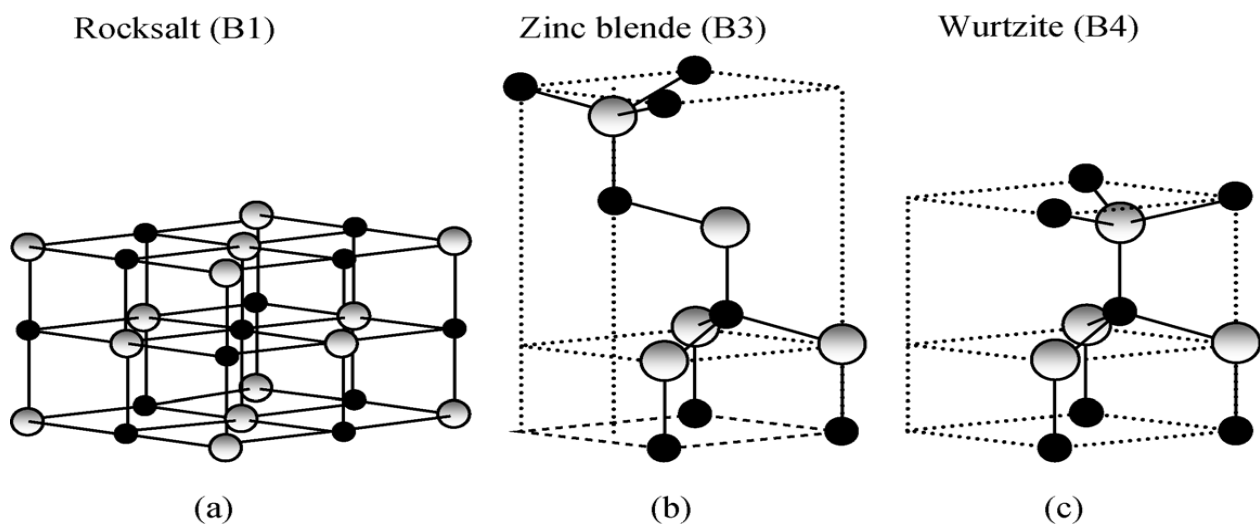
Figure 1.3 Crystal structures of ZnO: (a) cubic rock-salt(B1), (b) zinc blende (B3), and (c) wurztie (B4).
The shaded gray and black spheres denote Zn and O atoms, respectively [8].

1.3.2 LATTICE PARAMETERS

The wurtzite structure has a hexagonal unit cell with two lattice parameters, *a and c,* in the ratio of $c/a = \sqrt{8/3} = 1.633$. Each sub-lattice consists of one type of atom represented with respect to each other along the three fold c-axis by the amount of u=3/8=0.375 (in an ideal wurtzite structure) in fractional coordinates. The internal parameter u is defined as the length of the bond parallel to the *c*-axis (anion–cation bond length or the nearest-neighbor distance) divided by the *c* lattice parameter. The basal plane lattice parameter (the edge length of the basal plane hexagon) is universally depicted by *a*; the axial lattice parameter (unit cell height), perpendicular to the basal plane, is universally described by *c*. Each sublattice includes four atoms per unit cell, and every atom of one kind (group II atom) is surrounded by four atoms of the other kind (group VI), or vice versa, which are coordinated at the edges of a tetrahedron. The crystallographic vectors of wurtzite are $\vec{a} = a\left(\frac{1}{2}, \frac{\sqrt{3}}{2}, 0\right)$, $\vec{b} = a\left(\frac{1}{2}, \frac{-\sqrt{3}}{2}, 0\right)$, $\vec{c} = a(0, 0, \frac{c}{a})$ In Cartesian coordinates, the basis atoms are $(0, 0, 0), (0, 0, uc)$, $a\left(\frac{1}{2}, \frac{\sqrt{3}}{6}, \frac{c}{2a}\right)$, and $a\left(\frac{1}{2}, \frac{\sqrt{3}}{6}, [u + \frac{1}{2}]\frac{c}{a}\right)$.

Table 1.3 tabulates measured and calculated lattice parameters, c/a ratio, and u parameter reported by several groups for ZnO crystallized in wurtzite, zinc blende, and rocksalt structures for comparison. The zinc blende ZnO structure is metastable and can be stabilized only by heteroepitaxial growth on cubic substrates, such as ZnS [9], GaAs/ZnS [10], and Pt/Ti/SiO$_2$/Si [11], reflecting topological compatibility to overcome the intrinsic tendency of forming wurtzite phase. In the case of highly mismatched substrates, there is usually a certain amount of zinc blende phase of ZnO separated by crystallographic defects from the wurtzite phase. The symmetry of the zinc blende structure is given by space group $F\bar{4}3m$ in the Hermann–Mauguin notation and

$T_d{}^2$ in the Schoenflies notation and is composed of two interpenetrating face-centered cubic (fcc) sublattices shifted along the body diagonal by one-quarter of the length of the body diagonal. There are four atoms per unit cell and every atom of one type (group II) is tetrahedrally coordinated with four atoms of other type (group VI), and vice versa. Like other II–VI semiconductors, wurtzite ZnO can be transformed to the rocksalt (NaCl) structure at relatively modest external hydrostatic pressures. The reason for this is that the reduction of the lattice dimensions causes the interionic Coulomb interaction to favor the ionicity more over the covalent nature. The space group symmetry of the rocksalt type of structure is *Fm3m* in the Hermann–Mauguin notation and O_h^5 in the Schoenflies notation, and the structure is sixfold coordinated. However, the rocksalt structure cannot be stabilized by the epitaxial growth. In ZnO, the pressure-induced phase transition from the wurtzite (B4) to the rocksalt (B1) phase occurs in the range of 10 GPa associated with a large decrease in volume of about 17% [12].

Table 1.3 Measured and calculated lattice constants of wurtzite ZnO

a(Å)	*c*(Å)	*c/ a*	**u**	**Ref**
		1.633	0.375	Ideal
3.2496	5.2042	1.6018	0.3819	[38]
3.2501	5.2071	1.6021	0.3817	[39]
3.286	5.241	1.595	0.383	[40]

Zinc blende (4.619[13], 4.60[14], 4.463, 4.37and 4.47[15])

Rocksalt (4.271[16], 4.30[14])

1.3.3 THE BAND STRUCTURAL AND ENERGY BAND GAP

The band structure of ZnO was first calculated in 1969 using Greens function and followed up soon after with experimental results from x-ray induced photo-emission spectroscopy and UV photoemission measurements [17].

A very important property of any given semiconductor is its band structure, because many important properties such as the band gap and effective electron and hole masses are derived from it. ZnO is considered most suitable semiconductor among all his family members for ultraviolet lasing at room temperature, device application as well as possibilities to engineer the band gap, for this reason a clear understanding of the band structure is important to explain the electrical properties and many other phenomena because it determines the relationship between the energy and the momentum of the carrier. The electronic band structure of ZnO has been calculated by a number of groups [18, 19]. The results of a band structure calculation using the Local Density Approximation (LDA) and incorporating atomic self-interaction corrected pseudopotentials (SIC-PP) to accurately account for the Zn 3d electrons is shown in figure 1.4 [19]. The band structure is shown along high symmetry lines in the hexagonal Brillouin zone. Both the valence band maxima and the lowest conduction band minima occur at the Γ point, k=0 indicating that ZnO is a direct band gap semiconductor. The bottom 10 bands (occurring around −9 eV) correspond to Zn 3d levels. The next 6 bands from −5 eV to 0 eV correspond to O 2p bonding states. The first two conduction band states are strongly Zn localized and correspond to empty Zn 3s levels. The higher conduction bands (not illustrated here) are free-electron-like.

The O 2s bands (also not illustrated here) associated with core-like energy states, occur around −20 eV. The band gap as determined from this calculation is 3.77 eV.
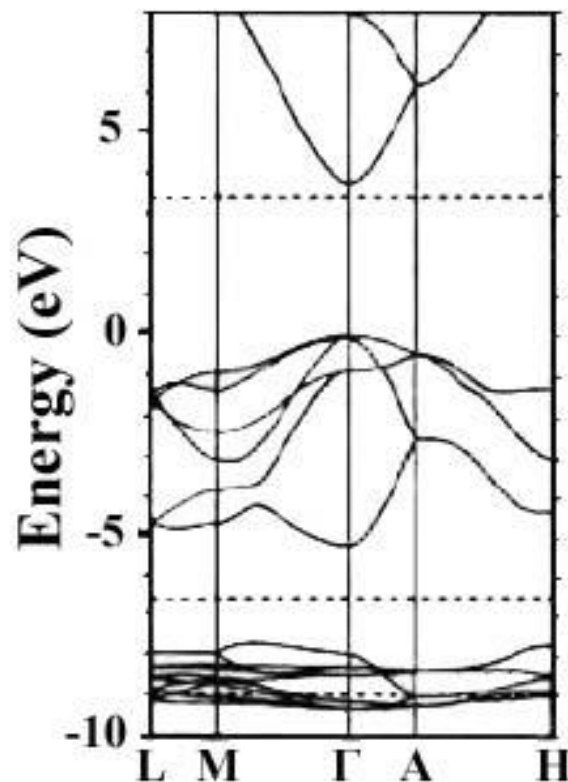
Figure 1.4 The band structure of bulk wurtzite ZnO calculated using self-interaction-corrected pseudopotentials (SIC-PP). This method is much more efficient at treating the d-bands than the standard LDA method [19]

There are several experimental methods to study the band structure of ZnO such as X-ray induced photoemission spectroscopy [20, 21], UV photoemission measurements [22, 23], angle-resolved photoelectron spectroscopy [24, 25], and low-energy electron diffraction [26]. These experimental tools greatly facilitate the understanding and improvement of theoretical calculations.

1.3.4 OPTICAL PROPERTIES OF ZnO

The optical properties are usually described by dielectric constant $\varepsilon(\omega)$, sometimes by refractive index $n(\omega)$, extinction coefficient $k(\omega)$ and absorption coefficient $\alpha(\omega)$. These features are very important to determine the optical and electronic properties of the crystal. The index of refraction of a material is a number that indicates the speed at which light moves through a material compared to how it moves through a vacuum. The extinction coefficient is an imaginary portion of the index of refraction that indicates the absorption loss when the wave passes through the sample. Optical constants give information about how the light moves through the sample and reflects off the material and can be used to measure the band gap of the material.

Optical properties and processes in ZnO as well as its refractive index were extensively studied many decades ago. The renewed interest in ZnO is fuelled and fanned by its prospects in optoelectronics applications owing to its direct wide band gap of 3.37 eV at room temperature with large exciton energy of 60 meV and efficient radiative recombination. The strong exciton binding energy, which is much larger than that of GaN (25 meV), and the thermal energy at room temperature (25 meV) can ensure an efficient exciton emission at room temperature under low excitation energy. Consequently, ZnO is recognized as a promising photonic material in the blue UV region. Optical transitions in ZnO have been studied by a variety of experimental techniques such as optical absorption, transmission, reflection, photoreflection, spectroscopic ellipsometry, photoluminescence, cathodoluminescence, calorimetric spectroscopy, etc. Room temperature PL spectra of ZnO typically consists of a UV emission band and a broad emission band, which is also called deep band emission (DBE). Figure 1.5 shows a typical PL spectrum of single crystal bulk ZnO at room temperature.
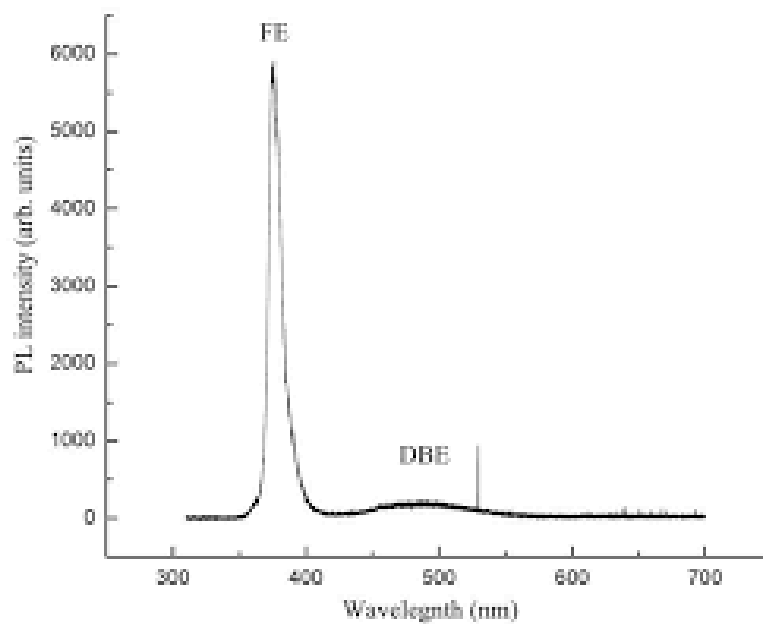
Figure 1.5 PL spectrum of single crystal bulk ZnO. The spectrum is normalized to the free exciton (FE) emission[*].

1.4 RARE EARTH ELEMENTS (REES)

The rare earth elements (REES) are a group of 17 chemical (metallic) elements, which appear in the periodic table. The group consists of the 15-lanthanide elements along with Yttrium and Scandium as shown in Fig. 1.7.

A mixture of rare earths was discovered in 1794 by J. Gadolin and ytterbium was separated from this mixture in 1878 by Mariganac, while the last rare earth element promethium (Pm) was separated by a nuclear reaction in 1974.Therefore, a period of more than 100 years separates the discovery of all the rare earth elements.

They share many similar properties, which is why they occur together in geological deposits. The 17 REEs are found in all REE deposits but their distribution and concentrations vary. They are referred to as 'rare' because it is not common to find them in commercially viable concentrations. REEs generally fall into one of two categories – light rare earths (LREE) (lanthanum, cerium, praseodymium, neodymium, promethium, samarium) and heavy rare earths (HREE) (europium, gadolinium, terbium, dysprosium, holmium, erbium, thulium, ytterbium, lutetium, scandium, and yttrium). With varying levels of uses and demand. REE mineral deposits are usually rich in either LREE or HREE, but rarely contain both in significant quantities. In general, they are vital to some of the world's fastest growing markets: clean energy and high technology. The rare earth elements are distinguished by their incomplete internal $4f$ shell. When diluted in solid hosts, the rare earth atoms become almost always trivalent ions, losing the two 6s and one $4f$ electrons. The $4f$ electrons are shielded from external fields by the two remaining electronic shells with larger radial extension $(5s^2 5p^6)$ [27].

Figure 1.6 A simplified Periodic Table with lanthanide elements [28].

1.4.1 COMMON APPLICATIONS OF RARE EARTH ELEMENTS

The range of applications in which they are used is extraordinarily wide, from the everyday (automotive catalysts and petroleum cracking catalysts, flints for lighters, pigments for glass and ceramics and compounds for polishing glass) to the highly specialized (miniature nuclear batteries, lasers repeaters, superconductors and miniature magnets).Separately, or as compounds, various rare earth metals are used also in the production of super alloys.

REES are now especially important and used extensively, in the defense industry. Some of their specific defense applications include anti-missile defense, aircraft parts, communications systems, electronic countermeasures, jet engines, rockets, underwater mine detection, missile guidance systems and space-based satellite power (Table1.3).

Table 1.4 Rare Earth Elements and some their Uses.

N⁰	Element	Symbol	Uses
1	Cerium	Ce	Catalyst, Fuel additive, Optical polish, Ceramic, Glasses And Phosphors
2	Dysprosium	Dy	Lasers, Magnets, Ceramic, Phosphors And Nuclear Applications
3	Erbium	Er	Ceramic, Glasses dyes, Optical Fibers, Lasers, Photography And Nuclear Applications
4	Europium	Eu	Phosphors, Lasers And Phosphors
5	Gadolinium	Gd	Lasers, Ceramic, Optical, Magnetic Detection And Medical Image Visualization
6	Holmium	Ho	Lasers, Ceramic, Magnets, Optics And Nuclear Applications
7	Lanthanum	La	Catalyst, Ceramic, Glasses , Phosphors And Pigments
8	Neodymium	Nd	Catalyst, Lasers, IR Filters And Magnets
9	Praseodymium	Pr	Ceramic, Glasses And Pigments
10	Promethium	Pm	Phosphors, Nuclear Batteries And Measuring Devices
11	Samarium	Sm	Magnets, Microwave Filters, Lasers And Nuclear Applications
12	Scandium	Sc	Aerospace, Lighting, Nuclear Applications And Semiconductors
13	Terbium	Tb	Lasers, Lighting And Phosphors
14	Thulium	Th	Electron Beam, Lasers And Medical Image Visualization
15	Yttrium	Y	Capacitors, Phosphors, Radars And Superconductors
16	Ytterbium	Yb	Lasers, Chemical Industry And Metallurgy
17	Lutetium	Lu	Catalyst And Medicine

1.4.2 ERBIUM(Er)

Erbium (Er) is a chemical element, a Rare-Earth Elements of the lanthanide series of the periodic table. Pure erbium is a silvery white metal that is relatively stable in air. It slowly reacts with water and quickly dissolves in diluted acids, except hydrofluoric acid (HF) because of formation of the protective fluoride (ErF_3) layer on the surface of the metal. Erbium is a very strong paramagnet above approximately 85 K (−188 °C, or −307 °F). Between 85 K and 20 K (−253 °C, or −424 °F) the metal is antiferromagnetic, and below about 20 K it is arranged in a conical ferromagnetic structure [29].

The element was discovered in 1842 as an oxide by Carl Gustaf Mosander, who originally called it terbia; in the confusion arising from the similarity in the properties of the rare-earth elements, the names of two, terbium and erbium, became interchanged [*30*]. The element occurs in many rare-earth minerals; among the more important are the laterite ionic clays, xenotime, and euxenite. Erbium also occurs in the products of nuclear fission. In Earth's crust, erbium is as abundant as tantalum and tungsten.

Natural erbium is a mixture of six stable isotopes: erbium-166 (33.5 percent), erbium-168 (26.98 percent), erbium-167 (22.87 percent), erbium-170 (14.91 percent), erbium-164 (1.6 percent), and erbium-162 (0.14 percent). Not counting nuclear isomers, a total of 30 radioactive isotopes of erbium are known. Their mass varies from 142 to 177. All the radioactive isotopes of erbium are relatively unstable: their half-lives range from 1

second (erbium-145) to 9.4 days (erbium-169). The element adopts a close-packed hexagonal structure with $a = 3.5592$ Å and $c = 5.5850$ Å at room temperature.

When raised to a high-energy state by absorption of infrared light, the Er^{3+}ion emits photons at wavelengths of 1.55 micrometres—one of the wavelengths commonly employed in fibre-optic signal transmission. Hence, the major use of erbium is in fibre-optic telecommunications, as a component of the signal amplifiers in long-distance telephone and data cables. Its compounds are used in lasers and as a pink colouring agent for glasses. Erbium-stabilized zirconia (ZrO_2) makes pink synthetic gems. Another small-scale use of erbium is in the intermetallic compound Er^3Ni, which has a high magnetic heat capacity around 4 K (−269 °C, or −452 °F), which is needed for effective regenerative heat exchange at low temperatures, and, therefore, the compound is employed as a regenerator material in low-temperature cryocoolers. Erbium behaves as a typical rare-earth element, forming compounds in which its oxidation state is +3, such as the pink oxide Er_2O_3. The Er^{3+} ion is pink in solution.

Electron shell configuration of Erbium is $1s^2, 2s^2 2p^6, 3s^2 \ 3p^6 \ 3d^{10}, 4s^2 \ 4p^6 \ 4d^{10} \ 4f^{12}, 5s^2 \ 5p^6, 6s^2$.

Erbium's everyday uses are varied. It is commonly used as a photographic filter, and because of its resilience, it is useful as a metallurgical additive. Other uses:

- Used in nuclear technology in neutron-absorbing control rods[31, 32].

- When added to vanadium as an alloy, erbium lowers hardness and improves workability [33].

- Erbium oxide has a pink color, and is sometimes used as a colorant for glass, cubic zirconia and porcelain. The glass is then often used in sunglasses and cheap jewelry[33].

- Erbium-doped optical silica-glass fibers are the active element in erbium-doped fiber amplifiers (EDFAs), which are widely used in optical communications [34]. The same fibers can be used to create fiber lasers. In order to work efficiently, erbium-doped fiber is usually co-doped with glass modifiers/homogenizers, often aluminum or phosphorus. These dopants help prevent clustering or Er-ions and transfer the energy more efficiently between the Er ions and the signal. Co-doping of optical fiber with Er and Yb is used in high-power Er/Yb fiber lasers. Erbium can also be used in erbium-doped waveguide amplifiers[31].

- An erbium-nickel alloy Er_3Ni has an unusually high specific heat capacity at liquid-helium temperatures and is used in cryocoolers; a mixture of 65% Er_3Co and 35% $Er_{0.9}Yb_{0.1}Ni$ by volume improves the specific heat capacity even more [35,36].

- A large variety of medical applications (i.e. dermatology, dentistry) utilize erbium ion's 2940 nm emission (see Er:YAG laser), which is highly absorbed in water (absorption coefficient about 12000/cm). Such shallow tissue deposition of laser energy is necessary for laser surgery, and the efficient production of steam for laser enamel ablation in dentistry.

1.5 RARE EARTH ELEMENTS DOPED ZnO

Semiconductors doped with rare earth ions are excellent phosphors of high efficiency and low degradation in addition to their unique physical and chemical properties [37]. II-VI compound semiconductors have been found to be unique host materials for doping of optically active impurities, which exhibit luminescence at room temperature [38]. Rare earth ions in II-VI semiconductors compounds have been studied since more than 50 years [39] in powders [40], bulk crystals [41], thin films [42], and epitaxial layers [43]. Recently, rare earths (RE) doped semiconductors have long been the topic of research owing to their prominent and desirable optical and magnetic properties. Typically, trivalent rare earth elements have very stable emissions, due to the 4f electrons, which are deeply buried and hence well shielded from the outer shells. This property of the rare earth elements makes it possible; to incorporate them into various hosts with different lattice and still preserve the typical rare earth emissions. Semiconductors such as ZnO, GaN, ZnSe doped with rare earth ions show evidence of electroluminescence; these materials are candidates for traditional semiconductor light emitting diodes and enable new technologies for highly distinguishable emissive flat panel displays.

Recently, the ZnO presented an interesting subject for doping with various elements such as transition metals and nobel metals. This is of course very suitable to improve the optoelectronic and photocatalytic properties because the incorporation of dopants generates lattice defects and changes consequently the band gap energy [44]. In particular, the doping with rare-earth elements has been extensively investigated, experimentally as well as theoretically.

Poongodi et al [45] deposited nanostructured Nd doped ZnO thin films on glass substrate by a sol–gel spin coating technique. The results show the degradation of

methylene blue dye and the decrease in grain size and light absorption over an extended visible region by Nd ion doping in ZnO film contributed equally to improve the photocatalytic activity.

Honglin et al [46] prepared the ZnO nanopowders doped with (La,Er,Nd) rare-earth by chemical method. The photoluminescence (PL) measurement revealed that pure and Res doped ZnO had different I_{UV}/I_{DLE} ratios, and the absorption spectra of doped ZnO exhibited enhanced optical absorption in visible region. Zhang et al [47] studied the electronic structure and magnetism of RE (RE = La, Ce, Pr, Nd and Eu) doped ZnO using generalized gradient approximation (GGA) and GGA+ U, it appeared the influence of a dopant on the electronic and magnetism properties of ZnO.

DU Fangli *et al* [48] prepared Ce-doped ZnO films by the sol-gel method with spin coating onto glass substrates. It was found that Ce-doped ZnO films showed a hexagonal wurtzite structure and had a (101) preferred orientation. The infrared emissivity increased with the temperature rising when the ZnO films were doped with 3 at % and 7 at % of Ce concentration. However, the infrared emissivity decreased with the temperature increasing when the ZnO film was doped with 5 at.% of Ce. This suggests that the infrared emissivity of the films is remarkably changed by controlling the Ce doping concentration.

Sofiani etal [49] deposited zinc oxide (ZnO) and cerium-doped zinc oxide (ZnO:Ce) films by reactive chemical pulverization spray pyrolysis technique using zinc and cerium chlorides as precursors. All deposited ZnO layers at the temperature 450ºC are polycrystalline and indicate highly c-axis oriented structure. The dimension of crystallites depends on incorporation of Ce atoms into the ZnO films. The photoluminescence spectra of the films have been studied as a function of the deposition parameters such as doping concentrations and post growth annealing.

Photoluminescence spectra were measured at the temperature range from 13 K to 320 K.

Eugenio Hernan Otal etal [50] studied the introduction and stability of the heavy lanthanide Er, into ZnO by HRTEM, XRD and thermal treatments. The applied synthesis route allows introducing the Er atoms in the lattice in a metastable state. The stability depends on the Er concentration. ZnO with Er concentrations of less than 2% are stable up to 800ºC, while higher concentrations result in a phase segregation at T > 700ºC. Unit cell parameters obtained from the Rietveld refinement of XRD patterns provide a conclusive evidence of the incorporation of the Er ions in the host ZnO matrix.

Fanyong Ran et al [51] have fabricated using erbium acetate as an Er source, transparent ZnO films doped with Er by sol–gel method through spin-coating on quartz substrates. The ZnO:Er films exhibit wurtzite structure with preferential orientation of the (002) plane. The film that annealed at 800ºC shows the highest degree of preferential orientation. Coalescence of small grains result in very large and irregularly shaped grains for the film annealed at 1000ºC. The estimated optical band gap of Er-doped ZnO films annealed at different temperatures is 3.28 eV, which is almost independent of annealing temperature and quite similar to that of undoped ZnO film.

REFERENCES

[1] Q. Zhao, X.Y. Xu, X.F. Song, X.Z. Zhang, D.P. Yu, C.P. Li, L. Guo, Appl. Phys. Lett. 88 (2006) 033102.

[2] W. Water, S.Y. Chu, Mater. Lett. 55 (2002) 67.

[3] GUO, H.G.; ZHOU, J.Z.; LIN, Z.G. ZnO nanorod light-emitting diodes fabricated by electrochemical approaches. Electrochemistry Communications, 2008. Vol. 10, No. 1, p. 146-150.

[4] ZHANG, Q.F.; DANDENEAU, C.S.; ZHOU, X.Y.; CAO, G.Z. ZnO Nanostructures for Dye-Sensitized Solar Cells. Advanced Materials, 2009. Vol. 21, No. 41, p. 4087-4108.

[5] Y. Li, G.S.Tompa, S. Liang, C. Gorla, C. Lu, J.Doyle, J Vac Sci Techol A 15 (1997) 1663.

[6] D.W. Palmer, Available from: http://www.semiconductors.co.uk, 2002.06.

[7] D, Florescu, L, G, Mourok, F, H, Pollack, D, C, Look, G, Cantwell, X, Li, J Appl Phys., 91(2002)890.

[8] Jin, B.J., S. Im, and S.Y. Lee, Violet and UV luminescence emitted from ZnO thin films grown on sapphire by pulsed laser deposition. Thin Solid Films, 2000. 366(1-2): p. 107-110.

[9] Kogure, T. and Bando, Y. (1993) Journal of Electron Microscopy, 47, 7903.

[10] Ashrafi, A.B.M.A., Ueta, A., Avramescu, A., Kumano, H., Suemune, I., Ok, Y.-W. and Seong, T.-Y. (2000) Applied Physics Letters, 76, 550.

[11] Kim, S.-K., Jeong, S.-Y. and Cho, C.-R. (2003) Applied Physics Letters, 82, 562.

[12] Bates, C.H., White, W.B. and Roy, R. (1962) Science, 137, 993.

[13] Ip, K., Heo, Y., Baik, K., Norton, D.P., Pearton, S.J. and Ren, F. (2004) Journal of Vacuum Science & Technology B, 22, 171.

[14] Kim, H.K., Han, S.H., Seong, T.Y. and Choi, W.K. (2000) Applied Physics Letters, 77, 1647.

[15] Liu, C.H., Zapien, J.A., Yao, Y., Meng, X.M., Lee, C.S., Fan, S.S., Lifshitz, Y. and Lee, S.T. (2003) High-density ordered ultraviolet light-emitting ZnO nanowire arrays. Advanced Materials, 15, 838.

[16]Yang, P., Yan, H., Mao, S., Russo, R., Johnson, J., Saykally, R., Morris, N., Pham, J., He, R. and Choi, H.-J. (2002) Controlled growth of ZnO nanowires and their optical properties. Advanced Functional Materials, 12, 323.

[17] U. Rossler, Energy bands of hexagonal 2-6 semiconductors. Physical Review,1969. 184(3): p. 733

[18] J. R. Chelikowsky, Solid State Commun. 22 (1977) 351.

[19] D. Vogel, P. Krüger, J. Pollmann, Phys. Rev. B 52 (1995) R14316.

[20] D. W. Langer, and C. J. Vesely, Phys. Rev. B 1970, 2, 4885.

[21] C. J. Vesely, R. L. Hengehold, and D. W. Langer, Phys. Rev. B 1972, 5, 2296.

[22] P. A. Powell, W. E. Spicer, and J. C. McMenamin, Phys. Rev. Lett 1971, 27, 97.

[23] R. A. Powell, W. E. Spicer, and J. C. McMenamin, Phys. Rev. B 1972, 6, 3056.

[24] R. T. Girard, O. Tjernberg, G. Ghiana, S. Söderholm, U. O. Karlsson, C. Wigren, H. Nylen, and I. Lindau, Surf. Sci. 1997, 373, 409.

[25] K. Ozawa, K. Sawada, Y. Shirotori, K. Edamoto, and M. Nakatake, Phys. Rev. B 2003, 68, 125417.

[26] C. B. Duke, A. R. Lubinsky, S. C. Chang, B. W. Lee, and P. Mark, Phsy. Rev. B 1977, 15, 4865.

[27] Leandro R. Tessler, Erbium in a-Si:H, Brazilian Journal of Physics, 1999.

[28] L. A. Riseberg and M. J. Weber, "Relaxation phenomena in Rare-Earth Luminescence", Progress in optics XIV, North Holland, 1976.

[29] Jackson, M. "Magnetism of rare earth." IRM Quarterly 3 (2000): 1-8.

[30] Mosander, Carl Gustav. "XXX. On the new metals, lanthanium and didymium, which are associated with cerium; and on erbium and terbium, new metals associated with yttria." The London, Edinburgh, and Dublin Philosophical Magazine and Journal of Science 23.152 (1843): 241-254.

[31] Emsley, John (2001). "Erbium". Nature's Building Blocks: An A-Z Guide to the Elements. Oxford, England, UK: Oxford University Press. pp. 136–139. ISBN 0-19-850340-7.

[32] Balygin, A. A., et al. "Use of Uranium-Erbium and Plutonium-Erbium Fuel in Rbmk Reactors." Safety Issues Associated with Plutonium Involvement in the Nuclear Fuel Cycle. Springer Netherlands, 1999. 121-130.

[33] Hammond, C. R. (2000). The Elements, in Handbook of Chemistry and Physics (81st ed.). CRC press. ISBN 0-8493-0481-4.

[34] Becker, P.C.; Olsson, N.A.; Simpson, J.R. (1999). Erbium-doped fiber amplifiers fundamentals and technology. San Diego: Academic Press. ISBN 978-0-12-084590-3.

[35] Kittel, Peter (ed.). Advances in Cryogenic Engineering 39a.

[36] Ackermann, Robert A. (1997). Cryogenic Regenerative Heat Exchangers. Springer. p. 58. ISBN 978-0-306-45449-3.

[37] N. Rakov, F. E. Ramos, G. Hirata and M. Xiao, Appl. Phys. Lett. 83, 272 (2003)

[38] H.Ishizumi and Y.Kanemitsu, Appl. Phys. Lett. 86, 253106 (2005)

[39] Hommel, D., et al. "Rare earths in II–VI compounds: Non-linear optical excitation processes at low and high doping levels." Journal of crystal growth 101.1 (1990): 393 403.

[40] Trapeznikova, Z. A. "On the Interaction of." Optics and Spectroscopy 6 (1959): 325.

[41] Anderson, W. W. "Tb 3+ as a Recombination Center in ZnS." Physical Review 136.2A (1964): A556.

[42] Hommel, D., et al. "Rare earths in II–VI compounds: Non-linear optical excitation processes at low and high doping levels." Journal of crystal growth 101.1 (1990): 393-403.

[43] Hirabayashi, Katsuhiko, Haruki Kozawaguchi, and Bunjiro Tsujiyama. "Color electroluminescent devices prepared by metal organic chemical vapor deposition." Japanese journal of applied physics 26.9R (1987): 1472

[44] Danli, Jian-Feng Huang, Li-Yun Cao, Microwave hydrothermal synthesis of Sr doped ZnO Crystallites with enhanced photocatalytic properties. Ceramics International 40(2014) 2647-2653

[45] Poongodi, Govindan, Rangasamy Mohan Kumar, and Ramasamy Jayavel. "Structural, optical and visible light photocatalytic properties of nanocrystalline Nd doped ZnO thin films prepared by spin coating method." Ceramics International 41.3 (2015): 4169-4175.

[46] Honglin, Li, et al. "Experimental and first-principles studies of structural and optical properties of rare earth (RE= La, Er, Nd) doped ZnO." Journal of Alloys and Compounds 617 (2014): 102-107.

[47] Zhang, X. J., et al. "First-principles prediction of electronic structure and magnetic ordering of rare-earth metals doped ZnO." Journal of Alloys and Compounds 617 (2014): 828-833.

[48] Du Fangli, Wang Ning , Zhang Dongmei , Shen Yingzhong , Journal Of Rare Earths, 28 (3) (June 2010) P. 391.

[49] Sofiani.Z , B. Derkowska, P. Dalasin´ ski, M. Wojdyła, S. Dabos-Seignon, M. Alaoui Srinivasan. G, J. Kumar, Journal of Crystal Growth, 310 (2008) 1841–1846.

[50] Eugenio Hernan Otal, Songhak Yoon, Myriam Aguirre, Anke Weidenkaff, Journal of Alloys and Compound,s 509S (2011) S364–S366.

[51] Fanyong Ran, Lei Miaob, Sakae Tanemura, Masaki Tanemura, Yongge Cao, Shigeru Tanaka, Noriyoshi Shibata, Materials Science and Engineering B, 148 (2008) 35–39.

CHAPTER II

2.1 INTRODUCTION

Density Functional Theory (DFT) is one of the most widely used methods for "ab initio" calculations of the structure of atoms, molecules, crystals, surfaces, and their interactions [1, 2]. The main idea of DFT is to describe a many-body interacting system via its particle density and not via its many-body wavefunction. Its significance is to reduce the 3N degrees of freedom of the N-body system to only three spatial coordinates through its particle density. It is used to calculate properties such as equilibrium geometries, electronic, optic, activation energies, and reaction energies.

In this chapter, we will discuss the general theory and historical background about DFT, as well as, we will introduce some important concepts in DFT.

2.2 THE DENSITY FUNCTIONAL THEORY (DFT)

Density functional theory is one of the most popular and successful quantum mechanical approaches to matter. It is a method in quantum mechanical modeling that studies the behavior of the material by solving the Schrödinger equation (SE) and finding the ground state of the system. Ground state is defined as the state in which the system has the lowest possible energy. The theory originates from the pioneering work due to Thomas [3] and Fermi [4] in the early thirties of the twentieth century and further refinements by Hartree [5], Dirac [6, 7], Fock [8] and Slater [9].

It was given a firm foundation by Hohenberg, Kohn and Sham almost forty years after the work of Thomas and Fermi. The original scheme as proposed by Hohenberg and Kohn (HK) [10] and Kohn and Sham (KS) [11] is a ground-state theory which provides a reliable and inexpensive method for the calculation of ground-state energy of an interacting many Fermionic system.

2.2.1 THE MANY-BODY SYSTEM AND BORN-OPPENHEIMER APPROXIMATION

The Hamiltonian of a many-body condensed-matter system consisting of nuclei and electrons can be written as:

$$\widehat{H} = \widehat{T}_T + \widehat{U}_T$$

$$\widehat{H} = \widehat{T}_n(\vec{R}) + \widehat{T}_e(\vec{r}) + \widehat{U}_{nn}(\vec{R}) + \widehat{U}_{ee}(\vec{r}) + \widehat{U}_{ne}(\vec{R}, \vec{r})$$

$$\widehat{H} = \sum_I -\frac{\hbar^2}{M}\frac{\nabla^2 \vec{R}_I}{2} + \sum_i -\frac{\hbar^2}{m}\frac{\nabla^2 \vec{r}_i}{2} + \frac{e^2}{4\pi\varepsilon_0}\sum_{I\neq J}\frac{+Z_I Z_J}{|\vec{R}_I - \vec{R}_J|} + \frac{e^2}{4\pi\varepsilon_0}\sum_{i\neq j}\frac{-1}{|\vec{r}_i - \vec{r}_j|}$$

$$+ \frac{e^2}{4\pi\varepsilon_0}\sum_{i,I}\frac{-Z_I}{|\vec{r}_i - \vec{R}_I|} \tag{2.1}$$

where the indexes I, J run on nuclei, i and j on electrons, R_I and M are positions and masses of the nuclei, r_i and m of the electrons, Z_I the atomic number of nucleus I.

The first term is the kinetic energy of the nuclei, the second term is the kinetic energy of the electrons, the third term is the potential energy of nucleus-nucleus Coulomb interaction, the fourth term is the potential energy of electron-electron Coulomb interaction and the last term is the potential energy of nucleus-electron Coulomb interaction. The time-independent Schrödinger equation for the system reads:

$$\widehat{H}\psi(\vec{R},\vec{r}) = E\,\psi(\vec{R},\vec{r}) \tag{2.2}$$

where $\psi(\vec{R},\vec{r})$ is the total wavefunction of the system. In principle, everything about the system is known if one can solve the above Schrödinger equation. However, it is impossible to solve it in practice. A so-called Born Oppenheimer (BO) approximation was made by Born and Oppenheimer [12] in 1927. Since the nuclei are much heavier than electrons (the mass of a proton is about 1836 times the mass of an electron), the nuclei move much slower (about two order of magnitude slower) than the electrons. Therefore we can separate the movement of nuclei and electrons. When we consider the movement of electrons, it is reasonable to consider the positions of nuclei are fixed, thus the total wavefunction can be written as:

$$\psi(\vec{r},\vec{R}) = \psi_n(\vec{R})\psi_e(\vec{r},\vec{R}) \tag{2.3}$$

where $\psi_n(\vec{R})$ describes the nuclei and $\psi_e(\vec{r},\vec{R})$ the electrons (depending parametrically on the positions of the nuclei). With the BO approximation, Eq. (2.2) can be divided into two separate Schrödinger equations:

$$\widehat{H}_e\,\psi_e(\vec{r},\vec{R}) = V(\vec{R})\,\psi_e(\vec{r},\vec{R}) \tag{2.4}$$

where

$$\hat{H}_e = -\sum_i \frac{\hbar^2}{m}\frac{\nabla^2 \vec{r}_i}{2} + \frac{1}{2}\sum_{I \neq J}\frac{Z_I Z_J e^2}{|\vec{R}_I - \vec{R}_J|} + \frac{1}{2}\sum_{i \neq j}\frac{-e^2}{|\vec{r}_i - \vec{r}_j|} - \sum_{i,I}\frac{Z_I e^2}{|\vec{r}_i - \vec{R}_I|} \qquad (2.5)$$

and

$$\left[\sum_I -\frac{\hbar^2}{M}\frac{\nabla^2 \vec{R}_I}{2} + V(\vec{R})\right]\psi_n(\vec{R}) = E'\psi_n(\vec{R}) \qquad (2.6)$$

Eq. (2.4) is the equation for the electronic problem with the nuclei positions fixed. The eigenvalue of the energy $V(\vec{R})$ depends parametrically on the positions of the nuclei. After solving Eq. (2.4), $V(\vec{R})$ is known and by applying it to Eq. (2.6), which has no electronic degrees of freedom, the motion of the nuclei is obtained. Eq. (2.6) is sometimes replace by a Newton equation, i.e., to move the nuclei classically, using ∇V as the forces. Then the whole problem is solved.

The significance of the BO approximation is to separate the movement of electrons and nuclei. Now we can consider that the electrons are moving in a static external potential $V_{ext}(r)$ formed by the nuclei, which is the starting point of DFT. The BO approximation was extended by Bohn and Huang known as Born-Huang (BH) approximation [13] to take into account more nonadiabatic effect in the electronic Hamiltonian than in the BO approximation.

2.2.2 THOMAS-FERMI-DIRAC APPROXIMATION

The very earliest attempt at using the density instead of the wavefunction was published only a year after Schrödinger's work independently by Enrico Fermi (14) and Llewellyn Thomas (15). In this method, they used the electron density $n(r)$ as the basic variable instead of the wavefunction. The total energy of a system in an external potential $V_{ext}(r)$ is written as a functional of the electron density $n(r)$) as:

$$E_{TF}[n(r)] = A_1 \int n(r)^{5/3}\, dr + \int n(r)\, V_{ext}(r) dr$$

$$+ \frac{1}{2} \iint \frac{n(r)n(r')}{|r-r'|}\, drdr' \tag{2.7}$$

where the first term is the kinetic energy of the non-interacting electrons in a homogeneous electron gas (HEG) with $A_1 = \frac{3}{10}(3\pi^2)^{2/3}$ in atomic units ($\hbar = m_e = e = 4\pi/\epsilon_0 = 1$). The kinetic energy density of a HEG is obtained by adding up all of the free-electron energy state $\varepsilon_k = k^2/2$ up to the Fermi wavevector $k_F = [3\pi^2 n(r)]^{1/3}$ as:

$$t_0[n(r)] = \frac{2}{2\pi^3} \int_0^{k_F} \frac{k^2}{2} 4\pi k^2 dk = A_1 n(r)^{5/3} \tag{2.8}$$

The second term is the classical electrostatic energy of the nucleus-electron Coulomb interaction. The third term is the classical electrostatic Hartree energy approximated by the classical Coulomb repulsion between electrons. In the original TF method, the exchange and correlation among electrons was neglected. In 1930, Dirac [16] extended the Thomas-Fermi method by adding a local exchange term $A_2 \int n(r)^{4/3}\, dr$ to Eq. (2.7) with, $A_2 = -\frac{3}{4}(3/\pi)^{1/3}$, which leads Eq. (2.7) to

$$E_{TF}[n(r)] = A_1 \int n(r)^{5/3}\, dr + \int n(r)\, V_{ext}(r) dr$$

$$+ \frac{1}{2} \iint \frac{n(r)n(r')}{|r-r'|}\, drdr' + A_2 \int n(r)^{4/3}\, dr \tag{2.9}$$

The ground state density and energy can be obtained by minimizing the Thomas- Fermi-Dirac equation (2.9) subject to conservation of the total number (N) of electrons. By using the technique of Lagrange multipliers, the solution can be found in the stationary condition:

$$\delta\left\{ E_{TFD}[n(r)] - \mu\left(\int n(r)\, dr - N \right) \right\} = 0 \tag{2.10}$$

where μ is a constant known as a Lagrange multiplier, whose physical meaning is the chemical potential (or Fermi energy at T=0 K). Eq. (2.10) leads to the Thomas-Fermi-Dirac equation,

$$\frac{5}{3}A_1 n(r)^{2/3} + V_{ext}(r) + \int \frac{n(r')}{|r - r'|}dr' + \frac{4}{3}A_2 n(r)^{1/3} - \mu = 0 \qquad (2.11)$$

which can be solved directly to obtain the ground state density.

The approximations used in Thomas-Fermi-type approach are so crude that the theory suffers from many problems. The most serious one is that the theory fails to describe bonding between atoms, thus molecules and solids cannot form in this theory. [17] Although it is not good enough to describe electrons in matter, its concept to use electron density as the basic variable illustrates the way DFT works.

2.2.3 THE HOHENBERG-KOHN (HK) THEOREMS

DFT was proven to be an exact theory of many-body systems by Hohenberg and Kohn [10] in 1964. It applies not only to condensed-matter systems of electrons with fixed nuclei, but also more generally to any system of interacting particles in an external potential $V_{ext}(r)$. The theory is based upon two theorems.

2.2.3.1 THE FIRST HOHENBERG-KOHN THEOREM

The ground state particle density $n(r)$ of a system of interacting particles in an external potential $V_{ext}(r)$ uniquely determines the external potential $V_{ext}(r)$, except for a constant. Thus, the ground state particle density determines the full Hamiltonian, except for a constant shift of the energy. In principle, all the states including ground and excited states of the many-body wave functions can be calculated. This means that the ground state particle density uniquely determines all properties of the system completely. For simplicity, here the ground state of the system is non- degenerate. It can be proven that the theorem is also valid for systems with degenerate ground states [18]. The proof is

based on minimum energy principle. Suppose there are two different external potentials $V_{ext}(r)$ and $V'_{ext}(r)$ which differ by more than a constant and lead to the same ground state density $n_0(r)$. The two external potentials would give two different Hamiltonians, $\hat{H}$ and $\hat{H}'$, which have the same ground state density $n_0(r)$ but would have different ground state wavefunctions, Ψ and Ψ' with $\hat{H}\Psi = E_0\Psi$ and $\hat{H}'\Psi' = E'_0\Psi'$ Since Ψ' is not the ground state of $\hat{H}$, it follows that

$$E_0 < \langle\Psi'|\hat{H}|\Psi'\rangle$$

$$< \langle\Psi'|\hat{H}'|\Psi'\rangle + \langle\Psi'|\hat{H} - \hat{H}'|\Psi'\rangle \qquad (2.12)$$

$$< E'_0 + \int n_0(r)[V_{ext}(r) - V'_{ext}(r)]dr$$

Similarly

$$E'_0 < \langle\Psi'|\hat{H}|\Psi'\rangle$$

$$< \langle\Psi'|\hat{H}|\Psi'\rangle + \langle\Psi'|\hat{H}' - \hat{H}|\Psi'\rangle \qquad (2.13)$$

$$< E_0 + \int n_0(r)[V'_{ext}(r) - V_{ext}(r)]dr$$

Adding Eq. (2.12) and (2.13) lead to the contradiction

$$E_0 + E'_0 < E_0 + E'_0 \qquad (2.14)$$

Hence, no two different external potentials $V_{ext}(r)$ can give rise to the same ground state density $n_0(r)$, i.e., the ground state density determines the external potential $V_{ext}(r)$, except for a constant. That is to say, there is a one-to-one mapping between the ground state density $n_0(r)$ and the external potential $V_{ext}(r)$, although the exact formula is unknown.

2.2.3.2 THE SECOND HOHENBERG-KOHN THEOREM

There exists a universal functional $F[n(r)]$ of the density, independent of the external potential $V_{ext}(r)$, such that the global minimum value of the energy functional $E[n(r)] = \int n(r) V_{ext}(r) dr + F[n(r)]$ is the exact ground state energy of the system and the exact ground state density $n_0(r)$ minimizes this functional. Thus, the exact ground state energy and density are fully determined by the functional $E[n(r)]$.

The universal functional $F[n(r)]$ can be written as

$$F[n(r)] \equiv T[n(r)] + E_{int}[n(r)] \tag{2.15}$$

where $T[n(r)]$ is the kinetic energy and $E_{int}[n(r)]$ is the interaction energy of the particles. According to variational principle, for any wave function Ψ', the energy functional $E[\Psi']$:

$$E[\Psi'] \equiv \langle \Psi' | \hat{T} + \hat{V}_{int} + \hat{V}_{ext} | \Psi' \rangle \tag{2.16}$$

has its global minimum value only when Ψ' is the ground state wavefunction Ψ_0, with the constraint that the total number of the particles is conserved. According to HK theorem I, Ψ' must correspond to a ground state with particle density $n'(r)$ and external potential $V'_{ext}(r)$, then $E[\Psi']$ is a functional of $n'(r)$. According to variational principle:

$$E[\Psi'] \equiv \langle \Psi' | \hat{T} + \hat{V}_{int} + \hat{V}_{ext} | \Psi' \rangle$$

$$= E[n'(r)]$$

$$= \int n'(r) V'_{ext}(r)\, dr + F[n'(r)]$$

$$> E[\Psi_0] \tag{2.17}$$

$$= \int n_0(r) V_{ext}(r) dr + F[n_0(r)]$$

$$= E[n_0(r)]$$

Thus, the energy functional $E[n(r)] = \int n(r) V_{ext}(r)dr + F[n(r)]$ evaluated for the correct ground state density $n_0(r)$ is indeed lower than the value of this functional for any other density $n(r)$. Therefore by minimizing the total energy functional of the system with respect to variations in the density $n(r)$; one would find the exact ground state density and energy.

The HK theorems can be generalized to spin density functional theory with spin degrees of freedom [19]. In this theory, there are two types of densities, namely, the particle density $n(r) = n_\uparrow(r) + n_\downarrow(r)$ and the spin density $s(r) = n_\uparrow(r) + n_\downarrow(r)$ where $\uparrow$ and $\downarrow$ denote the two different kinds of spins. The energy functional is generalized to $[n(r), s(r)]$. In systems with magnetic order or atoms with net spins, the spin density functional theory should be used instead of the original one-spin density functional theory. DFT can also be generalized to include temperature dependence and time dependence known as time-dependent density functional theory (TD-DFT) [20, 21].

Although HK theorems put particle density $n(r)$ as the basic variable, it is still impossible to calculate any property of a system because the universal functional $F[n(r)]$ is unknown. This difficulty was overcome by Kohn and Sham [11] in 1965, who proposed the well known Kohn-Sham ansatz.

2.2.3 THE KOHN-SHAM (KS) ANSATZ

Kohn-Sham (KS) ansatz put Hohenberg-Kohn theorems into practical use and makes DFT calculations possible with even a single personal computer [11]. This is part of the reason that DFT became the most popular tool for electronic structure calculations. The KS ansatz was so successful that Kohn was honored the Nobel prize in chemistry in 1998.

The KS ansatz is to replace the original many-body system by an auxiliary independent-particle system and assume that the two systems have exactly the same ground state density. It maps the original interacting system with real potential onto a fictitious non-interacting system whereby the electrons move within an effective Kohn-Sham single-particle potential VKS(r). For the auxiliary independent-particle system, the auxiliary Hamiltonian is

$$\widehat{H}_{KS} = -\frac{1}{2}\nabla^2 + V_{KS}(r) \tag{2.18}$$

in atomic units ($\hbar = m_e = e = 4\pi/\epsilon_0 = 1$) For a system with N independent electrons, the ground state is obtained by solving the N one-electron Schrödinger equations,

$$\left(-\frac{1}{2}\nabla^2 + V_{KS}(r)\right)\psi_i(r) = \varepsilon_i\psi_i(r) \tag{2.19}$$

where there is one electron in each of the N orbitals $\psi_i(r)$ with the lowest eigenvalues ε_i. The density of the auxiliary system is constructed from:

$$n(\vec{r}) = \sum_{i=1}^{N} |\psi_i(\vec{r})|^2 \tag{2.20}$$

which is subject to the conservation condition:

$$\int n(r)\,dr = N \tag{2.21}$$

The non-interacting independent-particle kinetic energy $T_S[n(r)]$ is given by,

$$T_S[n(r)] = -\frac{1}{2}\sum_{i=1}^{N}\int \psi_i^*(r)\nabla^2\psi_i(r)\,dr \tag{2.22}$$

Then the universal functional $F[n(r)]$ was rewritten as

$$F[n(r)] = T_S[n(r)] + E_H[n(r)] + E_{XC}[n(r)] \tag{2.23}$$

where, $E_H[n(r)]$ is the classic electrostatic (Hartree) energy of the electrons,

$$E_H[n(r)] = \frac{1}{2} \iint \frac{n(r)n(r')}{|r-r'|} \, dr dr' \tag{2.24}$$

moreover, $E_{XC}[n(r)]$ is the XC energy, which contains the difference between the exact and non-interacting kinetic energies and the non-classical contribution to the electron-electron interactions, of which the exchange energy is a part. Since the ground state energy of a many-electron system can be obtained by minimizing the energy functional $E[n(r)] = F[n(r)] + \int n(r) V_{ext}(r) dr$, subject to the constraint that the number of electrons N is conserved,

$$\delta \left\{ F[n(r)] + \int n(r) V_{ext}(r) dr - \mu \left(\int n(r) \, dr - N \right) \right\} = 0 \tag{2.25}$$

and the resulting equation is

$$\mu = \frac{\delta F[n(r)]}{\delta n(r)} + V_{ext}(r)$$

$$= \frac{\delta T_S[n(r)]}{\delta n(r)} + V_{KS}(r) \tag{2.26}$$

where μ is the chemical potential,

$$V_{KS}(r) = V_{ext}(r) + V_H(r) + V_{XC}(r)$$

$$= V_{ext}(r) + \frac{\delta E_H[n(r)]}{\delta n(r)} + \frac{\delta E_{XC}[n(r)]}{\delta n(r)} \tag{2.27}$$

is the KS one-particle potential with the Hartree potential $V_H(r)$

$$V_H(r) = \frac{\delta E_H[n(r)]}{\delta n(r)}$$

$$= \int \frac{n(r')}{|r-r'|} \, dr' \tag{2.28}$$

and the XC potential $V_{XC}(r)$

$$V_{XC}(r) = \frac{\delta E_{XC}[n(r)]}{\delta n(r)} \tag{2.29}$$

Equations (2.19), (2.20), (2.27) together are the well-known KS equations, which must be solved self-consistently because $V_{KS}(r)$ depends on the density through the XC potential. In order to calculate the density, the N equations in Eq. (2.19) have to be solved in KS theory as opposed to one equation in the TF approach. However an advantage of the KS method is that as the complexity of a system increases, due to N increasing, the problem becomes no more difficult, only the number of single-particle equations to be solved increases.

Although exact in principle, the KS theory is approximate in practice because of the unknown XC energy functional $E_{XC}[n(r)]$. An implicit definition of $E_{XC}[n(r)]$ can be given as

$$E_{XC}[n(r)] = T[n(r)] - T_S[n(r)] + E_{int}[n(r)] - E_H[n(r)] \qquad (2.30)$$

where $T[n(r)]$ and $E_{int}[n(r)]$ are the exact kinetic and electron-electron interaction energies of the interacting system respectively. It is crucial to have an accurate XC energy functional $E_{XC}[n(r)]$or potential $V_{XC}[n(r)]$in order to give a satisfactory description of a realistic condensed-matter system. The most widely used approximations for the XC potential are the local density approximation (LDA) and the generalized-gradient approximation (GGA).

The KS energy eigenvalues of Eq. (2.19) are not for the original interacting many-body system and have no physical meaning. They cannot be interpreted as one-electron excitation energies of the interacting many-body system, i.e., they are not the energies to add or subtract from the interacting many-body system, because the total energy of the interacting system is not a sum of all the eigenvalues of occupied states in equation (2.19), i.e., $E_{tot} \neq \sum_i^{occ} \varepsilon_i$. The only exception is the highest eigenvalue in a finite system which is the negative of the ionization energy, -I, because it determines the asymptotic long-range density of the bound system which is assumed to be exact. No

other eigenvalue is guaranteed to be correct by the KS theory. Nevertheless, within the KS theory itself, the eigenvalues have a well-defined meaning and they are used to construct physically meaningful quantities. They have a definite mathematical meaning, often known as the Slater-Janak theorem. The eigenvalue is the derivative of the total energy with respect to occupation of a state, i. e.

$$\varepsilon_i = \frac{dE_{total}}{dn_i}$$

$$= \int \frac{dE_{total}}{dn(r)} \frac{dn(r)}{dn_i} dr \qquad (2.31)$$

2.2.5 SOLVING KOHN-SHAM EQUATIONS

By using independent-particle methods, the KS equations provide a way to obtain the exact density and energy of the ground state of a condensed matter system. The KS equations must be solved consistently because the effective KS potential V_{KS} and the electron density $n(r)$ are closely related. This is usually done numerically through some self-consistent iterations as shown in Fig. 2.1.1. The process starts with an initial electron density, usually a superposition of atomic electron density, then the effective KS potential V_{KS} is calculated and the KS equation is solved with singleparticle eigenvalues and wavefunctions, a new electron density is then calculated from the wavefunctions. After this, self-consistent condition(s) is checked. Self-consistent condition(s) can be the change of total energy or electron density from the previous iteration or total force acting on atoms is less than some chosen small quantity, or a combination of these individual conditions. If the self-consistency is not achieved, the calculated electron density will be mixed with electron density from previous iterations to get a new electron density. A new iteration will start with the new electron density. This process continues until self-consistency is reached. After the self-consistency is reached, various quantities can be calculated including total energy, forces, stress, eigenvalues, electron density of states, band structure, etc...

The most timing consuming step in the whole process is to solve KS equation with a given KS potential V_{KS}.

Initial guess

$$n_\uparrow(r), n_\downarrow(r)$$

Calculate effective potential

$$V_{KS,\sigma}(r) = V_H[n] + V_{ext}(r) + V_{XC,\sigma}[n_\uparrow, n_\downarrow]$$

Solve KS equation

$$\left[-\frac{1}{2}\nabla^2 + V_{KS,\sigma}(r)\right]\psi_{i,\sigma}(r) = \varepsilon_{i,\sigma}(r)\psi_{i,\sigma}(r)$$

Calculate electron density

$$n_\sigma(r) = \sum_i \psi_{i,\sigma}^*(r)\psi_{i,\sigma}(r)$$

Self-consistent convergence?

No

Yes

Output quantities

Energy, forces, stress, eigenvalues, · · ·
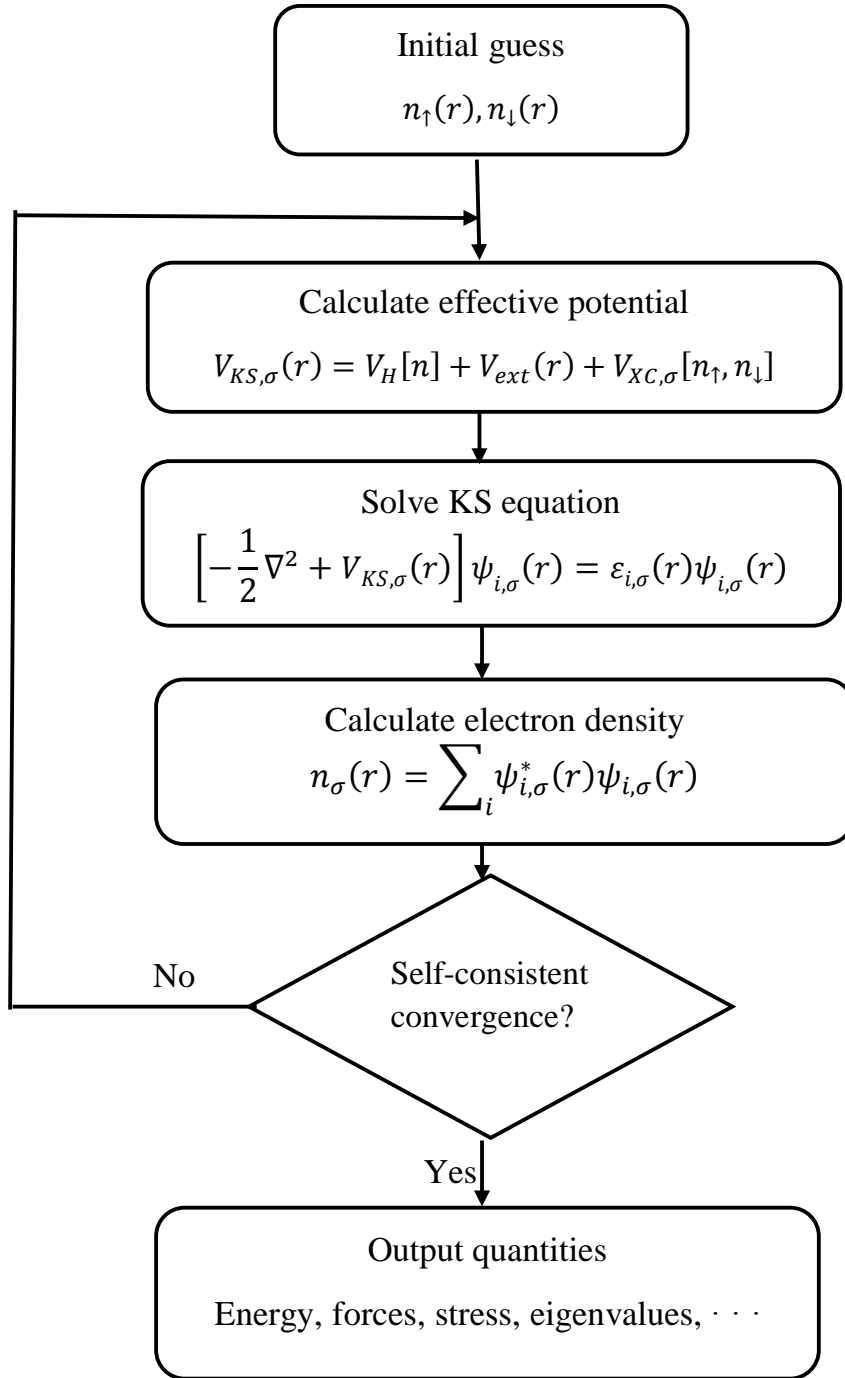
Figure 2.1 Flowchart of self-consistency loop for solving KS equations.

There are several different schemes to the calculation of the independent-particle electronic states in solids where boundary conditions are applied. They are basically classified into three types [22]:

1. Plane waves.

In this method, the wavefunctions (eigenfunctions of the KS equations) are expanded in a complete set of plane waves $e^{ik.r}$ and the external potential of nuclei are replaced by pseudopotentials, which include effects from core electrons. Such pseudopotentials have to satisfy certain conditions. Most widely used pseudopotentials nowadays include norm-conserving pseudopotentials [23] (NCPPs) and ultrasoft pseudopotentials [24] (USPPs). In norm-conserving pseudopotentials, five requirements should be satisfied:

a. the pseudo valence eigenvalues should agree with all-electron valence eigenvalues for the chosen atomic reference configuration;

b. the pseudo valence wavefunctions should match all-electron valence wavefunctions beyond a chosen core radius R_c;

c. the logarithmic derivatives of the pseudo and the all-electron wavefunctions should agree at R_c,

d. the integrated charge inside R_c for each wavefunction agrees (norm-conservation); and

e. the first energy derivative of the logarithmic derivatives of the all-electron and pseudo wavefunctions agree at R_c, and therefore for all $r \leq R_c$.

In ultrasoft pseudopotentials, the norm-conservation condition is not required so that the pseudo wavefunctions are much softer than pseudo wavefunctions in norm conserving pseudopotentials. As a result, it significantly reduces the number of plane waves needed to expand the wavefunctions (smaller energy cutoff for wavefunctions).

Plane waves have played an important role in the early orthogonalized plane wave [25-27] (OPW) calculations and are generalized to modern projector augmented wave [28-30] (PAW) method. Because of the simplicity of plane waves and pseudopotentials, computational load is significantly reduced in these methods and therefore it is most suitable for calculations of large systems. In this method, forces can be easily calculated and it can be easily developed to quantum molecular dynamics simulations as well as response to (small) external perturbations. However, results from plane wave methods using pseudopotentials are usually less accurate than results from all-electron full potential methods. Moreover, great care should be taken when one generates a pseudopotential and it should be tested to match results from all-electron calculations. The most widely used codes using plane waves and pseudopotentials are plane wave self-consistent field (now known as Quantum ESPRESSO) (PWscf), ABINIT and VASP.

2. Localized atomic (-like) orbitals.

The most well known methods in this category are linear combination of atomic orbitals (LCAO), also called tight-binding [31] (TB) and full potential non-orthogonal local orbital [32] (FPLO). The basic idea of these methods is to use atomic orbitals as the basis set to expand the one-electron wavefunction in KS equations.

In FPLO, in addition to the spherical average of the crystal potential, a so-called confining potential $V_{com} = (r/r_0)^m$ is used to compress the long-range tail of the local orbitals (wave functions), where m is the confining potential exponent with a typical value of 4, $r_0 = (x_0 r_{NN}/2)^{3/2}$ is a compression parameter with x_0 being a dimensionless parameter and r_{NN} the nearest neighbor distance. Therefore, the atomic-like potential is written as

$$V_{at}(r) = -(1/4\pi)\int V(r - R - \mathcal{T})\, d^3r + V_{com}(r) \quad (2.58)$$

where the first term is the spherical average of the crystal potential mentioned above. For systems containing atom(s) with partially filled 4f and 5f shells, the confining potential exponent m needs to be increased to 5 or 6. In practice, the dimensionless parameter x_0 is taken as a variational parameter in the self-consistent procedure.

3. Atomic sphere methods.

Methods in the class can be considered as a combination of plane wave method and localized atomic orbitals. It uses localized atomic orbital presentation near the nuclei and plane waves in the interstitial region. The most widely used methods are (full potential) linear muffin-tin orbital[33] (LMTO) as implemented in LMTART[30] by Dr. Savrasov and (full potential) linear augment plane wave[33-35] (LAPW) as implemented in WIEN2K[36].

REFERENCES

[1] F. Nogueira, M. A. L. Marques and C. Fiolhais, A Primer in Density Functional Theory, Springer Verlag, (2003).

[2] P. K. Chattraj (Ed.), J. Chem. Sci. 117, 1 (2005).

[3] L.H. Thomas, Proc. Cambridge Phil. Soc. 23, 542 (1926).

[4] E. Fermi, Z. Phys. 48, 73 (1928).

[5] D.R. Hartree, Proc. Cambridge Phil. Soc. 24, 89 (1928).

[6] P. A. M. Dirac, Proc. Royal Soc. (London) A, 123, 714, (1929).

[7] P.A.M. Dirac, Proc. Cambridge Phil. Soc. 26, 376 (1930).

[8] V. Fock, Z. Phys. 61, 126 (1930).

[9] J.C. Slater, Phys. Rev. 81, 385 (1951); J.C. Slater, Phys. Rev. 82, 538 (1951); J.C. Slater, Phys. Rev. 91, 52 (1953).

[10] P. Hohenberg and W. Kohn, Phys. Rev. 136, B864 (1964) .

[11] W. Kohn and L. J. Sham, Phys. Rev. 140, A1133 (1965).

[12] M. Born and R. Oppenheimer, Annalen der Physik 84, 457 (1927).

[13] M. Born and K. Huang, Dynamic Theory of Crystal Lattices. Oxford: Oxford University Press (1954).

[14] Fermi, Enrico. "Eine statistische Methode zur Bestimmung einiger Eigenschaften des Atoms und ihre Anwendung auf die Theorie des periodischen Systems der Elemente." Zeitschrift für Physik 48.1-2 (1928): 73-79.

 [15] Thomas LH (1927) the calculation of atomic fields. Mathematical Proceedings of the Cambridge Philosophical Society 23(05):542-548.

[16] P. A. M. Dirac, Proc. Cambridge Phil. Roy. Soc. 26, 376 (1930).

[17] E. Teller, Rev. Mod. Phys. 34, 627 (1962).

[18] M. Levy, Proc. Nat. Acad. Sci. USA 76, 6062 (1979).

[19] R. O. Jones and O. Gunnarsson, Rev. Mod. Phys. 61, 689 (1989).

[20] N. D. Mermin, Phys. Rev. 137, A1441 (1965).

[21] E. Runge and E. K. U. Gross, Phys. Rev. Lett. 52, 997 (1984).

[22] R. M. Matrin, Electronic Structure - Basic Theory and Practical Methods, Cambridge University Press (2004).

[23] D. R. Hamann, M. Shl¨uter, and C. Chiang, Phys. Rev. Lett. 43, 1494 (1979).

[24] D. Vanderbilt, Phys. Rev. B 41, 7892 (1990).

[25] W. C. Herring, Phys. Rev. 57, 1169 (1940).

[26] W. C. Herring and A. G. Hill, Phys. Rev. 58, 132 (1940).

[27] F. Herman, Rev. Mod. Phys. 30, 102 (1958).

[28] P. E. Bl¨ochl, Phys. Rev. B 50, 17953 (1994).

[29] G. Kresse and D. Joubert, Phys. Rev. B 59, 1758 (1999).

[30] N. A. W. Holzwarth, G. E. Matthews, A. R. Tackett, and R. B. Dunning, Phys. Rev. B 55, 2055 (1997).

[31] J. C. Slater and G. F. Koster, Phys. Rev. 94, 1498 (1954).

[32] K. Koepernik and H. Eschrig Phys. Rev. B 59, 1743 (1999).

[33] O. K. Anderson, Phys. Rev B 12, 3060 (1975).

[34] S. Y. Savrasov, Phys. Rev. B 54, 16470 (1996);S. Y. Savrasov, D. Y. Savrasov, ibid 54 16487 (1996).

[35] D.J. Singh, Plane Waves, Pseudopotentials and the LAPW Method, Kluwer Academic Publishers, Boston, Dordrecht, London (1994).

[36] P. Blaha, K. Schwarz, G. K. H. Madsen, D. Kvasnicka and J. Luitz, WIEN2K, (K. Schwarz, Techn. Univ. Wien, Austria, 2001).

CHAPTER III

3.1 INTRODUCTION

In this chapter, we are going to present the methodology used in the calculation of our work. We explain how the exchange-potential correlation can be treated through various approximations (LDA, GGA and GGA+U). We attempt to introduce the fundamental concepts of the linearized / augmented plane wave plus local orbitals (L/APW+lo). We show also the different versions of (L/APW+lo) and their main developing steps in terms of linearization, full potential, local orbitals and mixed basis sets. Then, we will submit the modified becke-johnson potential (mBJ) and the wien2k code.

3.2 EXCHANGE CORRELATION FUNCTION

The KS ansatz successfully maps the original interacting many-body system onto a set of independent single-particle equations and makes the problem much easier. In the meantime, without knowing the exact form of the XC energy functional $E_{XC}[n(r)]$, the KS equations are unsolvable. Although the exact XC energy functional $E_{XC}[n(r)]$ should be very complicated, simple but successful approximations to it have been made, which not only predict various properties of many systems reasonably well but also greatly reduce computational costs, leading to the wide use of DFT for electronic structure calculations.

3.2.1 THE LOCAL DENSITY APPROXIMATION (LDA)

Kohn and Sham introduced the Local Density Approximation (LDA) in 1965 [1]. It is the most widely used one. In LDA, the XC energy per electron at a point r is considered the same as that for a homogeneous electron gas (HEG) that has the same electron density at the point r. The total exchange-correlation functional $E_{XC}[n(r)]$ can be written as,

$$E_{XC}^{LDA}[n(r)] = \int n(r) \in_{XC}^{hom} \left(n(r)\right) dr$$

$$= \int n(r) \left[\in_X^{hom} \left(n(r)\right) + \in_C^{hom} \left(n(r)\right)\right] dr \qquad (3.1)$$

$$= E_X^{LDA}[n(r)] + E_C^{LDA}[n(r)]$$

For spin unpolarized systems and

$$E_{XC}^{LDA}[n_\uparrow(r), n_\downarrow(r)] = \int n(r) \in_{XC}^{hom} \left(n_\uparrow(r), n_\downarrow(r)\right) dr \qquad (3.2)$$

for spin polarized systems [2], where the XC energy density $\in_{XC}^{hom} \left(n(r)\right)$ is a function of the density alone, and is decomposed into exchange energy density $\in_X^{hom} \left(n(r)\right)$ and correlation energy density $\in_C^{hom} \left(n(r)\right)$ so that the XC energy functional is

decomposed into exchange energy functional $E_X^{LDA}[n(r)]$ and correlation energy

functional $E_C^{LDA}[n(r)]$ linearly. Note that $E_{XC}^{LDA}[n_\uparrow(r), n_\downarrow(r)]$ is not written in the way

$$E_{XC}^{LDA}[n_\uparrow(r), n_\downarrow(r)] = \int \left[n_\uparrow(r) \in_{XC,\uparrow}^{hom} (n_\uparrow(r)) + n_\downarrow(r) \in_{XC,\downarrow}^{hom} (n_\downarrow(r)) \right] dr \qquad (3.3)$$

as one may think. The exchange energy functional $E_X^{LDA}[n(r)]$ employs the expression

for a HEG by using it pointwise, which is known analytically as [3]

$$E_X^{LDA}[n(r)] = \int n(r) \in_X^{hom} (n(r)) dr$$

$$= -\frac{3}{4} \left(\frac{3}{\pi} \right)^{1/3} \int n(r)^{4/3} \, dr \qquad (3.4)$$

where

$$\in_X^{hom} (n(r)) == -\frac{3}{4} \left(\frac{3}{\pi} \right)^{1/3} n(r)^{1/3} \qquad (3.5)$$

is the exchange energy density of the unpolarized HEG introduced first by Dirac [3].

Analytic expressions for the correlation energy of the HEG are unknown except in the

high and low density limits corresponding to infinitely weak and infinitely strong

correlations. The expression of the correlation energy density of the HEG at high

density limit has the form

$$\in_C = A\ln(r_s) + B + r_s(C\ln(r_s) + D) \qquad (3.6)$$

and the low density limit takes the form

$$\in_C = \frac{1}{2} \left(\frac{g_0}{r_s} + \frac{g_1}{r_s} + \cdots \right) \qquad (3.7)$$

where the Wigner-Seitz radius r_s is related to the density as

$$\frac{4}{3} \pi r_s^3 = \frac{1}{n} \qquad (3.8)$$

In order to obtain accurate values of the correlation energy density at intermediate

density, accurate quantum Monte Carlo (QMC) simulations for the energy of the HEG

are needed and have been performed at several intermediate density values [4].

Most local density approximations to the correlation energy density interpolate these accurate values from QMC simulations while reproducing the exactly known limiting behavior. Depending on the analytic forms used for ϵ_C, different local density approximations were proposed including Vosko-Wilk-Nusair [5] (VWM), Perdew-Zunger [6] (PZ81), Cole-Perdew [7] (CP) and Perdew-Wang [8] (PW92).

For spin polarized systems, the exchange energy functional is known exactly from the result of spin-unpolarized functional:

$$E_X[n_\uparrow(r), n_\downarrow(r)] = \frac{1}{2}(E_X[2n_\uparrow(r)] + E_X[2n_\downarrow(r)]) \qquad (3.9)$$

The spin-dependence of the correlation energy density is approached by the relative spin-polarization:

$$\zeta(r) = \frac{n_\uparrow(r) - n_\downarrow(r)}{n_\uparrow(r) + n_\downarrow(r)} \qquad (3.10)$$

The spin correlation energy density $\epsilon_C(n(r), \zeta(r))$ is so constructed to interpolate extreme values $\zeta = 0, \pm 1$ corresponding to spin-unpolarized and ferromagnetic situations.

The XC potential $V_{XC}(r)$ in LDA is

$$V_{XC}^{LDA} = \frac{\delta E_{XC}^{LDA}}{\delta n(r)}$$

$$= \epsilon_{XC}(n(r)) + n(r)\frac{\partial \epsilon_{XC}(n(r))}{\partial n(r)} \qquad (3.11)$$

Within LDA, the total energy of a system is:

$$E_{tot}[n(r)] = T_S[n(r)] + E_H[n(r)] + E_{XC}[n(r)] + \int n(r)V_{ext}(r)dr$$

$$E_{tot}[n(r)] = \sum_i^{occ} \left\langle \psi_i(r) \left| -\frac{1}{2}\nabla^2 \right| \psi_i(r) \right\rangle + E_H[n(r)] + E_{XC}[n(r)] + \int n(r)V_{ext}(r)dr$$

$$E_{tot}[n(r)] = \sum_{i}^{OCC} \left\langle \psi_i(r) \left| -\frac{1}{2}\nabla^2 + V_H[n(r)] + V_{XC}[n(r)] + V_{ext}(r) \right| \psi_i(r) \right\rangle$$

$$- \sum_{i}^{OCC} \langle \psi_i(r)| + V_H[n(r)]|\psi_i(r)\rangle$$

$$- \sum_{i}^{OCC} \langle \psi_i(r)| + V_{XC}[n(r)]|\psi_i(r)\rangle$$

$$- \sum_{i}^{OCC} \langle \psi_i(r)| + V_{ext}[n(r)]|\psi_i(r)\rangle + E_H[n(r)] + E_{XC}[n(r)]$$

$$+ \int n(r)V_{ext}(r)dr$$

$$= \sum_{i}^{OCC} \varepsilon_i - \frac{1}{2}\int \frac{n(r)\,n(r')}{|r-r'|} dr dr' + \int n(r)\big(\in_{XC}(r) - V_{XC}(r)\big)dr$$

$$= \sum_{i}^{OCC} \varepsilon_i - \frac{1}{2}\int \frac{n(r)\,n(r')}{|r-r'|} dr dr' + \int n(r)^2 \frac{\partial \in_{XC}(n(r))}{\partial n(r)} dr \qquad (3.12)$$

As mentioned before, $E_{tot} \neq \sum_{i}^{OCC} \varepsilon_i$.

The LDA is very simple; corrections to the exchange-correlation energy due to the inhomogeneities in the electronic density are ignored. However, it is surprisingly successful and even works reasonably well in systems where the electron density is rapidly varying. One reason is that LDA gives the correct sum rule to the exchange-correlation hole. That is, there is a total electronic charge of one electron excluded from the neighborhood of the electron at r. In the meantime, it tends to underestimate atomic ground state energies and ionization energies, while overestimating binding energies. It makes large errors in predicting the energy gaps of some semiconductors. Its success and limitations lead to approximations of the XC energy functional beyond the LDA, through the addition of gradient corrections to incorporate longer range gradient effects

(GGA), as well as LDA+U method to account for the strong correlations of the d electrons in transition elements and f electrons in lanthanides and actinides.

3.2.2 GENERALIZED-GRADIENT APPROXIMATION (GGA)

As mentioned above, the LDA neglects the in homogeneities of the real charge density, which could be very different from the HEG. The XC energy of inhomogeneous charge density can be significantly different from the HEG result. This leads to the development of various generalized-gradient approximations (GGAs) which include density gradient corrections and higher spatial derivatives of the electron density and give better results than LDA in many cases. Three most widely used GGAs are the forms proposed by Becke [9] (B88), Perdewet al [10], and Perdew, Burke and Enzerhof [11] (PBE).

The definition of the XC energy functional of GGA is the generalized form in Eq. (3.2) of LSDA to include corrections from density gradient $\nabla n(r)$ as

$$E_{XC}^{LDA}[n_\uparrow(r), n_\downarrow(r)] = \int n(r) \in_{XC}^{hom} \big(n(r)\big)(n_\uparrow(r), n_\downarrow(r), |\nabla n_\uparrow(r)|, |\nabla n_\downarrow(r)|, \dots) \, dr$$

$$= \int n(r) \in_X^{hom} \big(n(r)\big) F_{XC}(n_\uparrow(r), n_\downarrow(r), |\nabla n_\uparrow(r)|, |\nabla n_\downarrow(r)|, \dots) \, dr$$
$$(3.13)$$

where F_{XC} is dimensionless and $\in_{XC}^{hom} \big(n(r)\big)$ is the exchange energy density of the unpolarized HEG as given in Eq. (3.5). FXC can be decomposed linearly into exchange contribution F_X and correlation contribution FC as $F_{XC} = F_X + F_C$. For a detailed treatment of F_X and F_C in different GGAs [12].

GGA generally works better than LDA, in predicting bond length and binding energy of molecules, crystal lattice constants, and so on, especially in systems where the charge density is rapidly varying. However, GGA sometimes overcorrects LDA results in ionic

crystals where the lattice constants from LDA calculations fit well with experimental data but GGA will overestimate it. Nevertheless, both LDA and GGA perform badly in materials where the electrons tend to be localized and strongly correlated such as transition metal oxides and rare-earth elements and compounds. This drawback leads to approximations beyond LDA and GGA.

3.2.3 LDA+U METHOD

Strongly correlated systems usually contain transition metal or rare earth metal ions with partially filled d or f shells. Because of the orbital-independent potentials in L(S) DA and GGA, they cannot properly describe such systems. For example, L(S) DA predicts transition metal oxides to be metallic with itinerant d electrons because of the partially filled d shells. Instead, these transition metal oxides are Mott insulators and the d electrons are well localized. In order to properly describe these strongly correlated systems, orbital-dependent potentials should be used for d and f electrons.

There are several approaches available nowadays to incorporate the strong electron-electron correlations between d electrons and f electrons. Of these methods including the self-interaction correction (SIC) method [13], Hartree-Fock (HF) method [14], and GW approximation [15], LDA+U method [16] is the most widely used one.

In the LDA+U method, the electrons are divided into two classes: delocalized s, p electrons which are well described by LDA (GGA) and localized d or f electrons for which an orbital-dependent term $\frac{1}{2} U \sum_{i \neq j} n_i n_j$ should be used to describe Coulomb $d - d$ or $f - f$ interaction, where n_i are $d-$ or $f-$orbital occupancies. The total energy in L(S) DA+U method is given as [16]:

$$E_{tot}^{LDA+U}[\rho_\sigma(r), \{n_\sigma\}] = E^{LSDA}[\rho_\sigma(r)] + E^U[\{n_\sigma\}] - E_{dc}[\{n_\sigma\}] \qquad (3.14)$$

where σ denotes the spin index, $\rho_\sigma(r)$ is the electron density for spin-σ electrons and $\{n_\sigma\}$ is the density matrix of d or f electrons for spin-σ, the first term is the standard LSDA energy functional, the second term is the electron-electron Coulomb interaction energy given by[16]

$$E^U[\{n_\sigma\}] = \frac{1}{2} \sum_{\{m\},\sigma} \{\langle m, m''|V_{ee}|m', m'''\rangle n_{mm',\sigma} n_{m''m''',-\sigma}$$

$$- (\langle m, m''|V_{ee}|m', m'''\rangle$$

$$- \langle m, m''|V_{ee}|m''', m'\rangle) n_{mm',\sigma} n_{m''m''',\sigma}\} \tag{3.15}$$

where m denotes the magnetic quantum number, and V_{ee} are the screened Coulomb interactions among the d or f electrons. The last term in Eq. (3.14) is the double counting term, which removes an averaged LDA energy contribution of these d or f electrons from the LDA energy. It isgiven by [16]

$$E_{dc}[\{n_\sigma\}] = \frac{1}{2} UN(N-1) - \frac{1}{2} J[N_\uparrow(N_\uparrow - 1) + N_\downarrow(N_\downarrow - 1)] \tag{3.16}$$

where $N_\sigma = Tr(n_{mm',\sigma})$ and $N = N_\uparrow + N_\downarrow$. U and J are screened Coulomb and exchange parameters.

As a simple approximation, if the exchange and non-sphericity is neglected, Eq. (3.14) is simplified to [16]

$$E_{tot}^{LDA+U} = E_{LDA} + \frac{1}{2} U \sum_{i \neq j} n_i n_j - \frac{1}{2} UN(N-1) \tag{3.17}$$

The orbital energies ε_i are derivatives of Eq. (3.17) with respect to orbital occupations n_i:

$$\varepsilon_i = \frac{\partial E}{\partial n_i} = \varepsilon_{LDA} + U\left(\frac{1}{2} - n_i\right) \tag{3.18}$$

In this simple consideration, the LDA orbital energies are shifted by $-U/2$ for occupied orbitals ($n_i = 1$) and by $+U/2$ for unoccupied orbitals ($n_i = 0$), resulting in lower and

upper Hubbard bands separated by U, which opens a gap at the Fermi energy in transition metal oxides.

In the general case, the effective single-particle potential is

$$V_{mm',\sigma} = \frac{\partial (E^U[\{n_\sigma\}] - E_{dc}[\{n_\sigma\}])}{\partial n_{mm',\sigma}}$$

$$= \sum_{\{m\}} \{\langle m, m''|V_{ee}|m', m'''\rangle n_{m''m''',-\sigma}$$

$$- (\langle m, m''|V_{ee}|m', m'''\rangle - \langle m, m''|V_{ee}|m''', m'\rangle) n_{m''m''',\sigma}\} - U\left(N\right.$$

$$\left. - \frac{1}{2}\right) + J\left(N_\sigma - \frac{1}{2}\right) \tag{3.19}$$

which is used in the effective single-particle Hamiltonian

$$\widehat{H} = \widehat{H}_{LSDA} + \sum_{mm'} |inlm\sigma\rangle V_{mm',\sigma} \langle inlm'\sigma| \tag{3.20}$$

where i denotes the site, n the main quantum number, and l the orbital quantum number. The matrix elements of V_{ee} can be expressed in terms of complex spherical harmonics and effective Slater integrals F_k as [17]

$$\langle m, m''|V_{ee}|m', m'''\rangle = \sum_k a_k(m, m', m'', m''')F_k \tag{3.21}$$

where $0 \leq k \leq 2l$ and

$$a_k(m, m', m'', m''') = \frac{4\pi}{2k+1} \sum_{q=-k}^{k} \langle lm|Y_{kq}|lm'\rangle \langle lm''|Y_{kq}^*|lm'''\rangle \tag{3.22}$$

$$F_k \approx \iint_0^\infty dr_1 dr_2 (r_1 R_i(r_1))^2 (r_2 R_i(r_2))^2 \frac{r_<^k}{r_>^{k+1}} \; For \; k > 0 \tag{3.23}$$

Here, $r_<$ is the smaller of r_1 and r_2 and $r_>$ the larger. The relations between the Slater integrals and the screened Coulomb and exchange parameters U and J are:

$U = F_0; \quad J = (F_2 + F_4)/14$, For $3d$ or $4d$ systems,

$U = F_0; \quad J = (286F_2 + 195F_4)/6435$, For $4f$ or $5f$ systems, $\tag{3.24}$

The ratio F_4/F_2 and F_6/F_2 are taken from atomic situations. $F_4/F_2 \sim 0.625$ for *3d* transition elements [18] and $F_4/F_2 \sim 0.625$, $F_6/F_2 \sim 1/2$ for *4f* lanthanides.

The screened Coulomb parameter U can be calculated from the constraint LDA method [19], so that the LDA+U method remains a first principle method (no adjustable parameters). For the double-counting term, there are two different treatments: the so-called around mean field (AMF) and fully localized limit (FLL) (called atomic limit) approaches. The former is more suitable for small U systems [20] and the latter is more suitable for large U systems [21]. The energies for the double counting are given by [41]

$$E_{AMF}^{dc} = \frac{1}{2} \sum_{m \neq m', \sigma\sigma'} \left[U_{mm'} - \delta_{\sigma,\sigma'} J_{mm'} \right] \bar{n}\bar{n}$$

$$= \frac{1}{2} UN^2 - \frac{U + 2lJ}{2l+1} \frac{1}{2} \sum_\sigma N_\sigma^2 \qquad (3.25)$$

$$E_{FLL}^{dc} = \frac{1}{2} \sum_{m \neq m', \sigma\sigma'} \left[U_{mm'} - \delta_{\sigma,\sigma'} J_{mm'} \right] \bar{n}_\sigma \bar{n}_{\sigma'}$$

$$= \frac{1}{2} UN(N-1) - \frac{1}{2} J \sum_\sigma N_\sigma(N_\sigma - 1) \qquad (3.26)$$

where $\bar{n} = N/2(2l+1)$ is the average occupation of the correlated orbitals and $\bar{n}_\sigma = N_\sigma(2l+1)$ is the average occupation of a single spin of the correlated orbitals. Note that, Eq. (3.26) is the same as Eq. (3.16).

3.2.4 THE MODIFIED BECKE-JOHNSON POTENTIAL

The method described above belongs to the so-called generalized KS framework [22] mixing DFT and Hartree-Fock (HF) theories. Nevertheless, if one wants to stay inside the true Kohn Sham framework and use a method that can lead to KS gaps close to the experimental band gaps, the potential proposed by Becke and Johnson (BJ) [23], which was designed to reproduce the exact exchange potential in atoms, can be a good starting

point. The multiplicative BJ potential, which does not contain any empirical parameters, reads:

$$v_x^{BJ}(\vec{r}) = v_x^{BR}(\vec{r}) + \frac{1}{\Pi}\sqrt{\frac{5}{6}}\sqrt{\frac{t(\vec{r})}{n(\vec{r})}} \tag{3.27}$$

where

$$t(\vec{r}) = \frac{1}{2}\sum_{i=0}^{N} \nabla\psi_i^*(\vec{r}) \cdot \nabla\psi_i(\vec{r}) \tag{3.28}$$

is the KS kinetic-energy density and

$$v_x^{BJ}(\vec{r}) = -\frac{1}{b(\vec{r})}\left(1 - e^{-x(\vec{r})} - \frac{1}{2}x(\vec{r})e^{-x(\vec{r})}\right) \tag{3.29}$$

is the Becke Roussel (BR) exchange potential, which was proposed to model the Coulomb potential created by the exchange hole. In equation (3.29), x is determined from a nonlinear equation involving $n, \nabla n(\vec{r}), \nabla^2 n(\vec{r})$ and t, and b is calculated with

$$b = [x^3 e^{-x(\vec{r})}/(8\Pi n)]^{1/3} \tag{3.30}$$

It has been shown that the BJ potential can be further improved for the description of band gaps by using a modified version developed by Tran and Blaha (TB-mBJ) which introduces a parameter to change the relative weights of the two terms in the BJ potential:

$$v_x^{BJ-mBJ}(\vec{r}) = cv_x^{BR}(\vec{r}) + (3c - 2)\frac{1}{\Pi}\sqrt{\frac{5}{6}}\sqrt{\frac{t(\vec{r})}{n(\vec{r})}} \qquad (3.31)$$

with

$$c = \alpha + \beta\left(\frac{1}{V_{cell}}\int_{cell}\frac{\nabla n(\vec{r}')}{n(\vec{r}')}d^3(\vec{r}')\right)^{1/2} \qquad (3.32)$$

where V_{cell} is the unit cell volume and α and β are two free parameters whose values are $\alpha = -0.012$ and $\beta = 1.023$ bohr $^{(1/2)}$ according to a fit to experimental results. The way in which this linear combination is written makes sure that for any value of c the LDA exchange potential is recovered for a constant electron density. For c= 1 the original BJ potential is recovered. This potential has yield satisfying results for many different systems, including transition-metal compounds [24–26].

3.3 FULL POTENTIAL LINEARIZED / AUGMENTED PLANE WAVE PLUS LOCAL ORBITALS - FP-L/APW+LO

3.3.1 AUGMENTED PLANE WAVE (APW) METHOD

APW method is the most popular techniques for the solution of the electronic structure using Kohn-Sham (KS) equations. Slater proposed the technique in 1937 [27, 28].

In this approach, In the APW scheme the unit cell is partitioned into two types of regions: (i) spheres centered around all constituent atomic sites r_α with a radius R_α, and (ii) the remaining interstitial region, abbreviated as I (see Figure 3.1). In this case, the wave functions are expanded into PWs each of which is augmented by atomic solutions in the form of partial waves, i.e. a radial function times spherical harmonics. In particular, radial solutions of Schrödinger's equation are employed inside non-overlapping atom centered spheres and plane waves in the remaining interstitial zone.

The introduction of such a basis set is due to the fact that close to the nuclei the potential and wave functions are very similar to those in an atom, while between the atoms then are smoother. The APWs consist of :

$$
\varphi(r) = \begin{cases} \sum_{lm} a^{\alpha}_{lm} u^{\alpha}_{lm}(r, \varepsilon) & r < R_{\alpha} \\ \Omega^{-1/2} \sum_{G} C_G \, exp\big(i(\vec{k} + \vec{G}).\vec{r}\big) & r \in I \end{cases}
\tag{3.33}
$$

From (3.33) φ is the wave function, Ω is the unit cell volume, $\vec{r}$ is the position inside sphere α with the polar coordinates $\vec{r}$, $\vec{k}$ is a wave vector in the irreducible Brillouin zone (IBZ) and u_{lm} is the numerical solution to the radial Schrödinger equation at the energy ε .The KS orbitals $\psi(r)$ are expressed as a linear combination of APWs $\varphi(r)$. Inside the MT sphere a KS orbital can only be accurately, described if ε in the APW basis functions is equal to the eigenenergy,ε_i. Therefore, a different energy-dependent set of APW basis functions must be found for each eigenenergy. C_G and a_{lm} are expansion coefficients; E_l is a parameter (set equal to the band energy) and V the spherical component of the potential in the sphere.

$$
\left[-\frac{d^2}{dr^2} + \frac{l(l+1)}{r^2} + V(r) - E_l \right] r \, u_{lm}(r) = 0
\tag{3.34}
$$

Slater has motivated the use of these functions by noting that plane waves are the solutions of the Schrödinger's equation in a constant potential and radial functions are solutions in a spherical potential. This approximation to the potential is called "muffintin" (MT). Since the continuity on the spheres boundaries needs to be guaranteed on the dual representation defined in Eq. (3.33), constraint must be imposed. In the APW method, this is done by defining the u_{lm} in terms of C_G in the spherical harmonic expansion of the plane waves.
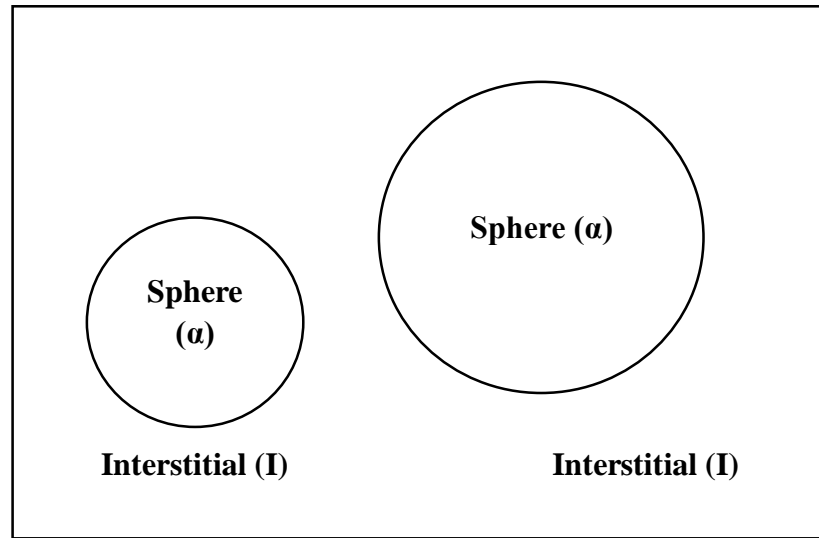
Figure 3.1 Adaptation of the basis set by dividing the unit cell into atomic spheres and interstitial regions.

In the APW technique, continues basis sets (functions) are used, which cover all the space within the sphere. However, APW is a commonly used technique for the calculations of the structural, electronic, optical and magnetic properties of solids but even then, it has some disadvantages. One example of the limitation of this technique is; it cannot be extended beyond the average spherical muffin-tin approximation. The basis functions, for this approach, have a kink at the border of the muffin-tin and hence at the boundary their derivatives are discontinues. Another drawback of this approach is the radial function $u_{lm}(r, E_l)$ is dependent upon energy, which leads a nonlinear eigenvalue problem. This can cause numerical complications if u_l become very small at the empty sphere boundary.

3.3.2 LINEARIZED AUGMENTED PLANE WAVE (LAPW) METHOD

The APW technique is modified by Anderson and is called LAPW method [29]. The LAPW approach solves the problems of APW method i.e., the basis functions and their first derivative were discontinues at the muffin-tin boundary between core and

interstitial region. To solve the problem Ander- son introduced a linearization scheme

and that is why he used the term linearized augmented plane wave method (LAPW).

He launched an additional term in the basis within the MT sphere. In the LAPW

technique inside the MT region, the radial wave function is linearized by a linear

combination of $u_{lm}(r, E_l)$ and $\dot{u}_{lm}(r, E_l)$[30-32]:

$$\varphi(r) = \begin{cases} \sum_{lm}[a_{lm}^{\alpha}u_{lm}^{\alpha}(r, \varepsilon) + b_{lm}^{\alpha}\dot{u}(r)]Y_{lm}(\vec{r}), & r < R_{\alpha} \\ \Omega^{-1/2}\sum_{G}C_{G}exp\left(i(\vec{k} + \vec{G}).\vec{r}\right), & r \in I \end{cases} \tag{3.35}$$

where the b_{lm} are coefficients for the energy derivative analogous to the a_{lm}. The basis

functions inside the spheres are linear combinations of a radial functions $u_l(r)Y_{lm}(r)$

and their energy derivatives $u_l(r)Y_{lm}(r)$ and $\dot{u}_l(r)Y_{lm}(r)$ are the augmenting

functions. The u_l are defined as in the APW method (Eq. 3.34) and the energy

derivative, $\dot{u}_l(r)Y_{lm}(r)$, satisfies the following equation:

$$\left[-\frac{d^2}{dr^2} + \frac{l(l+1)}{r^2} + V(r) - E_l\right]r\dot{u}_{lm}(r) = r\,u_{lm}(r) \tag{3.36}$$

The LAPWs provide a sufficiently flexible basis to properly describe eigen functions

with eigen energies near the linearization energy, which can be kept fixed. This scheme

allows us to obtain all eigen energies with a single diagonalization in contrast to APW.

The LAPWs are plane waves in the interstitial zone of the unit cell, which match the

numerical radial functions inside the spheres with the requirement that the basis

functions and their derivatives are continuous at the boundary. In this method no shape

approximations are made and consequently such a procedure is often called "full-

potential LAPW" (FP-LAPW). The much older muffin-tin approximation corresponds

to retain only the $l = 0$ and $m = 0$ component in Eq. (3.36). A spherical average inside

the spheres and the volume average in the interstitial region is thus taken.

Inside atomic sphere a linear combination of radial functions times spherical harmonics, $Y_{lm}(r)$, is used. The linear combination of $u_l(r)$ and $\dot{u}_l(r)$ constitute the socalled "linearization" of the radial function. $u_l(r)$ and $\dot{u}_l(r)$ are obtained by numerical integration of the radial Schrödinger equation on a radial mesh inside the sphere. The LAPWs have more variational freedom inside the spheres than APWs. This greater exibility is due to the presence of two radial functions instead of one; non-spherical potentials inside spheres can be now treated with no difficulty. There is however, a price to be paid for the additional exibility of the LAPWs: the basis functions must have continuous derivatives and consequently higher plane wave cut-offs are required to achieve a given level of convergence. The solution of the KS equations are expanded in this combined basis according to the linear variation method:

$$\psi_k = \sum_n c_n \varphi_{kn} \tag{3.37}$$

and the coefficients c_n are determined by the Rayleigh-Ritz variational principle. The convergence of this basis set is controlled by a cut-off parameter $R_{mt} \times K_{max}$, where R_{mt} is the smallest atomic sphere radius in the unit cell and K_{max} is the magnitude of the largest K_n vector in Eq. (3.37).

3.3.3 AUGMENTED PLANE WAVE PLUS LOCAL ORBITAL (APW+LO) METHOD

The APW basis functions can also be modified just like the LAPW ones by introducing local orbitals. Sjosted et al. [30] improved APW by introducing local orbital (lo), i.e., APW+lo basis. As in the APW approach, the radial wavefunction is evaluated at fixed energy but this new technique includes another type of orbital's for flexibility. These orbitals are denoted by lo instead of LO in the LAPW [31]:

$$\varphi(r) = \begin{cases} \left[a_{lm}^{\alpha,l0}u_{lm}^{\alpha}(r,\varepsilon) + b_{lm}^{\alpha,l0}\dot{u}(r)\right]Y_{lm}(\vec{r}), & r < R_{\alpha} \\ 0, & r \in I \end{cases} \qquad (3.38)$$

The normalization condition that the function $\varphi(r)$ at the MT radii is zero determines the two coefficients in the equation. In this approach $\dot{u}_l$ does not depend upon the plane waves and is included only for the selected set of the l quantum numbers. The energy derivative term in the APW+lo, method is only included in just a few lo's and not in every plane wave like that in the LAPW one. Therefore we are not sure that the energy linearization of APW+lo basis is accurate like LAPW, though it converges faster than LAPW and gives the same accuracy as LAPW technique [32].

3.3.4 FULL-POTENTIAL LINEARIZED AUGMENTED PLANE WAVE METHOD (FP-LAPW)

The muffin-tin approximation was frequently used in 1970 in the APW and LAPW techniques [33]. The potential is assumed to be constant in the interstitial region while spherical symmetric in the muffin-tin region. These approximations are effective in highly coordinated systems like face centered metallic structures. These approaches are not very efficient in the calculations of the structural and electronic properties of covalent bonded and open structure solids. For these type compounds, the calculated results show inconsistency with the experimental results. In order to obtain better predications for these properties of compounds, no shape approximation is used. These compounds are treated with FP-LAPW method. The FP-LAPW method combines the LAPW basis with the treatment of the full potential without including any shape approximation in both interstitial and muffin-tin regions [33]. In FP-LAPW approach, the potential is expanded in two regions in such away that (a) inside the atomic sphere it is in the lattice harmonics and (b) inside interstitial region as Fourier series [33]:

$$V(\vec{r}) = \sum_{LM} V_{LM}(r) Y_{LM}(\vec{r}) \qquad (3.39)$$

$$V(\vec{r}) = \sum_{LM} V_K exp(i\vec{k}.\vec{r}) \qquad (3.40)$$

Where (3.39) for inside the atomic sphere, while (3.40) for outside the atomic sphere. This form is known as full-potential scheme. The selection of the radii of the sphere in muffin-tin approximation is very critical but not in the FP-LAPW.

3.4 THE WIEN2K CODE

The WIEN2k package is a computer program written in Fortran that performs quantum mechanical calculations on periodic solids. It was originally developed by Peter Blaha and Karl Heinz Schwarz from the Institute of Materials Chemistry of the Vienna University of Technology. The first public release of the code was done in 1990. Then, the next releases were WIEN93, WIEN97, and WIEN2k. It basically uses the full-potential (linearized) augmented plane-wave and local-orbitals [FP-(L)APW+lo] basis set to solve the Kohn–Sham equations of density functional theory.

This package allows to study most of the electronic structure properties of a crystalline solid: electron density, density of states (DOS), various types of spectra, magnetism (ferromagnetic, antiferromagnetic and non-magnetic configurations), non-collinear magnetism, band structure, Fermi surface, deferent exchange-correlation potentials including the local density approximation (LDA), various generalized gradient approximation (GGA) (Perdew-Wang [8] or Perdew-Burke-Ernzerh of [11], Wu-Cohen [34]), meta-GGA [35, 36] and the LDA+U method [16] in various flavors for the double counting terms, as well as the socalled Tran-Blaha modified Becke-Johnson potential [24], and hybrid functional [37].

REFERENCES

[1] W. Kohn and L. J. Sham, Phys. Rev. 140, A1133 (1965).

[2] U. von Barth and L. Hedin, J. Phys. C: Solid State Phys. 5, 1629 (1972).

[3] P. A. M. Dirac, Proc. Cambridge Phil. Roy. Soc. 26, 376 (1930).

[4] D. M. Ceperley and B. J. Alder, Phys. Rev. Lett. 45, 566 (1980).

[5] S. H. Vosko, L. Wilk and M. Nusair, Can. J. Phys. 58, 1200 (1980).

[6] J. P. Perdew and A. Zunger, Phys. Rev. B 23, 5048 (1981).

[7] L. A. Cole and J. P. Perdew, Phys. Rev. A 25, 1265 (1982).

[8] J. P. Perdew and Y. Wang, Phys. Rev. B 45, 13244 (1992).

[9] A. D. Becke, Phys. Rev. A 38, 3098 (1988).

[10] J. P. Perdew, J. A. Chevary, S. H. Vosko, K. A. Jackson, M. R. Pederson, and C. Fiolhais, Phys. Rev. B 46, 6671 (1992).

[11] J. P. Perdew, K. Burke, and M. Ernzerhof, Phys. Rev. Lett. 77, 3865 (1996).

[12] R. M. Matrin, Electronic Structure - Basic Theory and Practical Methods, Cambridge University Press (2004).

[13] A. Svane and O. Gunnarsson, Phys. Rev. Lett. 65, 1148 (1990).

[14] S. Massida, M. Posternak and A. Baldereschi, Phys. Rev. B 48, 5058 (1993).

[15] L. Hedin, Phys. Rev. 139, A796 (1965).

[16] V. I. Anisimov, F. Aryasetiawan and A. I. Lichtenstein, J. Phys. Condens. Matter 9, 767 (1997).

[17] J. C. Slater, Quamtem Theory of Atomic Structure, (McGraw-Hill, New York, 1960), Vol. 1.

[18] F. M. F. de Groot, J. C. Thole, and G. A. Sawatzky, Phys. Rev. B 42, 5459 (1990).

[19] V. I. Anisimov, J. Zaanen and O. K. Andersen, Phys. Rev. B 44, 943 (1991).

[20] Czyzyk and G. A. Sawatzky, Phys. Rev. B 49, 14211 (1994).

[21] V. I. Anisimov, I. V. Solovyev, M. A. Korotin, M. T. Czyzyk. and G. A. Sawatzky, Phys. Rev. B 48, 16929 (1993).

[22] Seidl, A., Görling, A., Vogl, P., Majewski, J. A., & Levy, M. (1996). Generalized Kohn-Sham schemes and the band-gap problem. Physical Review B, 53(7), 3764.

[23] A. D. Becke and E. R. Johnson, J. Chem. Phys. 124, 221101 (2006).

[24] F. Tran and P. Blaha, Phys. Rev. Lett. 102, 226401 (2009).

[25] D. Koller, F. Tran, and P. Blaha, Phys. Rev. B 83, 195134 (2011).

[26] D. J. Singh, Phys. Rev. B 82, 205102 (2010).

[27] J.C. Slater, Phys. Rev. **51**, 151 (1937)

[28] J. C. Slater, Advances in Quantum Chemistry, **1**, 35 (1964).

[29] O. K. Andersen, \Linear methods in band theory," Phys. Rev. B 12, 3060 (1975).

[30] E. Sjstedt, L. Nordstrm, D. J. Singh, "An alternative way of linearizing the augmented plane-wave method," Solid State Comm. 114, 15 (2000).

[31] G. K. H. Madsen, P. Blaha, K. Schwarz, E. Sjstedt, L. Nordstrm, "Effcient linearization of the augmented plane-wave method," Phys. Rev. B 64, 195134 (2001).

[32] D. D. Koelling and G. O. Arbman, "Use of energy derivative of the radial solution in an augmented plane wave method: application to copper," J. Phys. F: Metal Phys. 5, 2041 (1975).

[33] K. Schwarz, "DFT calculations of solids with LAPW and WIEN2k," Journal of Solid State Chemistry 176, 319-328 (2003).

[34] Z. Wu and R. E. Cohen, Phys. Rev. B 73, 235116 (2006).

[35] J. P. Perdew, S. Kurth, J. Zupan, and P. Blaha, Phys. Rev. Lett. 82, 2544 (1999).

[36] J. Tao, J. P. Perdew, V. Starovenov, and G. Scuseria, Phys. Rev. Lett. 91, 146401 (2003).

[37] F. Tran and P. Blaha, Phys. Rev. B 83, 235118 (2011).

CHAPTER IV

4.1 INTRODUCTION

we chose ZnO to be our field study, Because it is highly doped with atomic impurities, and there now exists considerable academic research efforts to control ZnO doping to both improve existing physical properties and add new material dimensionalities, including varying the optoelectronic, magnetic , magneto-optic, electromagnetic, thermoelectric and piezoelectric properties ..

In this chapter, we used GGA approximation to explore the structural, electronic and optic properties of pure zinc blende (ZB) ZnO phase and several compositions of Zn$_{1-x}$Er$_x$O alloys for (x = 0, 0.25, 0.50, 0.75, 1).

4.2 COMPUTATIONAL DETAILS

All calculations have been carried out using density functional theory with help of the full-potential linearized augmented plane-wave (FP-LAPW) method as implemented in WIEN2k package [1,2], which self-consistently finds the eingenvalues and eingen function of the Kohn-Sham [3] equations for the system. We have used the Generalized Gradient Approximation (GGA) as parameterized by Perdew, Burke and Ernzenhorf [4] and modified Becke-Johnson (mBJ) approximation [5] for electronic and optical properties. The valence electron configurations used in the calculations are Zn ($3d^{10}$ $4s^2$), O ($2s^2$ $2p^4$), Er ($4f^{12}$ $5s^2$ $5p^6$ $6s^2$) respectively. We adopted a 8 atoms simple cubic supercell in which the Zn substitution by Er correspond to 25%, 50%, 75% and 100% of concentration (Fig. 1).To investigate the effect of Er doping and the effect of Er doping on the structural geometry of ZnO. The simulated super cells for above mentioned concentrations are optimized over a range $\pm$ 10 around the equilibrium volume and then values of the lattice constants are evaluated by fitting the obtained data (variation of the unit cell volume versus energy) into Murnaghan equation of state [6]. The wave function, charge density and potential were expanded by spherical harmonic functions inside non-overlapping spheres surrounding the atomic sites (muffin-tin spheres) and by a plane-wave basis set in the remaining space of the unit cell (interstitial region). The maximum l quantum number for the wave function expansion inside atomic spheres was confined to l_{max}=10. The charge density was Fourier expanded up to G_{max}= 9 (Ry)$^{1/2}$. The convergence parameter $R_{MT}K_{max}$ (Where K_{max} is the maximum modulus for the reciprocal lattice vector, and R_{MT} is the average radius of the muffin tin spheres) which controls the size of the basis set in these calculations, was set to 7. The reciprocal space is sampled by a 5×5×5 Monkhorst–Pack mesh [7] with sufficient

125 k-vectors in the irreducible Brillouin zone. The iteration process is repeated until

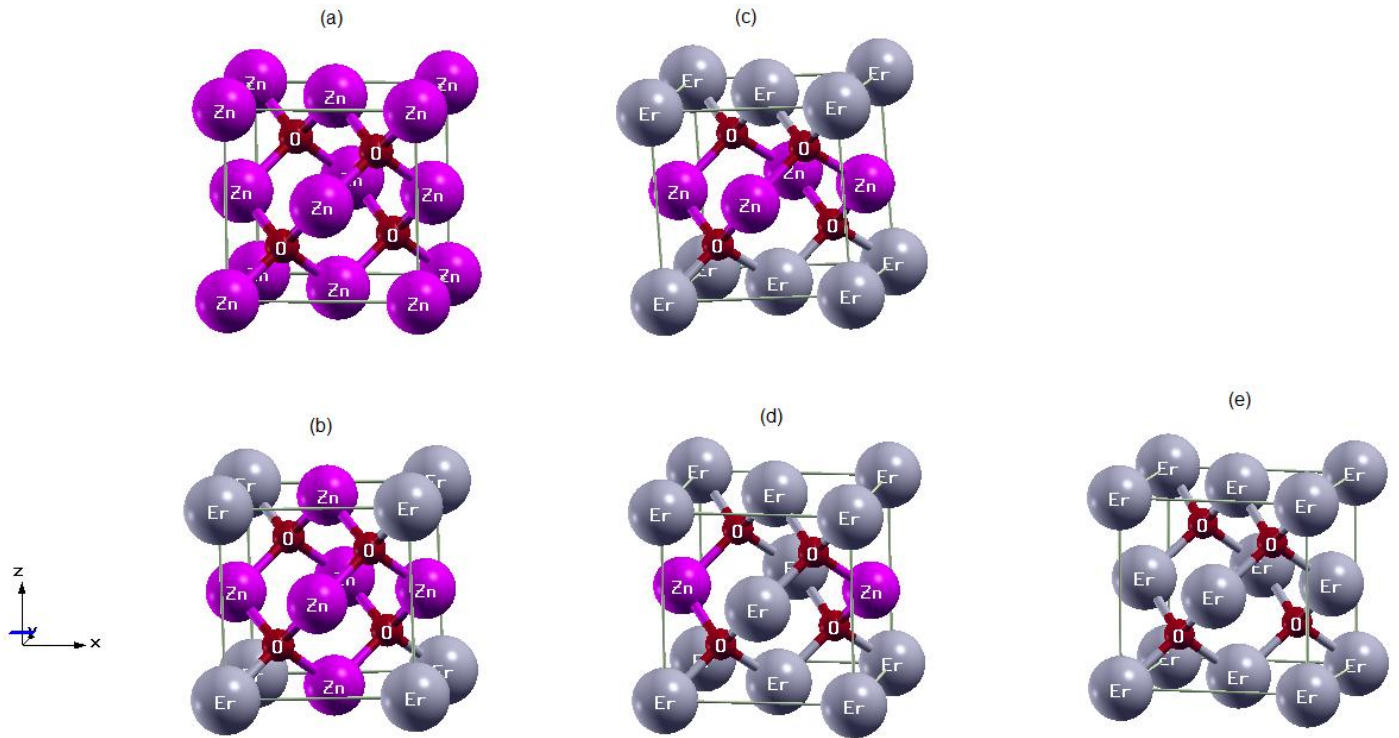the calculated total energy of the crystal converges to less than 10^{-5} Ry.

Figure 4.1 Supercell of Zn$_{1-x}$Er$_x$O alloys : (a) pure ZnO   (b) Zn$_{75}$Er$_{25}$O   (c) Zn$_{50}$Er$_{50}$O   (d) Zn$_{25}$Er$_{75}$O   (e) ErO.

4.3 STRUCTURAL PROPERTIES

4.3.1 STRUCTURAL PROPERTIES OF ZnO

The structural properties of Zn$_{1-x}$Er$_x$O alloys were studied for (x= 0, 0.25, 0.50, 0.75, 1). They are obtained by a minimization of the total energy depending on the volume for ZnO and Er doped ZnO in the zincblende structure (see Fig 4.1).We compute the lattice constants, bulk modulus and the pressure derivative of the bulk modulus by fitting the total energy versus volume according to the Murnaghan's equation of state [6]:

$$E(V) = E_0 + \frac{B_0 V}{B_0'} \left[\frac{(V_0/V)^{B_0}}{B_0' - 1} + 1 \right] - \frac{B_0 V_0}{B_0' - 1} \qquad (4.1)$$

where E$_0$ and V$_0$are the energy and volume at equilibrium. B and B$'$are the bulk modulus and it's the pressure derivative.

The equilibrium structural properties such as the lattice constants, bulk modulus, pressure derivative and total energy are computed using the GGA scheme. The obtained results are summarized and compared with some available experimental and theoretical data in Table 4.1.

The optimized lattice constant is 4.552 A^0 for pure ZnO, which is in good agreement with the experimental data 4.47 A^0 [8] and other theoretical results [9-13].

 The lattice constants calculated for pure ZnO is very close to the experimental results, proving that our calculation parameters are valid. The lattice parameter a calculated for ZnO is 1.8% greater than the experimental value, indicating that the GGA scheme overestimates the lattice constant [14].

As well as our result of bulk modulus B of ZB ZnO is in reasonable agreement with experimental results and previous theoretical studies [10, 15].
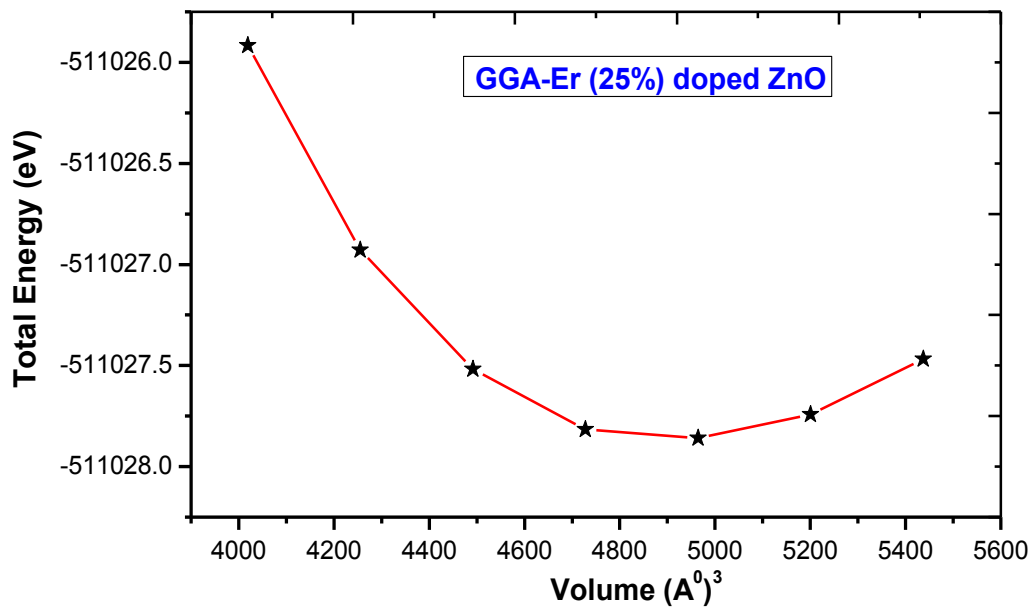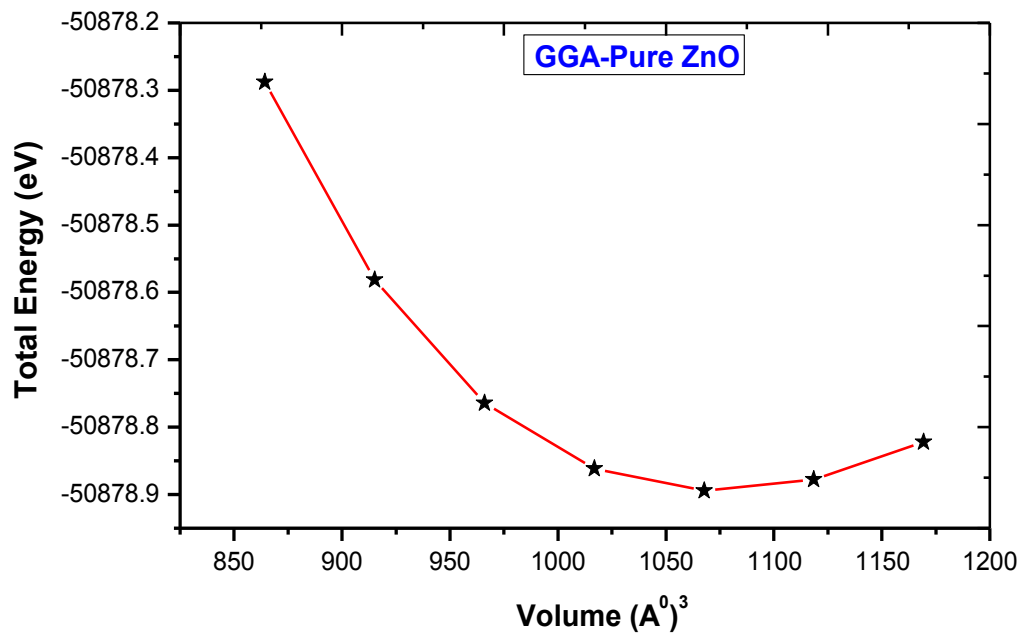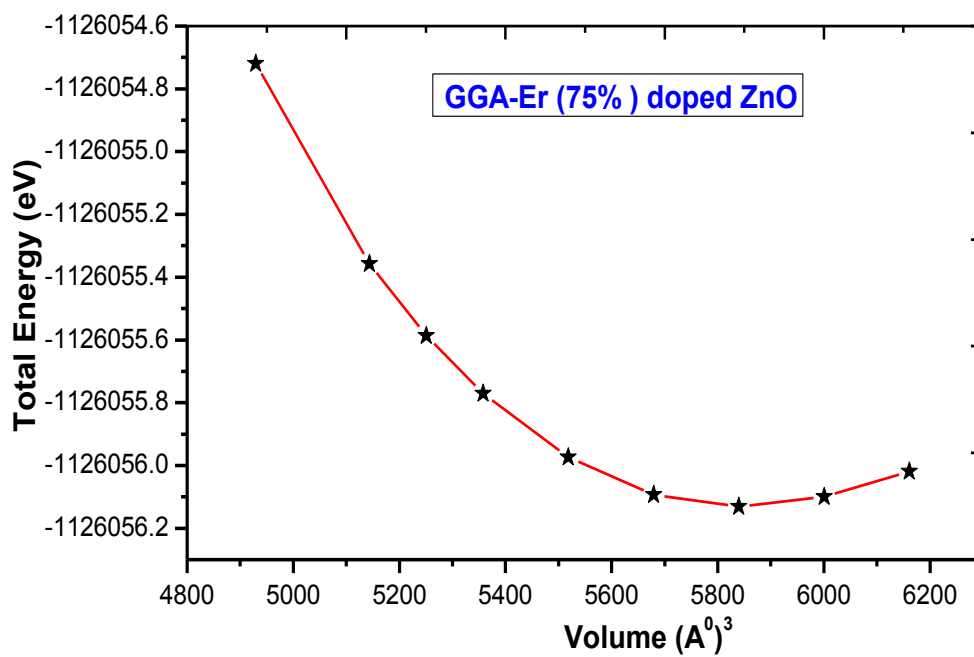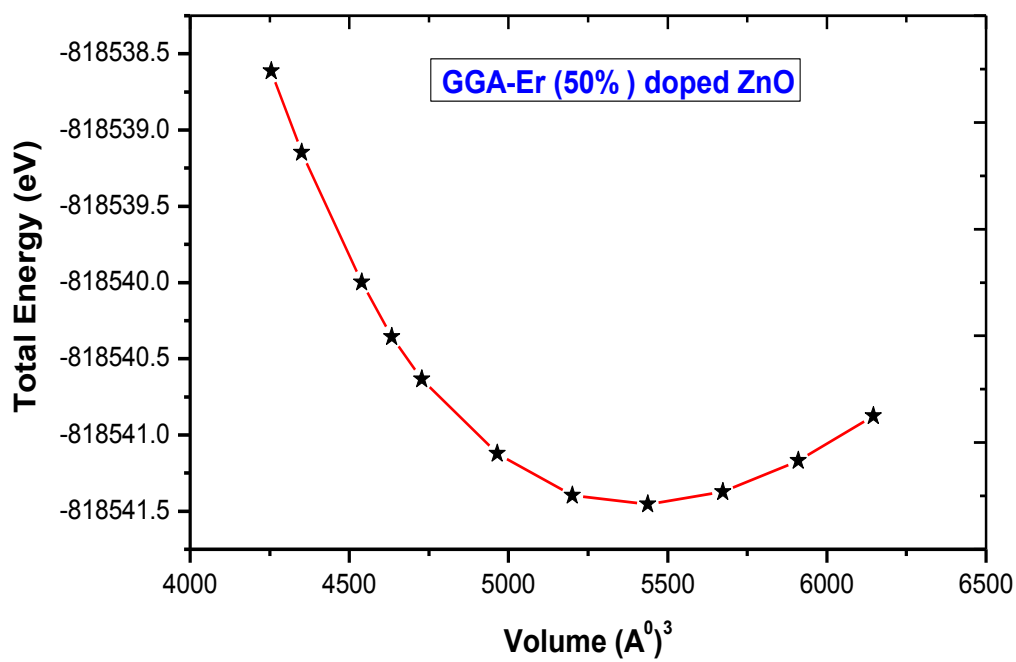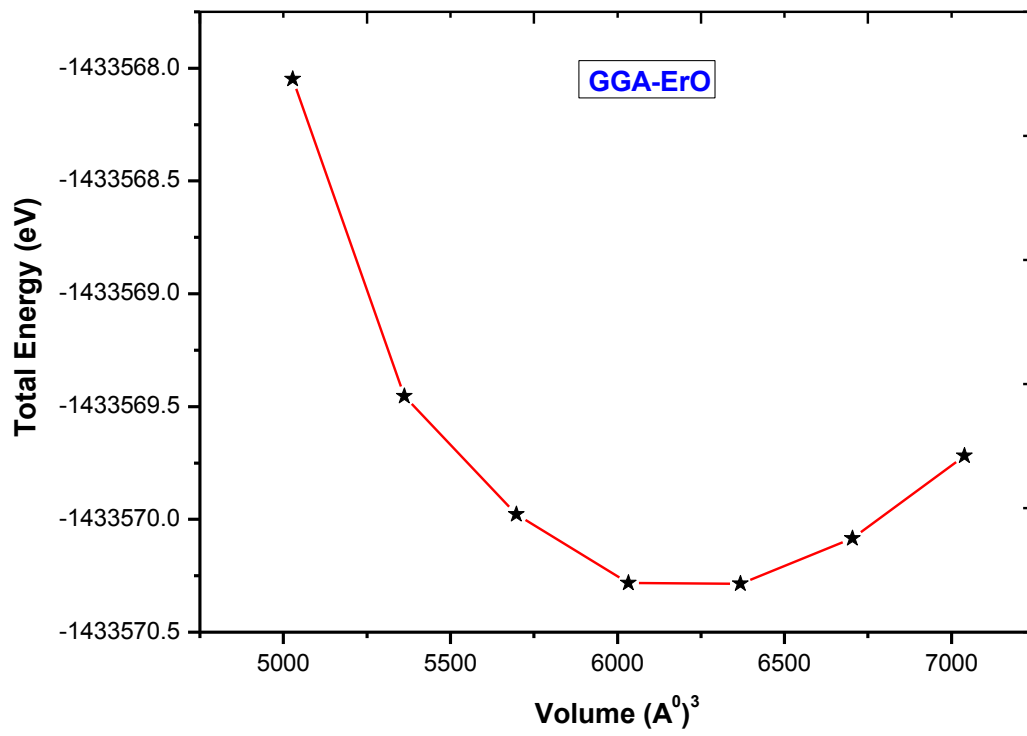
Figures 4.2 Total energys as a function of the volumes for Zn$_{1-x}$Er$_x$O alloys with

GGA approximation

Table 4.1 Lattice constants a, bulk modulus B, and pressure derivations of the bulk B' of pure ZnO.

	Prestent	**Other Calculations**	**Expriment**
a (Å)	4.552	4.614 [13], 4.53 [9] 4.62 [15]	4.47
B (GPa)	145.8	129.7 [15], 139.32 [16] 165.9 [10]	-
B'	4.24	4.33 [10] 4.096 [15]	-

4.3.2 STRUCTURAL PROPERTIES OF Zn$_{1-x}$Er$_x$O ALLOYS

In this case, we Substituted 25%, 50%, 75 and 100% from Er to Zn atoms in ZnO compound and performed the optimization (Fig 4.1). Our results of structural optimization for Er doped ZnO summarized in Table 4.2.

 The lattice constants and pressure derivative calculated for Zn$_{1-x}$Er$_x$O alloys clearly increase when we doped Zinc Oxide compound with Erbium, but the bulk modulus decreases.

In fact, to the best of our knowledge, there are no experimental values for the structural properties of Zn$_{1-x}$Er$_x$O alloys.

Table 4.2 Lattice constants a, bulk modulus B, and pressure derivations of the bulk B'
of Zn$_{1-x}$Er$_x$O alloys

Er-doped ZnO %	Lattice constants *(a)* (Å)	Bulk modulus B (GPa)	Pressure derivative B'
25%	4.759	122.45	4.31
50%	4.919	114.13	4.11
75%	5.047	103.53	3.52
100%	5.137	98.98	5.12

Fig. 4.3 illustrates the relation between lattice constant (a) and composition of dopant

(x), where the lattice constant increase to increasing of composition of dopant.

The calculated bulk modulus for Zn$_{1-x}$Er$_x$O decreases with rise of X, as shown in

Fig.4.4.

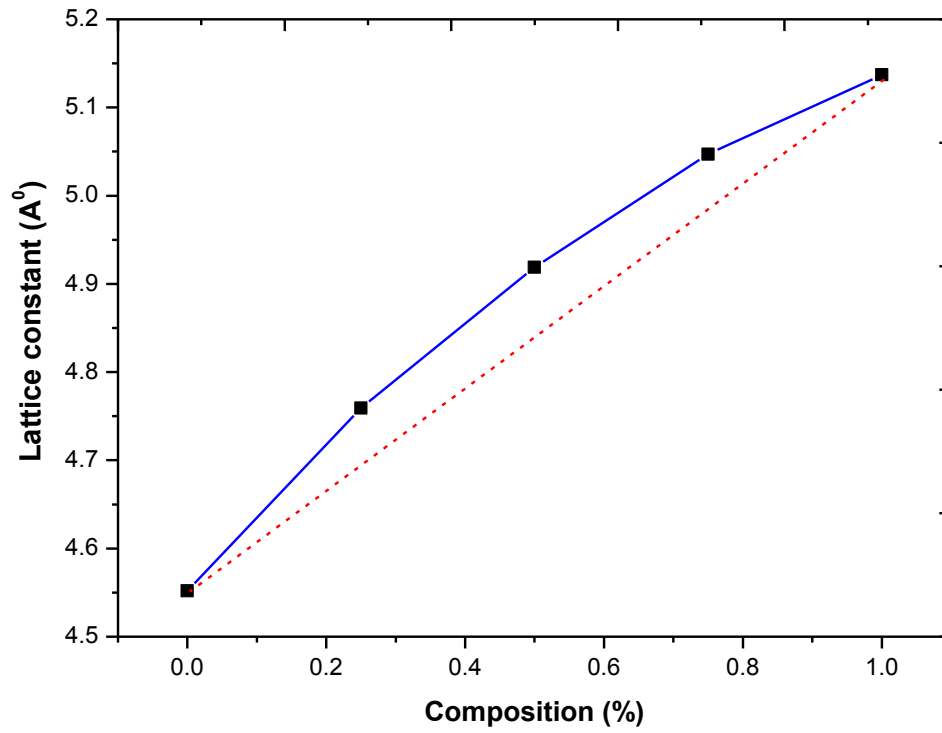Figure 4.3 Lattice Constant a as a function of Composition X for Zn$_{1-x}$Er$_x$O alloys.

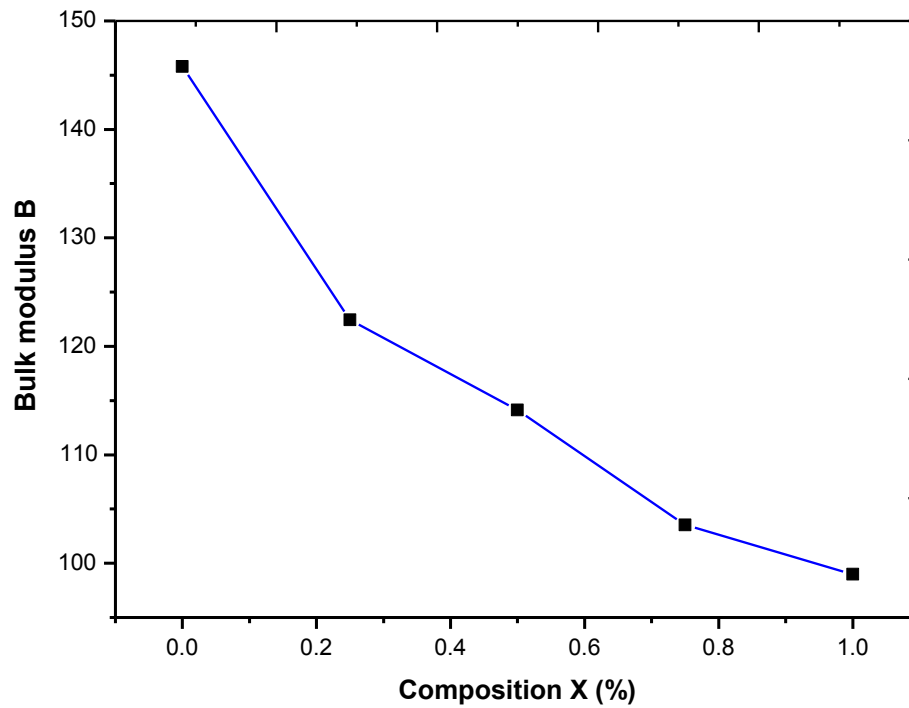Figure 4.4 Bulk modulus B as a function of Composition X for Zn$_{1-x}$Er$_x$O alloys.

4.4 ELECTRONIC PROPERTIES OF PURE ZnO AND Zn$_{1-x}$Er$_x$O ALLOYS

4.4.1 ELECTRONIC PROPERTIES OF PURE ZnO

Fig 4.5 displays the electronic band structures of zincblend ZnO using GGA approximation. It appeared that ZnO has a direct band gap semiconductor. The calculated energy band gap is 0.623 eV at Γ high symmetry point, which is close to the previous theoretical reports [17, 18], which are lower than the experimental value [19]. The underestimation of the band gap is mainly a scribed that the GGA or the local density approximation (LDA) calculation has the limitation in reproducing well the unoccupied electronic states [20].
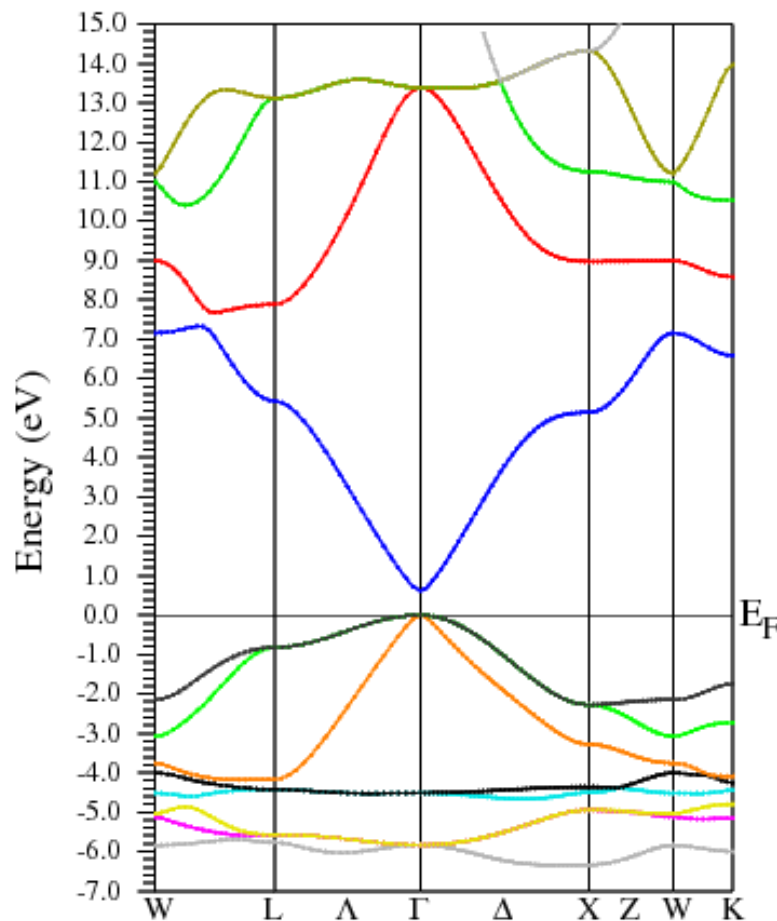

Figure 4.5 Band structure of pure ZnO using GGA calculation.

The total DOS and partial DOS of pure illustrated in Fig. 4.6. The valence band of pure ZnO is mainly consisted by three separated regions: the deep region -17.82 to -17 eV, which mainly originated from O 2s states, the middle region of -6.43 to 0 eV, which mainly derived from Zn 3d states and a part of O 2p states.

The valence band for pure ZnO mainly consists of the 2p, 2s states of O and 3d states of Zn. and the conduction band of ZnO dominated by the state of Zn 4s and 3p and 2pstates of O.
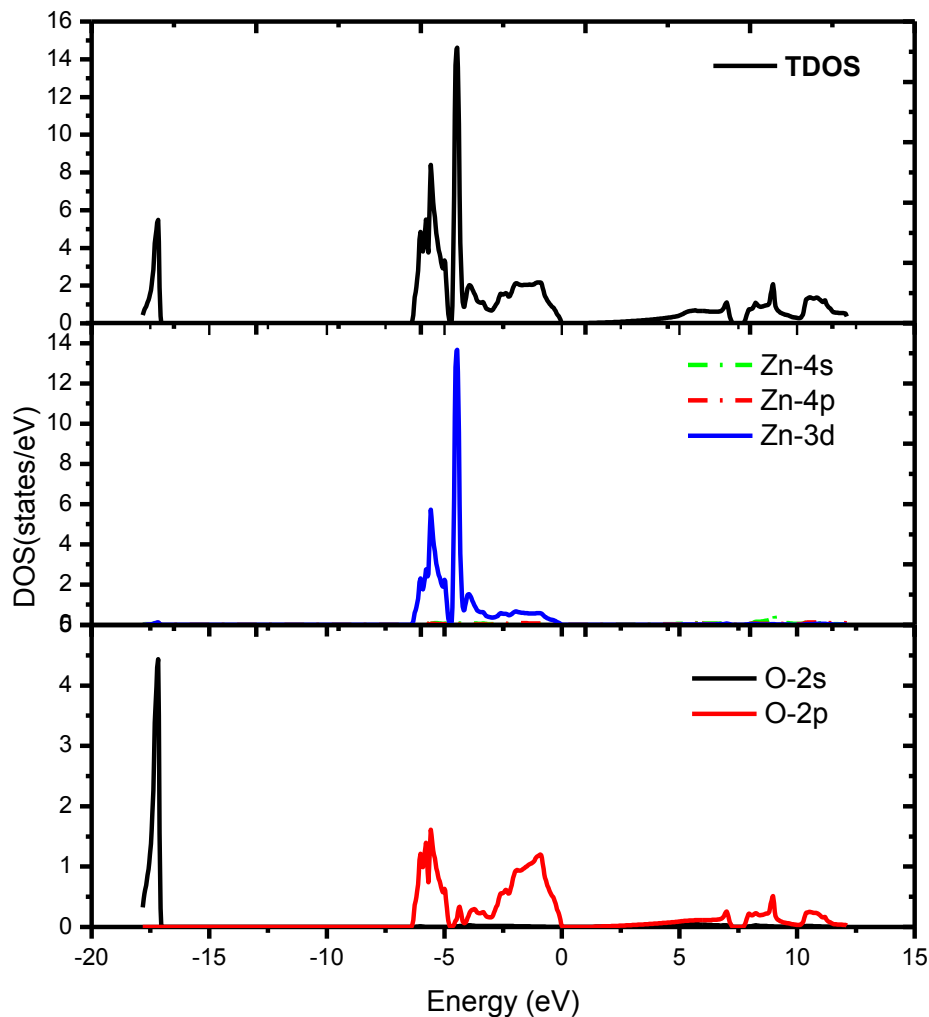

Figure 4.6 Total DOS and partial DOS of pure ZnO using GGA calculation.

4.4.2 ELECTRONIC PROPERTIES OF Zn$_{1-x}$Er$_x$O ALLOYS

The electronic properties of Zn$_{1-x}$Er$_x$O also performed by GGA calculation. The band gap results of Zn$_{1-x}$Er$_x$O(x= 0, 0.25, 0.50, 0.75, 1) are listed in Table 4.3. Our results appeared that all compounds are semiconductors and they have a direct bands gap at Γ high symmetry point.

Fig.4.7 shows the relation between the band gap and the concentration of impurity (metal erbium). It can be noted that the band gap varies with the proportion of impurity. It is found that E$_g$ increases with the Er component.

Table 4.3 The band gap of Zn$_{1-x}$Er$_x$O alloyes compared to exprimental and other theoretical calculations .

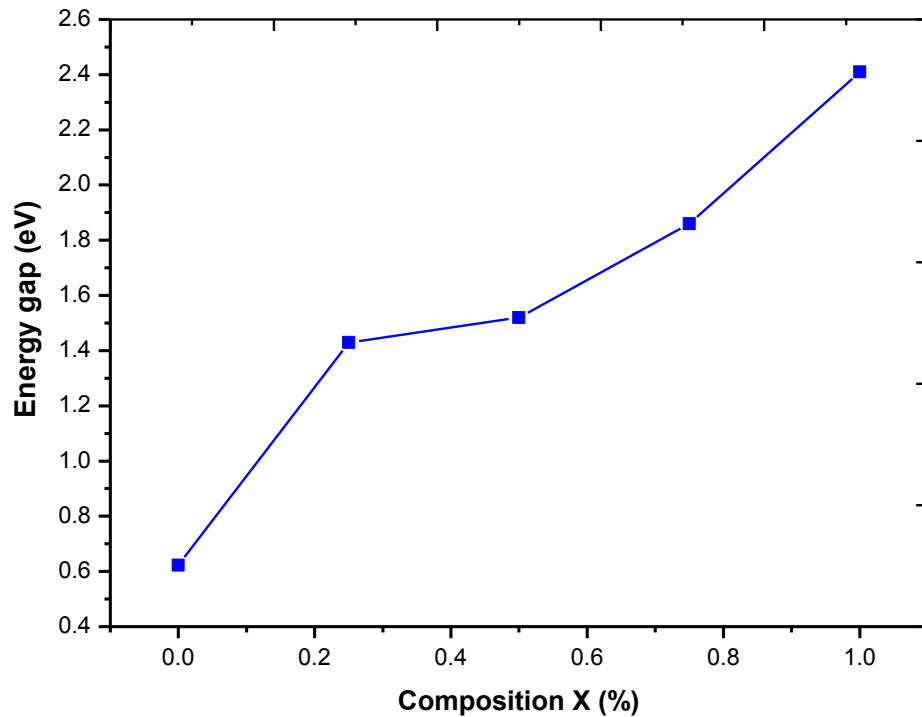| Zn$_{1-x}$Er$_x$O	Present	Experimental	Other calculations
0	0.623	3.3 [3]	0.641[21]0.73 [22] 0.804[15]
0.25	1.43	-	-
0.50	1.52	-	-
0.75	1.86	-	-
1	2.41	-	-

Figure 4.7 The energy band gap as a function of Composition X for Zn$_{1-x}$E$_x$O alloys.

The electronic band structures, total DOS and partial DOS of Zn$_{1-x}$Er$_x$O by GGA calculation illustrated in Fig. 4.8 and Fig.4.9 respectively.

They are shown that the Fermi-level move towards higher energy direction and enter into the conduction band, exhibiting n-type behavior after doping. The position of 4f-Er is observed localizes around the Fermi level yielding to the movement of the upper valence band downward. The Fermi level is shifted upward into the conduction band with the presence of 4f-Er state.
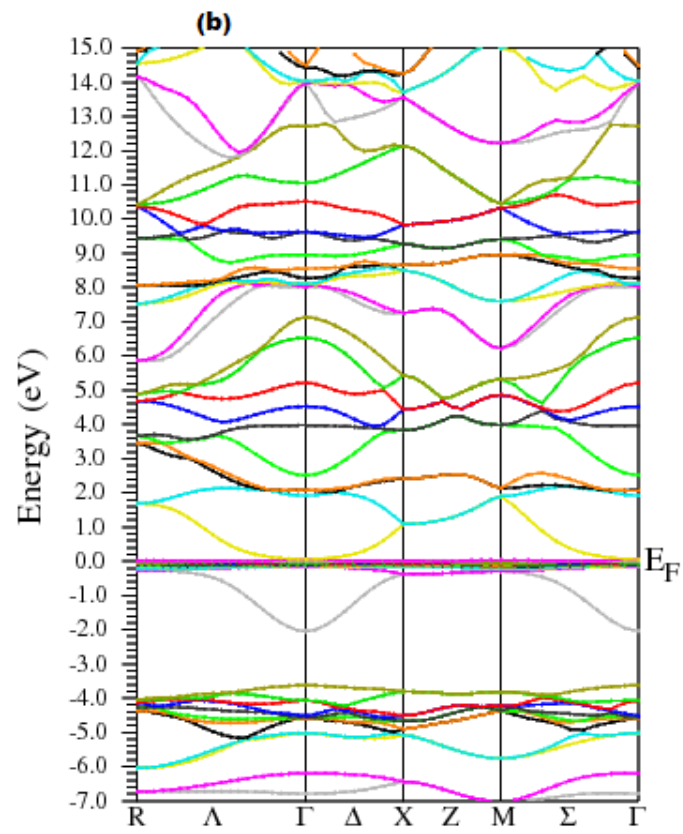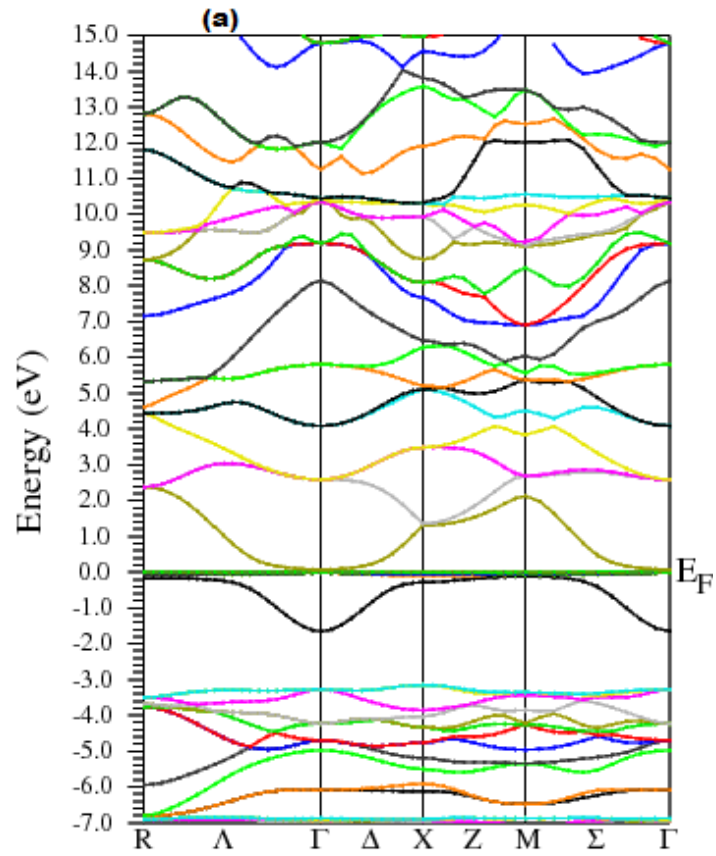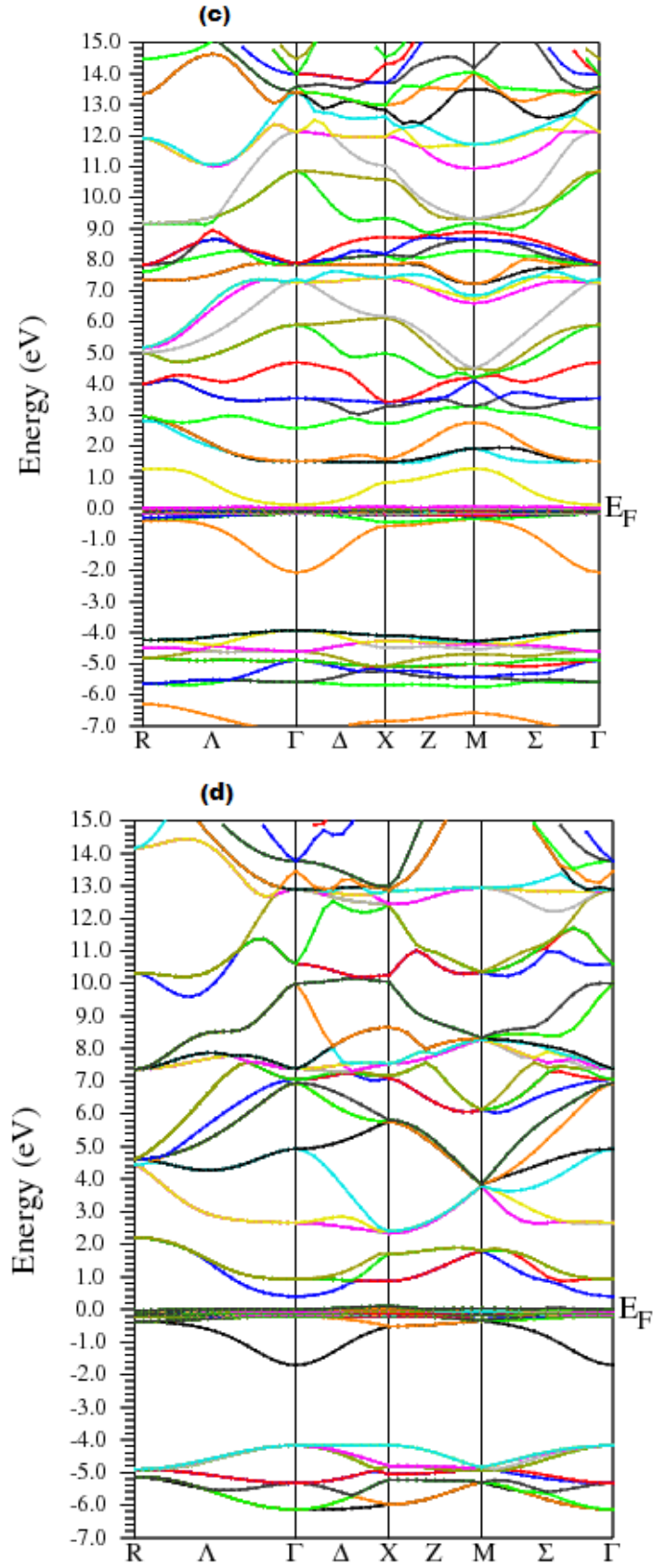
Figure 4.8 The electronic band structures of Zn$_{1-x}$Er$_x$O: (a) Zn$_{25}$Er$_{75}$O (b) Zn$_{50}$Er$_{50}$O (c) Zn$_{75}$Er$_{25}$O (d) ErO

(b)

(c)
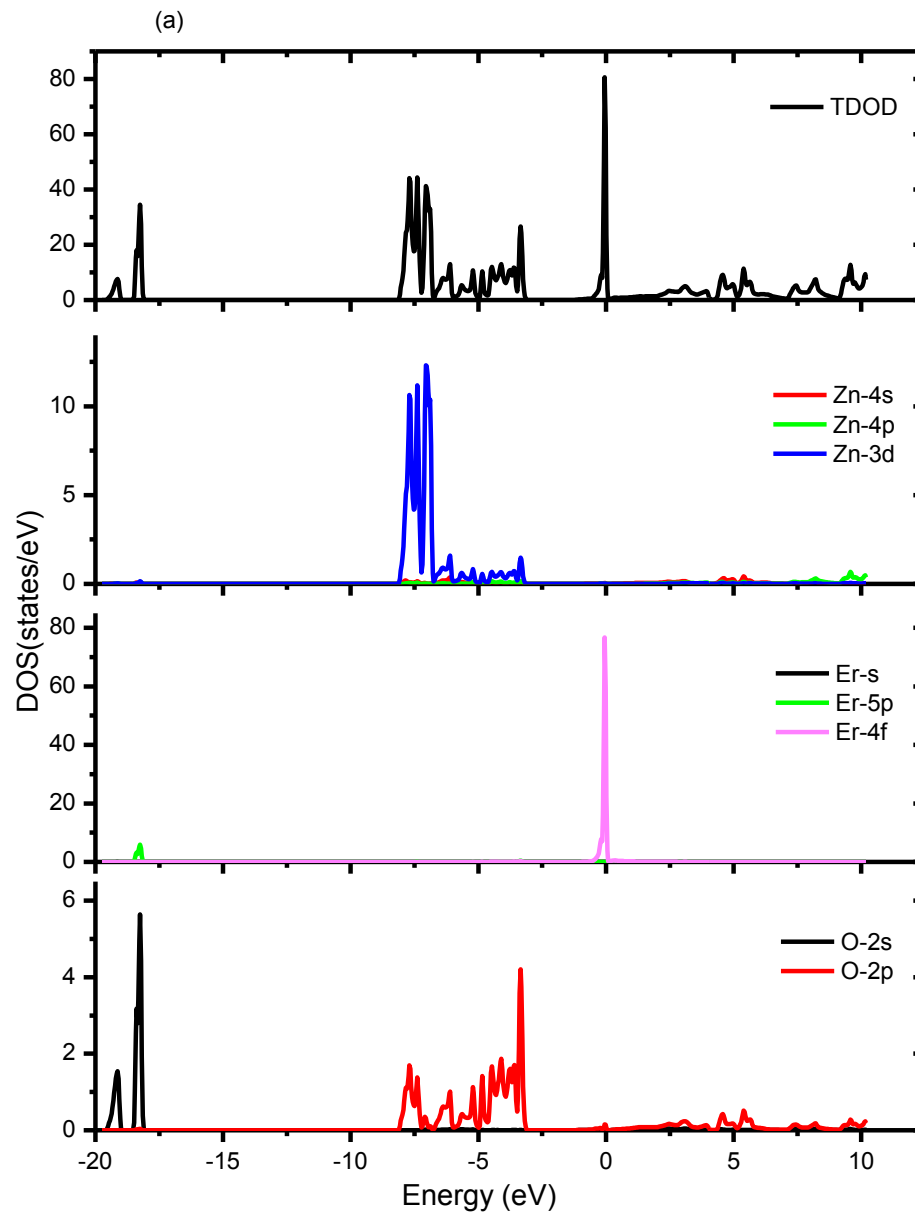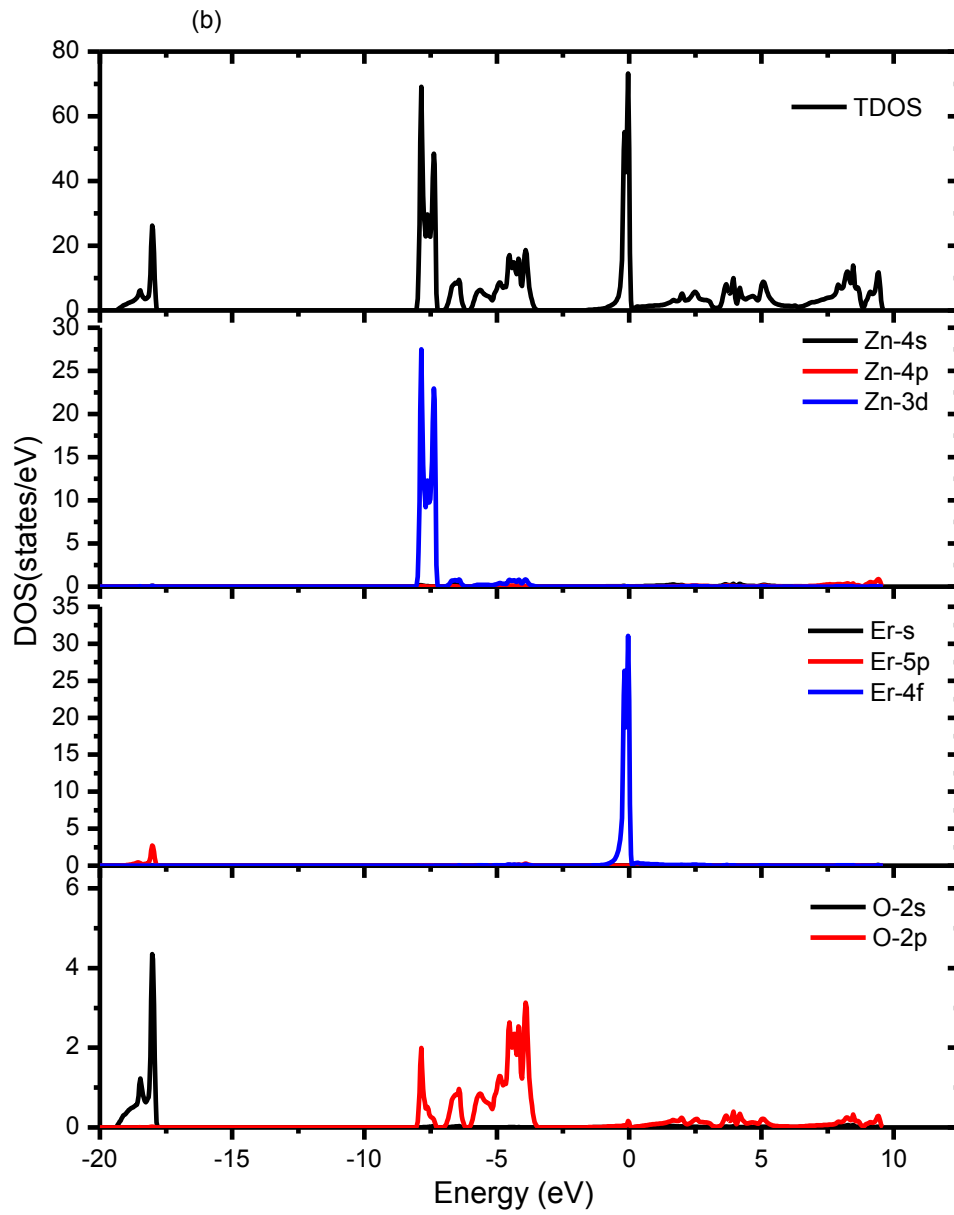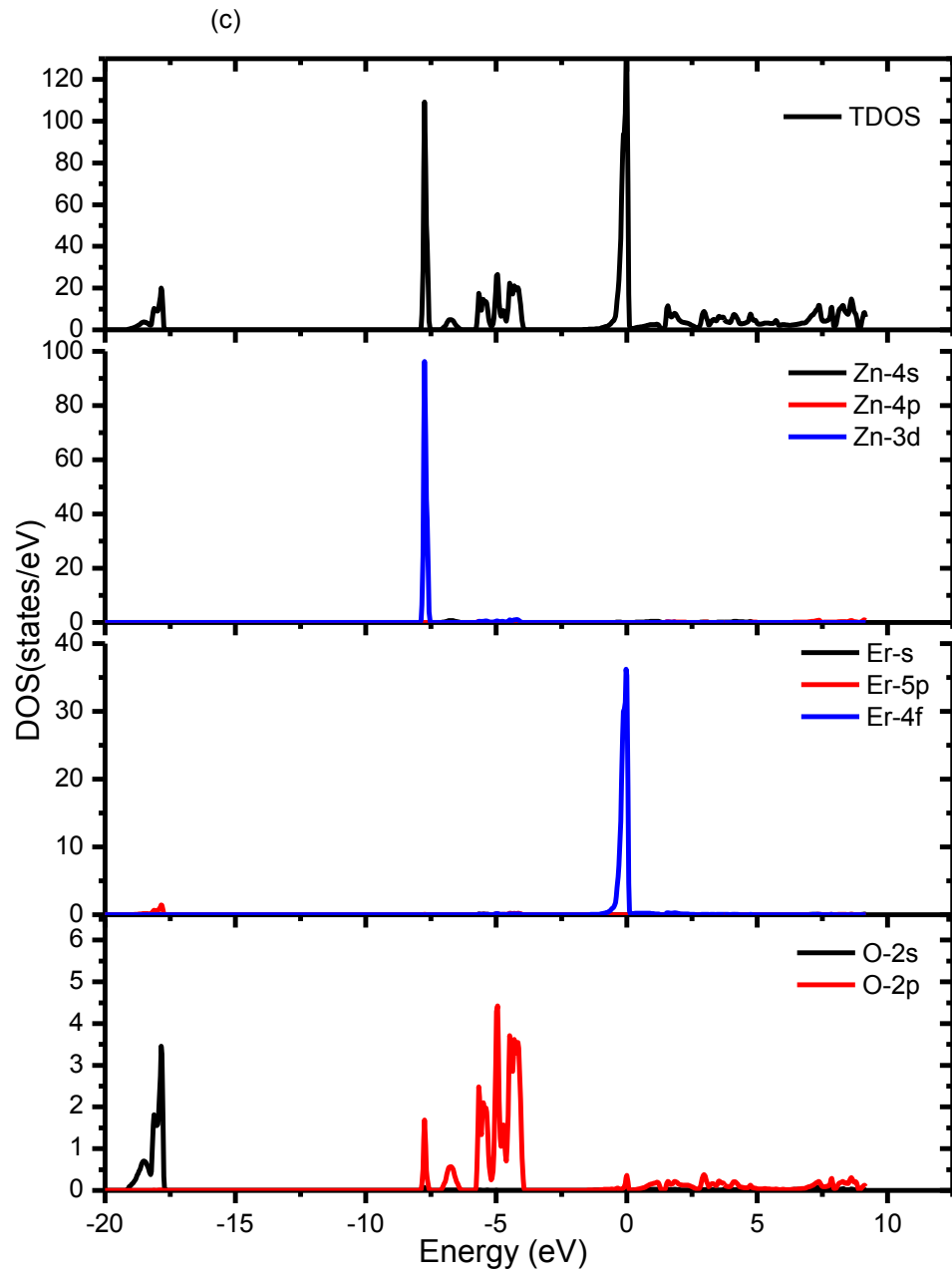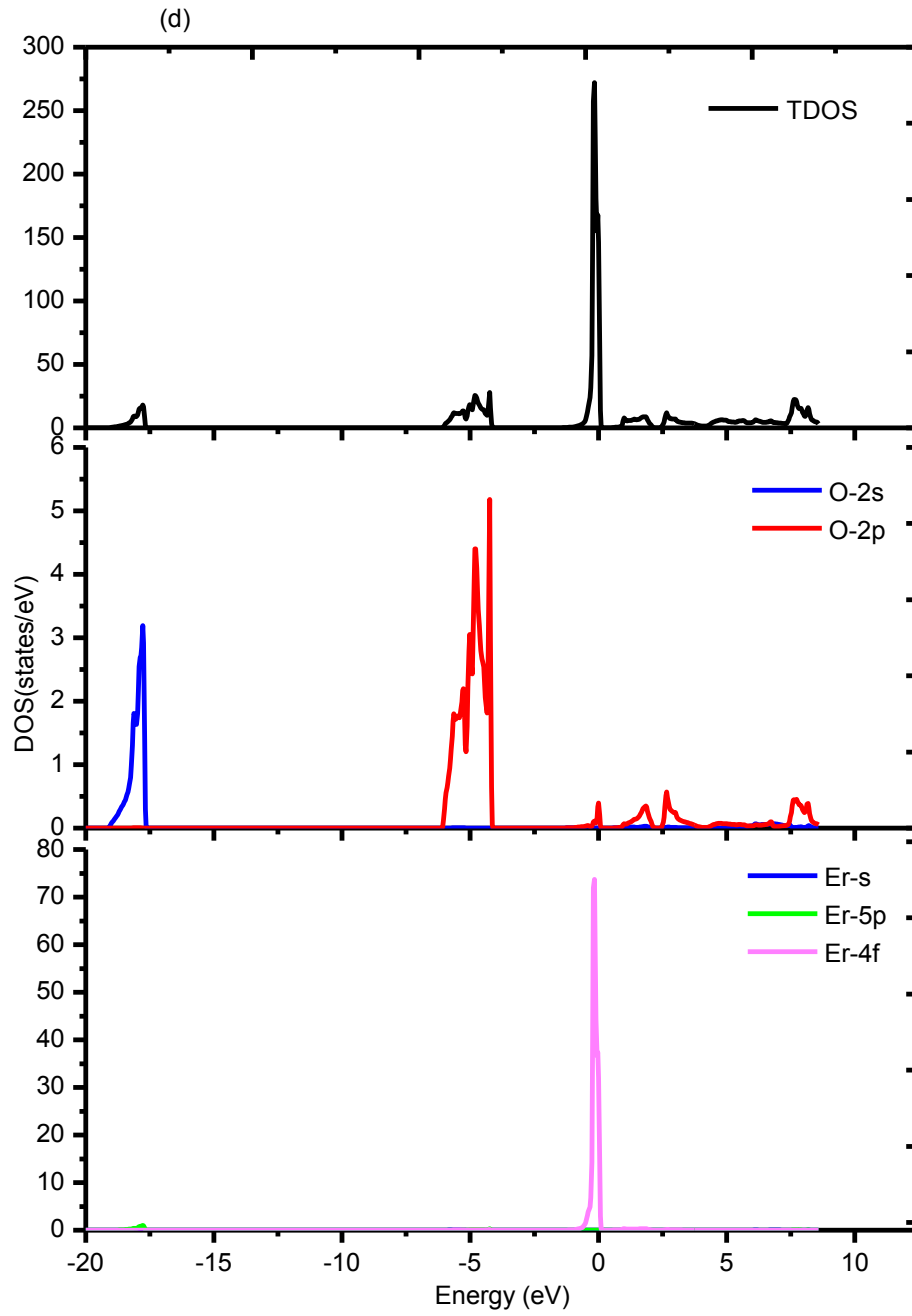
Figure 4.9 The partical and total Donsity of states (DOS) of of Zn$_{1-x}$Er$_x$O: (a) Zn$_{25}$Er$_{75}$O (b) Zn$_{50}$Er$_{50}$O (c) Zn$_{75}$E$_{r25}$O (d) ErO

CONCLUSIONS

In summary of this chapter, we investigated the structural and electronic properties of Zn$_{1-x}$Er$_x$O. Our results of structural properties are agreement with the theatrical and experimental values. We have investigated the composition dependence of the lattice constant, bulk modulus, band gap. We studied the behavior of the equilibrium volume, bulk modulus and the band gap of Zn$_{1-x}$Er$_x$O alloys as a function of the calculated band structures and density of states indicate a semiconducting character of the involved materials. We observed effect of Er on electronic and optical properties of Zn$_{1-x}$Er$_x$O for(x= 0, 0.25, 0.50, 0.75, 1).

REFERENCES

[1] P. Blaha, K. Schwarz, G. K. H. Madsen, D. Kvasnicka and J. Luitz, J. wien2k. An augmented plane wave + local orbitals program for calculating crystal properties, Karlheinz Schwarz, Techn. Wien, Austria, 2001.

[2] G. K. H. Madsen, P. Blaha, K. Schwarz, E. Sjöstedt and L. Nordström, Phys. Rev. B 64 (2001) 195134.

[3] W. Kohn and L. J. Sham, Phys. Rev. A 140 (1965)1133.

[4] J.P. Perdew, S. Burke and M. Ernzerhof, Phys. Rev. Let 77 (1996) 3865.

[5] F. Tran and P. Blaha, Phys. Rev. Lett. 102 (2009) 226401.

[6] F.D.Murnaghan, Proc.Natl.Acad.Sci.USA30 (1944)244–247.

[7] H. J. Monkhorst and J. D. Pack, Phys. Rev. B 13 (1976) 5188.

[8] A. Ashrafi and C. Jagadish, J. Appl. Phys. 102 (2007) 071101

[9] H. Dixit, R. Saniz, D. Lamoen, B. Partoens, J. Phys.:Condens. Matter 22 (2010) 125505.

[10] S. Cui, W. Feng, H. Hu, Z. Feng and Y. Wang, J. Alloys Compd 476 (2009) 306.

[11] B. Amrani, R. Ahmed and F. El Haj Hassan, Comput. Mater. Sci. 40 (2007) 66.

[12] A. JemmyCinthia, G. Sudhapriyanga, R. Rajeswarapalanichamy and M. Santhosh, Procedia Materials Science 5 (2014) 1034.

[13] H. Liu, H. Mao, M. Somayazulu, Y. Ding, Y. Meng and D. Husermann, Phys. Rev. B 70 (2004) 094114.

[14] F. El Haj Hassan, B .Amrani, J. Phys. Condens. Matter 19 (2007) 386234–386243.

[15] M. R. Boufatah and A. E. Merad. Mater. Sci. Semicon. Process. 19 (2014) 179.

[16] M. Kalay, H. H. Kart, S. Ö. Kart and T. Çağin, J. Alloys Compd. 484 (2007) 431.

[17]   L. Zhao, P.F.Lu, Z.Y.Yu, X.T.Guo, Y.Shen, H.Ye, G.F.Yuan, L.Zhang, The electronic and magnetic properties of (Mn,N)-codoped ZnO from first principles, J.Appl.Phys.108(2010)113924.

[18]   T.Souza, I.daCunha Lima, M.Boselli, Carrier induced ferromagnetism in Mn-doped ZnO:Monte Carlo simulations, Appl.Phys. Lett.(2008)152511–152513.

[19]   A. Meng, X.J. Li, X.L. Wang, Z.J. Li, Ceram. Int. 40 (2014) 9303–9309.

[20]   N.N. Lathiotakis, A.N. Andriotis, M. Menon, Phys. Rev. B 78 (2008) 193311–193314.

[21]   S. Zh. Karazhanov, P. Ravindrana, A. Kjekhusa, H. Fjellva, U. Grossnerc and B.G. Svenssonc, J. Cryst. Grow. 287(2006) 162.

[22]X. D. Zhang, M. L. Guo, W. X. Li, C. L. Liu, arXivpreprint arXiv:1210.0163 (2012).

CHAPTER V

5.1. INTRODUCTION

In this chapter, we will investigate the electronic and optical properties of pure ZnO and Erbium doped Zinc Oxide by density functional theory (DFT) with modified Becke-Johnson exchange potential (mBJ). We attempt to see the influence of Erbium (25%) to electronic and optical properties of ZB ZnO such as the energy gap, the upper valence bandwidth (UVBW), the total valence bandwidth (TVBW), the dielectric constant and   absorption coefficients.

5.2 ELECTRONIC PROPERTIES

5.2.1 ELECTRONIC PROPERTIES OF PURE ZnO

Electronic band structures and total density of states obtained with mBJ potential are shown in Figure 5.1 for pure ZnO. It is clear that ZnO is a direct band gap semiconductor with a calculated band gap of 2.58 eV at Γ high symmetry point, which is in good agreement with those of experimental and other sophistical calculations as seen in Table 5.1. Other principle features of the calculated band structures such as the upper valence bandwidth (UVBW), the total valence bandwidth (TVBW) and the splitting δd_{Zn} and δf_{Er} are given in the same table. The total and partial densities of states DOS of pure ZnO are presented in Figure 5.2. It elucidates that the valence band for pure ZnO mainly consists of the 2p, 2s states of O and 3d states of Zn. The upper valence band of the width 5.755 eV is dominated by 2p state of O, while its 2s state is localized in the lower level of VB at -18.64 eV.
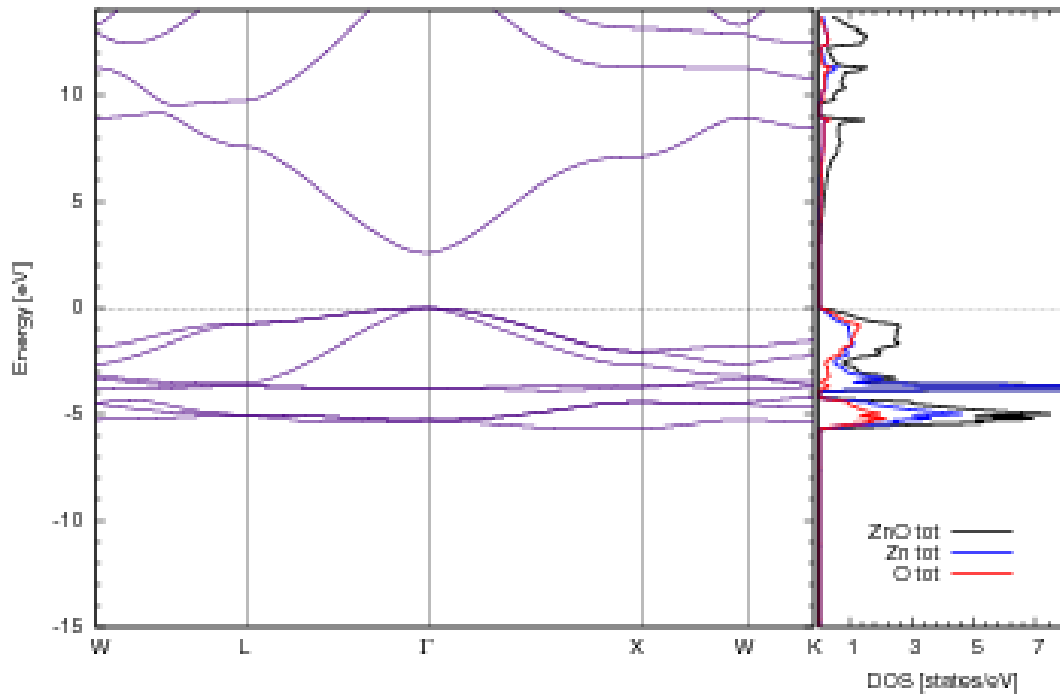
Figure 5.1 Band structures and total DOS for pure ZnO by mBJ potential.

Table 5.1 Calculated principle features of band structures for pure and Er-doped ZnO.

	Pure ZnO			Er-doped ZnO
	Present	**Exp**	**Other calc**	
E_g	2.58	3.3 [9]	0.50 [1][a] 0.73 [2][a] 2.59 [3][b] 0.804 [3][a] 2.47 [4][c]	2.98
UVBW	5.755			4.521
TVBW	19.293			17.719
δd_{Zn}	5.755			4.521
δf_{Er}	-			3.708
Occupied States	0			1.870

[a] GGA calculation.

[b] mBJ+LDA calculation

[c] GW calculation

Below the valence band maximum (VBM), the 3d Zn states give rise in the same energy width of that of 2p O. As a result, the hybridization is formed between 2p O and 3d Zn states. It is worth noticing that the level position of 3d Zn is corrected via mBJ potential compared to the GGA one (see Table 2). This correction contributes to the enhanced energy band gap. Good agreement is achieved with other experimental and hybrid functional PBE0 values.

The lowest conduction band (CBM) is attributed to the Zn 4s states and O 2p states which is well compared to the experimental and theoretical data.
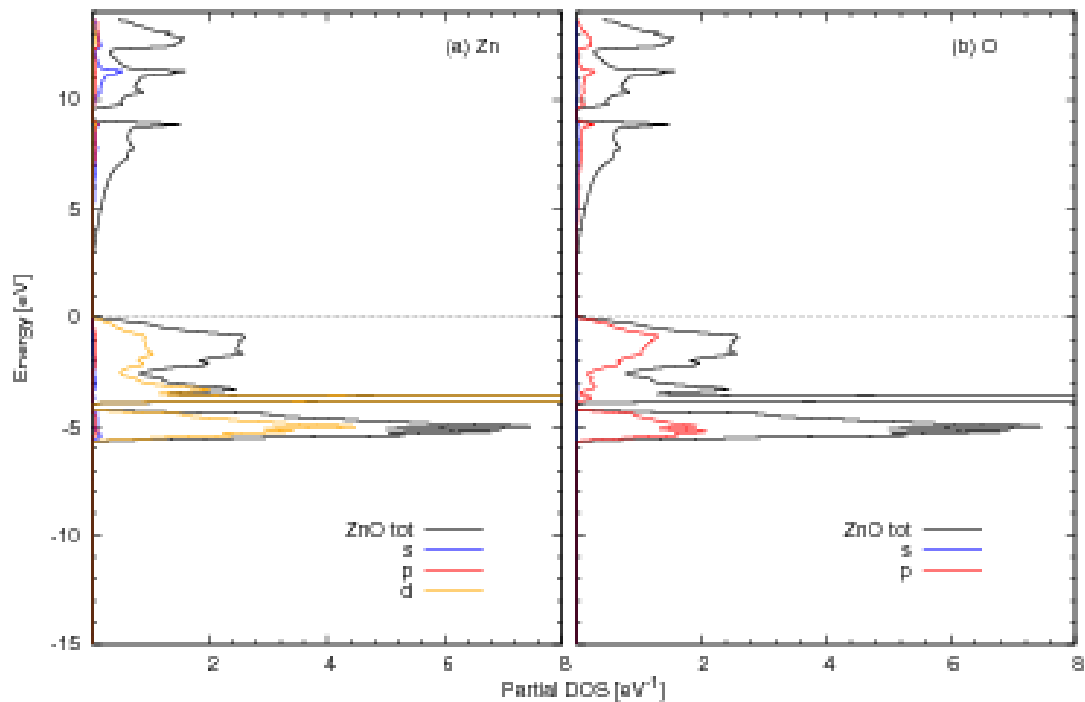
Figure 5.2 Partial density of states (DOS) for pure ZnO using mBJ potential..

5.2.2 ELECTRONIC PROPERTIES OF ER DOPED ZnO

The total density of states DOS and band structure of Er-doped ZnO are illustrated in Figure 5.3. The estimated electronic energy gap (2.98 eV) is observed under Fermi level in the range from −1.74 eV to−4.72 eV. Figure 5.4 is given the partial density of states (DOS) for Er-doped ZnO using mBJ potential.

The position of 4f-Er is observed localizes around the Fermi level yielding to the movement of the upper valence band downward. The resulting value of the optical energy band gap is then 4.72 eV obtained by mBJ potential. Therefore, the Fermi level is shifted upward into the conduction band with the presence of 4f-Er state.
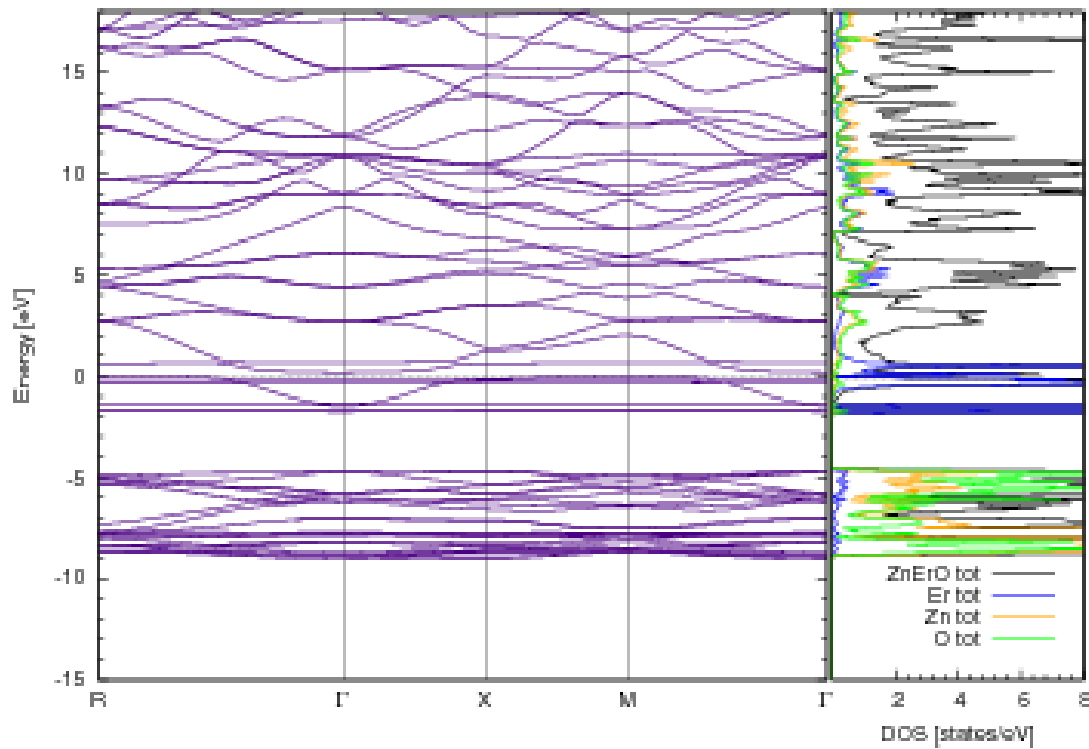
Figure 5.3 Band structures and total DOS for Er-doped ZnO by mBJ potential.

Consequently, this later state acts as donor giving rise to the *n*-type metallic conductivity. Wu et al [5] have explained this feature for the case of Ga doped ZnO as follow: The occupied states in the bottom of the conduction band can be regarded as an additional energy barrier that must be overcome before the electron can be excited from the valence to the conduction bands. This barrier also causes the increasing of the optical band gap to 4.72 eV. We can notice from this feature that this significant effect of Er in ZnO had a strong modification in optoelectronic properties. Detailed information about the positions of several contributed states is listed in Table 5.1for pure and Er doped ZnO.

Figure 5.4 Partial density of states (DOS) for Er-doped ZnO using mBJ potential.

5.3. OPTICAL PROPERTIES

To investigate the optical properties of materials, it is necessary to calculate the imaginary part of the dielectric function $\varepsilon_2(\omega)$. Because the optical properties are usually described by dielectric function $\var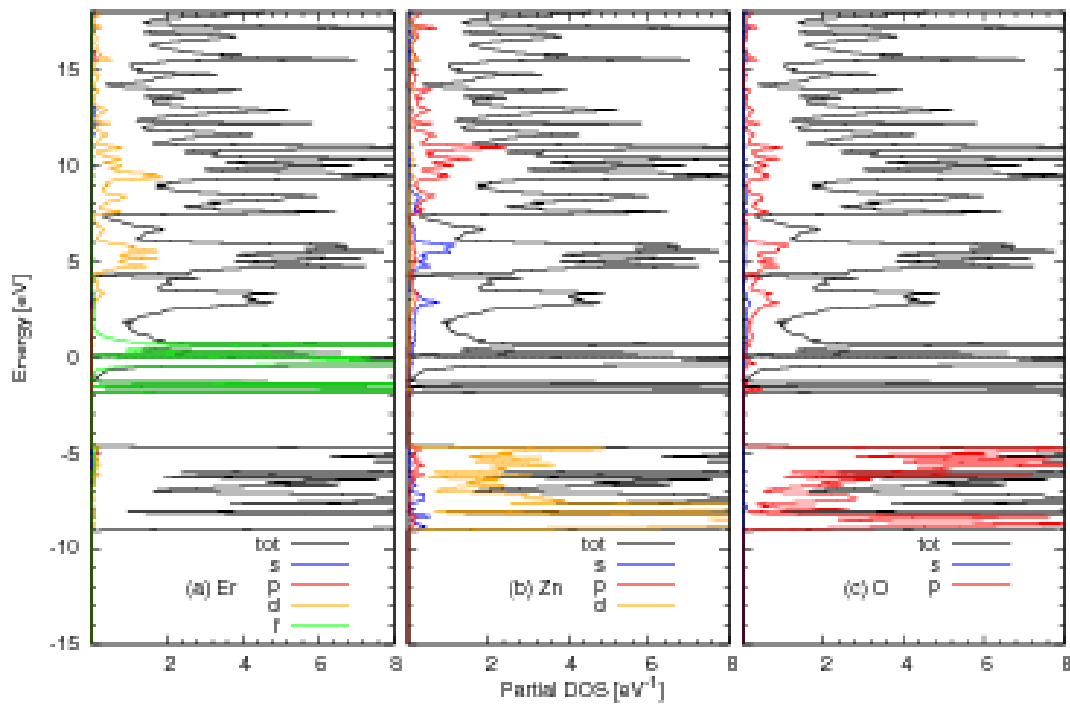epsilon(\omega)$, sometimes by refractive index $n(\omega)$, extinction coefficient $k(\omega)$ and absorption coefficient $\alpha(\omega)$. These features are very important to determine the optical and electronic properties of the crystal.

5.3.1 DIELECTRIC FUNCTION

The dielectric function describe as $\varepsilon(\omega) = \varepsilon_1(\omega) + i\varepsilon_2(\omega)$.where$\varepsilon_1(\omega)$ represents the dielectric real part and $\varepsilon_2(\omega)$ is the dielectric imaginary part.

The real part of dielectric function$\varepsilon_1(\omega)$, represents the dispersion of the incident photons by the materials, while the imaginary part $\varepsilon_2(\omega)$ results from the inter band transition between occupied states below Fermi level and unoccupied state on top Fermi level due the photon absorption. In fact, the absorption coefficient, reflectivity, and transmittance are also calculated from the dielectric function.

The dielectric imaginary part is given mathematically as following:

$$\varepsilon_2(\omega)_{\alpha\beta} = \frac{4\pi^2 e^2}{m^2 \omega^2} \sum_{if} \int \langle f|P_\alpha|i\rangle \langle i|P_\beta|f\rangle \, W_i \big(1 - W_f\big) \delta\big(E_f - E_i - \hbar\omega\big) d^3 k \qquad (5.1)$$

where $\langle f|P_\alpha|i\rangle$ and $\langle i|P_\beta|f\rangle$ are dipole matrix elements, f and i are final and the initial states respectively, W_i (resp. W_f) is the Fermi distribution function centred at E_i(resp. E_f).The real part $\varepsilon_1(\omega)$ is computed from $\varepsilon_2(\omega)$ using the Kramers– Kronig relation in the form:

$$\varepsilon_2(\omega)_{\alpha\alpha} = 1 + \frac{2}{\pi} P \int_0^\infty \frac{\omega' \varepsilon_2(\omega')_{\alpha\alpha}}{\omega'^2 - \omega^2} d\omega' \qquad (5.2)$$

where P and ω are the constant of integration and the frequency of the incident photons.

105

Figure 5.5 displays $\varepsilon_1(\omega)$ and $\varepsilon_2(\omega)$ of pure and Er doped ZnO. The real part $\varepsilon_1(\omega)$ represents the dispersion of the incident photons by the materials, while the imaginary part $\varepsilon_2(\omega)$ of the dielectric function of pure ZnO and Er-doped ZnO is important to determine the different transitions due to photons absorption in these two cases, from occupied to unoccupied states.

In this work, we have not used scissor operator since the mBJ potential is known to improve the band gap very closely to the experimental one as it is remarked for our pure ZnO (see Table 2). Therefore we expected that the calculated optical properties of pure and Er doped ZnO are more improved compared to other classical approximations (GGA or LDA).

From 5.5 (a), the calculated static dielectric function $\varepsilon_1(0)$ given at 0 frequency is 2.26, 11.94 for ZnO and Er doped-ZnO respectively. The value of ZnO agree with the reported results, for instances, (LDA+U) [6] and (GGA+mBJ) [7].The figure shows also a significant increase of the dielectric function under doping with Er. Figure 5.5 (b) shows the imaginary part $\varepsilon_2(\omega)$ of the dielectric function. For pure ZnO, we found that the peak observed at 2.58 eV, which corresponds to the energy band gap value, corresponds to the transition from O 2p occupied sates at (VBM) to the Zn 4s unoccupied states at (CBM).The others peaks viewed at high energies result from the transitions between various occupied to unoccupied states from the valence band to the conduction band. For Er doped ZnO, a new high peak is observed at low energy near 1.2 eV. This latter is due to the transition between Er 4f donor occupied states located around Fermi level and the Zn 4s and Zn 4p unoccupied states in the conduction band.
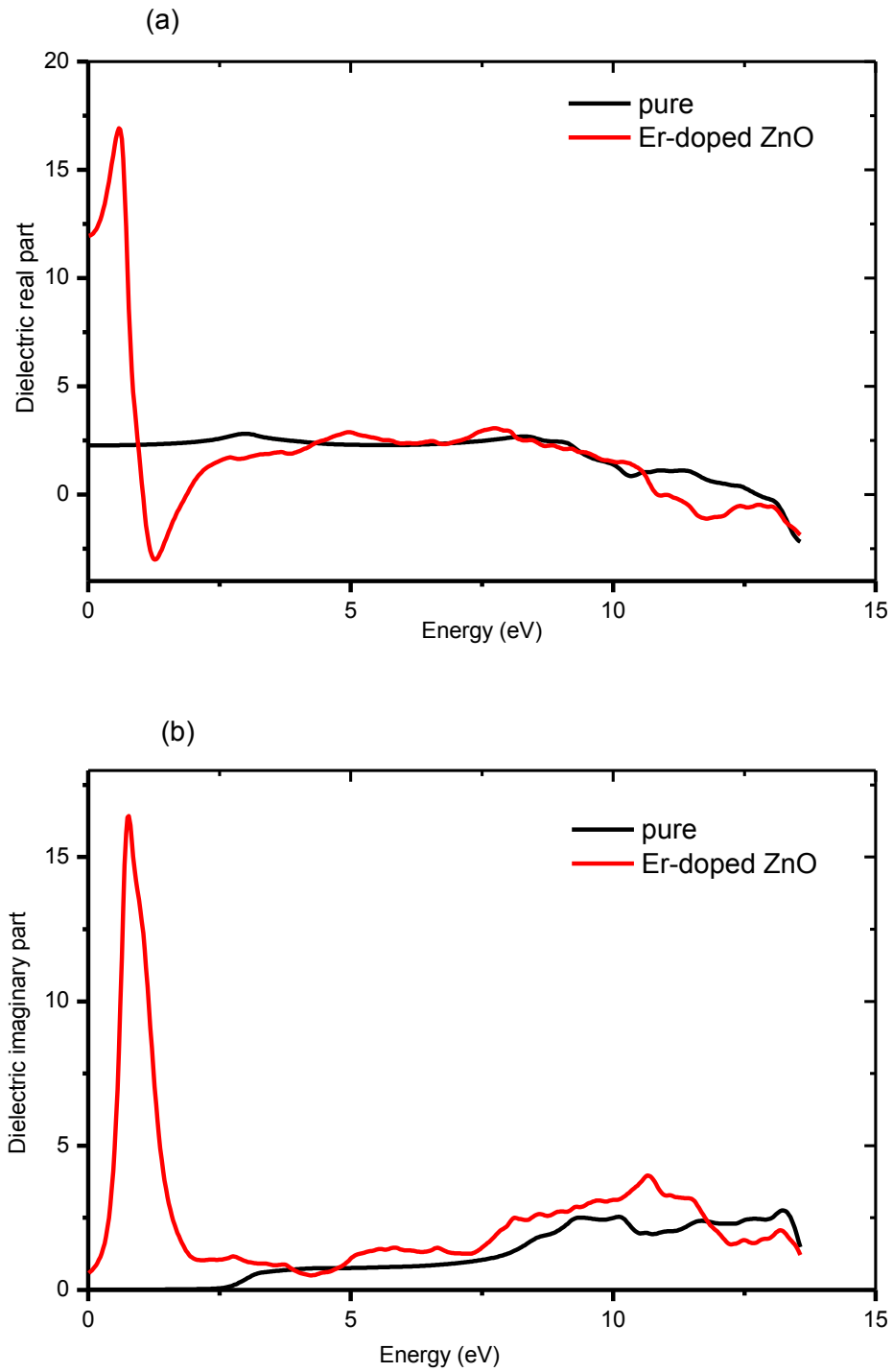
Figure 5.5 The dielectric functions of pure and Er-doped ZnO: (a) Real part and (b) imaginary part.

5.3.2 REFRACTIVE INDEX AND THE EXTINCTION COEFFICIENT

The refractive index is a very important physical parameter related to the microscopic atomic interactions and the design, analysis of heterostructure lasers and other wave-guiding semiconductor devices. It can be described by:

$$n(\omega) = \sqrt{\frac{|\varepsilon_2(\omega)| + \varepsilon_1(\omega)}{2}} \tag{5.3}$$

where ε_1 (ω) is the dielectric real part and ε_2 (ω) is the dielectric imaginary part.

Whereas, extinction coefficient define as a measure of the rate of diminution of transmitted light via scattering and absorption for a medium. It is written in following form:

$$L(\omega) = \frac{\varepsilon_2(\omega)}{\varepsilon_1^2(\omega) + \varepsilon_2^2(\omega)} \tag{5.4}$$

Figure 5.6 illustrates the calculated refractive index n (ω) and the extinction coefficient k(ω). The static refractive indices are deduced from the figure 5 (a) as 1.50 and 3.46 for pure and Er- doped ZnO respectively. Similar values are observed for pure ZnO compared to those reported in the literature [8]. Increasing behavior can be found with Er doping which consequently affects considerably the exciton energy (60 meV for ZnO).
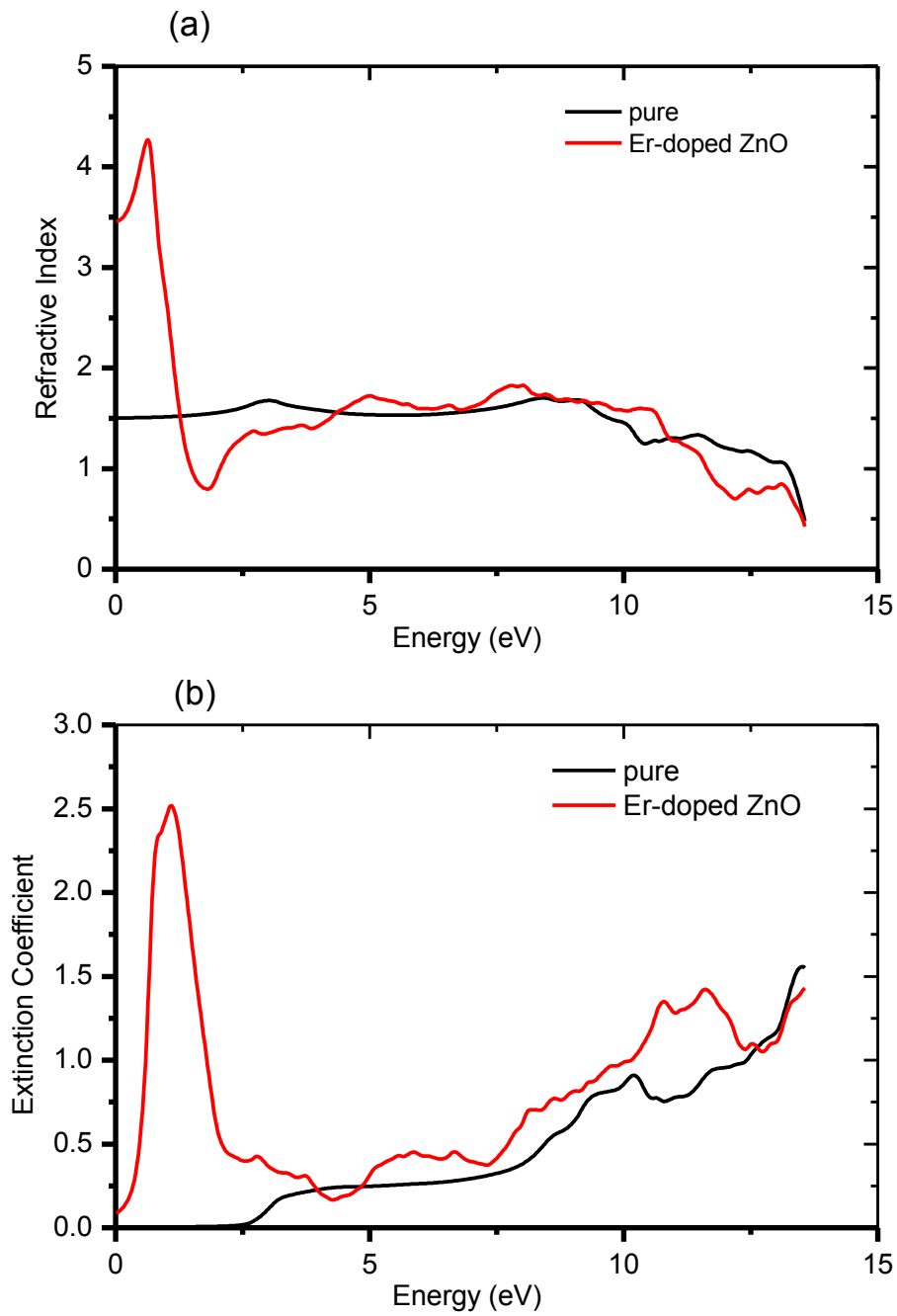
Figure 5.6 (a) the refractive index and (b) the extinction coefficient, of pure ZnO and Er-doped ZnO.

5.3.3 THE ABSORPTION COEFFICIENT

The absorption coefficient is a measure of the rate of decrease in the intensity of electromagnetic radiation (as light) as it passes through a given substance. It given symbolically as

$$\alpha(\omega) = \sqrt{2}\,\omega \left[\sqrt{\varepsilon_1^2(\omega) + \varepsilon_2^2(\omega)} - \varepsilon_2(\omega) \right]^{1/2} \tag{5.5}$$

The absorption coefficient is displayed in figure 5.7 for IR, Visible and UV regions. For pure ZnO, the absorption coefficient decreased of drastically from UV to visible regions finally vanished. We see that the Er doping has increased the coefficient absorption in all spectra regions unless in a small region in UV domain which can be neglected (as seen in the figure). Furthermore, red shift is also achieved under Er doping indicating the importance of its 4f donor occupied states.
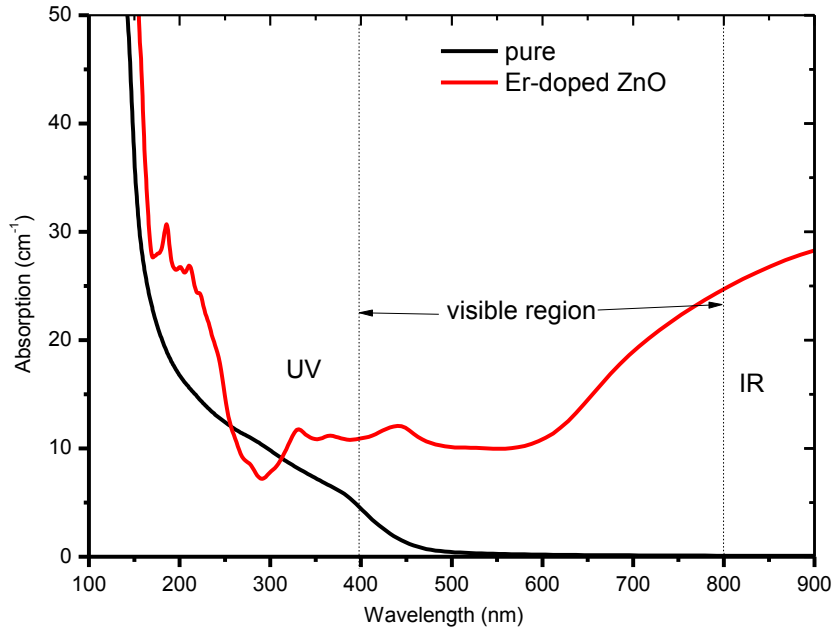
Figure 5.7 The absorption coefficient of pure and Er-doped ZnO.

CONCLUSION

In summary of this chapter, a theoretical investigation of the structural, electronic and optical properties of pure zinc blend ZnO and Er-doped ZnO has been reported. This study has been done using DFT with mBJ approximation. It is found that, the calculated energy band gap and the lattice parameter of pure ZnO are close to the experimental ones and in a good agreement with other theoretical calculations. The good agreement between our mBJ band gap with experimental one for pure ZnO supports our choice of no using the scissor operator for optical properties for both pure and Er-doped ZnO. It is also shown that, the incorporation of Er in ZnO affects considerably the electronic and optical properties compared with pure ZnO. For example, the optical energy gap has increased by 83% under Er doping. From imaginary dielectric function, we have established that red shift is also achieved under Er doping indicating the importance of its 4f donor occupied states.

REFERENCES

[1] X. D. Zhang, M. L. Guo, W. X. Li, C. L. Liu, arXiv preprint arXiv:1210.0163 (2012).

[2] Z. Chunying, W. Jing and Z. Cheng, J. Semiconductors 33 (2012) 072001.

[3] M. R. Boufatah and A. E. Merad. Mater. Sci. Semicon. Process. 19 (2014) 179.

[4] H. Dixit, R. Saniz, D. Lamoen, B. Partoens, J. Phys.: Condens. Matter 22 (2010) 125505.

[5] H. C. Wu, Y. C. Peng C. C. Chen, Optical Materials 35 (2013) 509.

[6] L. Honglin, L. Yingbo, L. Jinzhu and Y. Ke, J. Alloys Compd 617 (2014) 102.

[7] A. Slassi, Optik-International Journal for Light and Electron Optics 126 (2015) 4751.

[8] G. Murtaza, I. Ahmad, B. Amin, A. Afaq, F. Ghafoor and A. Benamrani, Physica B: Condensed Matter 406 (2011) 2632.

[9] Ü. Özgür, Ya. I. Alivov, C. Liu, A. Teke, M. A. Reshchikov, S. Doğan, V. Avrutin, S.-J. Cho and H. Morkoç, J. App. Phys. 98 (2005) 041301.

GENERAL CONCLUSION

GENERAL CONCLUSON

We can summarize our work in thesis to the following: The structural and electronic properties of Erbium Zinc Oxide alloys for (x = 0, 0.25, 0.50, 0.75, 1) are investigated using DFT with GGA approximation. The structural optimization is performed by calculating the total energies for different volumes around the equilibrium cell volume V_0 of Erbium Zinc Oxide. Obtained results of structural properties of pure ZnO are agreement with the theatrical and experimental studies.

The lattice constants calculated for pure ZnO is very close to the experimental results, proving that our calculation parameters are valid. It is 1.8% greater than the experimental value, indicating that the GGA scheme overestimates the lattice constant. Likewise, other structural properties of pure ZnO are agreement to theoretical and experimental investigations. Furthermore, the structural properties of Erbium Zinc Oxide alloys are calculated but to the best of our knowledge, there are no experimental values for them.

In other hand, the electronic properties of Erbium Zinc Oxide alloys are calculated. Our obtained energy band gaps of Erbium Zinc Oxide alloys are underestimated values because we used the GGA approximation.

The calculated band structures and density of states indicate a semiconducting character of the involved materials.

We observed effect of Er on electronic properties of Erbium Zinc Oxide for(x= 0, 0.25, 0.50, 0.75, 1) where, the energy gaps increase with increasing of composition and the Fermi-level move towards higher energy direction and enter into the conduction band, exhibiting n-type behavior after doping. As well, the position of 4f-Er is observed

localizes around the Fermi level yielding to the movement of the upper valence band downward.

To improve electronic properties of pure ZnO and Er-doped ZnO we used a new potential, it called modified Becke-Johnson exchange potential (mBJ). We observed that energy band gaps of pure ZnO and Er-doped ZnO are enhanced.

It is found that, the calculated energy band gap and the lattice parameter of pure ZnO are close to the experimental ones and in a good agreement with other theoretical calculations. The good agreement between our mBJ band gap with experimental one for pure ZnO supports our choice of no using the scissor operator for optical properties for both pure and Er-doped ZnO.

In addition, a theoretical investigation of the optical properties of pure zinc blend ZnO and Er-doped ZnO has been reported. This study has been done using DFT with mBJ approximation.

It is shown that, the incorporation of Er in ZnO affects considerably the optical properties compared with pure ZnO. For example, the optical energy gap has increased by 83% under Er doping. From imaginary dielectric function, we have established that red shift is also achieved under Er doping indicating the importance of its 4f donor occupied states and the absorption coefficient increased in all spectra regions unless in a small region in ultra violet (UV) domain which can be neglected.

Original research article

DFT investigation of structural, electronic and optical properties of pure and Er-doped ZnO: Modified Becke-Johnson exchange potential

CrossMark

E.A. Alkahtani [a,b], A.E. Merad [a,*], M.R. Boufatah [a], A. Benosman [c]

[a] Solid State Physics Team, Theoretical Physics Laboratory, Faculty of Sciences, A. Belkaïd University, Box 119, 13000, Tlemcen, Algeria
[b] Physics Department, Khawlan Education Faculty, Sana'a University, Yemen
[c] Theoretical Physics Laboratory, Faculty of Sciences, A. Belkaïd University, Box 119, 13000, Tlemcen, Algeria

A B S T R A C T

The structural, electronic and optical properties of pure ZnO and Er-doped ZnO are investigated by density functional theory (DFT) with generalized gradient approximation plus modified Becke-Johnson exchange potential (GGA + mBJ). The obtained results of electronic and optical properties were improved. Good agreement with the experimental and theoretical studies is obtained for pure ZnO since the results of Er-doped ZnO in zinc blend structure are considered as new predictions. The energy gap value of Er-doped ZnO is found to increase with Erbium incorporation, affecting the absorption coefficients in all spectra regions. Red shift is also achieved under Er doping indicating the importance of its 4f donor occupied states. Similar behavior is observed in the literature for Er-doped ZnO in wurtzite structure.

© 2016 Elsevier GmbH. All rights reserved.

1. Introduction

ZnO is one of the potential candidates in several technological applications such as, optoelectronic, solar cells, and photocatalyst [1,2] due to its high exciton binding energy (60 meV) and its wide band gap (∼3.3 eV) [3]. It is known as an n-type semiconductor material. Recently, the ZnO presented an interesting subject for doping with various elements such as transition and noble metals. This is of course very suitable to improve the optoelectronic and photocatalytic properties because the incorporation of dopants generates lattice defects and changes consequently the band gap energy [4]. In particular, the doping with rare-earth elements has been extensively investigated, experimentally as well as theoretically. Poongodi et al. [5] deposited nanostructured Nd doped ZnO thin films on glass substrate by a sol–gel spin coating technique. The results show the degradation of methylene blue dye and the decrease in grain size and light absorption over an extended visible region by Nd ion doping in ZnO film, contributed equally to improve the photocatalytic activity. Honglin et al. [6] prepared the ZnO nanopowders doped with (La,Er, Nd) rare-earth by chemical method. The photoluminescence (PL) measurement revealed that pure and REs doped ZnO had different I_{UV}/I_{DLE} ratios, and the absorption spectra of doped ZnO exhibited enhanced optical absorption in visible region. Zhang et al. [7] studied the electronic structure and magnetism of RE (RE = La,
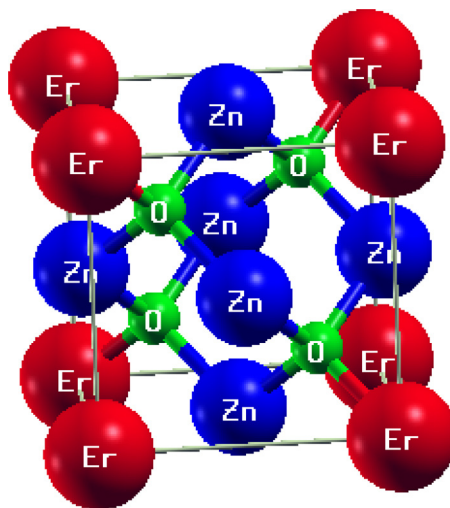
Fig. 1. Unit supercell of zinc blend Er doped ZnO.

Ce, Pr, Nd and Eu) doped ZnO using generalized gradient approximation (GGA) and GGA + U. It appeared the influence of dopant on the electronic and magnetic properties of ZnO.

In particular, the attractive interest of Erbium (Er)-doped semiconductors in optical applications such as light-emitting and laser diodes, is because of the sharp photoluminescence (PL) at 1.54 μm from the intra-4f shell transition in Er^{3+} ions [8]. The majority of works carried out the above properties at low temperature (77 K) precluding their use at room temperature [9]. However, few reports for Er doped ZnO in thin film or wurtzite phases have been experimentally investigated showing the PL spectra at room temperature, as given in the work of Honglin [6]. Consequently, no further theoretical understanding on the correlation between their properties is clarified. Therefore, it is still important to present a theoretical investigation of structural, electronic and optical properties of such material in order to enlighten the correlation between them.

Erbium can be found in three magnetic phases: ferromagnetic below 19 K, antiferromagnetic between 19 and 80 K and paramagnetic above 80 K [8]. In this work, we aimed to study the effect of Er doped ZnO in comparison with pure ZnO, modeled in paramagnetic phase that is observed at high temperature.

On the theoretical side, the density functional theory (DFT) has treated successfully the structural, electronic and optical properties of semiconductors [10]. However, it underestimates the fundamental band gap energy of most semiconductor oxides. In order to obtain a correct band gap, there are many theoretical approximation methods such as DFT + U, which is used to improve the band gap. Unfortunately, these schemes are computationally expensive compared to the LDA or GGA. Also, the recently proposed Tran–Blaha modified version of the Becke–Johnson potential (TB-mBJ) [11] has proved to be a successful method for accurate band gaps of semiconductors and insulators better than GGA + U and LDA + U [12]. Therefore, we used mBJ potential, in addition to GGA approximation, to study the electronic and optical properties of pure and Er doped ZnO.

Structural, electronic and optical properties are obtained for 25% of Er doped ZnO in zinc blend structure by caring out a first principles calculations based on density functional theory (DFT). In general, it is shown that this structure is similar to wurtzite one in electronic and optical band structure [13]. This work is considered as an extension of our recent studies realized on ZnO-ZB [13]. Our results were discussed qualitatively as well as quantitatively in comparison with few experimental available results.

2. Computational details

All calculations have been carried out using density functional theory with help of the full-potential linearized augmented plane-wave (FP-LAPW) method as implemented in WIEN2k package [14,15], which self-consistently finds the eingen values and eingen function of the Kohn-Sham [16] equations for the system. We have used the Generalized Gradient Approximation (GGA) as parameterized by Perdew, Burke and Ernzenhorf [17] and modified Becke-Johnson (mBJ) approximation [11] for electronic and optical properties.

The valence electron configurations used in the calculations are $Zn(3d^{10}\,4s^2)$, $O(2s^2\,2p^4)$, $Er(4f^{12}\,5s^2\,5p^6\,6s^2)$ respectively. We adopted an 8 atoms simple cubic supercell which corresponds to 25% of Er concentration (Fig. 1).

The wave function, charge density and potential were expanded by spherical harmonic functions inside non-overlapping spheres surrounding the atomic sites (muffin-tin spheres) and by a plane-wave basis set in the remaining space of the unit cell (interstitial region). The maximum l quantum number for the wave function expansion inside atomic spheres was confined to $l_{max} = 10$. The charge density was Fourier expanded up to $G_{max} = 9$ $(Ry)^{1/2}$. The convergence parameter $R_{MT}K_{max}$ (Where K_{max} is the maximum modulus for the reciprocal lattice vector, and R_{MT} is the average radius of the muffin tin

Table 1
Calculated equilibruim lattice constant (*a*), bulk modulus (B) and its first pressure derivative (B') for pure and Er doped ZnO.

	a (Å)			B (GPa)			B'		
	Our work	Exp.	Calcul.	Our work	Exp.	Calcul.	Our work	Exp.	Calcul.
Pure ZnO	4.552	4.47 [20]	4.614 [25] 4.53 [21] 4.62 [13]	145.8	–	129.7 [13] 139.32 [26] 165.9 [22]	4.24	–	4.33 [22] 4.096 [13]
Er doped ZnO	4.759	–	–	122.5	–	–	4.31	–	–

Table 2
Calculated principle features of band structures for pure and Er-doped ZnO given in (eV).

	Pure ZnO				Er doped ZnO			
	Our work		Exp.	Calcul.	Our work		Exp.	Calcul.
	GGA	mBJ			GGA	mBJ		
Eg	0.62	2.58	3.3 [3]	0.50 [26][a] 0.73 [27][a] 2.59 [13][b] 0.804 [13][a] 2.47 [21][c]	1.43	2.98	–	–
UVBW	6.462	5.755	–	–	5.136	4.521	–	–
TVBW	17.823	19.293	–	–	16.701	17.719	–	–
δd$_{Zn}$	6.462	5.755	–	–	5.136	4.521	–	–
δf$_{Er}$	–	–	–	–	1.395	3.708	–	–
Occupied states	0	0	–	–	1.273	1.870	–	–

[a] GGA calculation.
[b] LDA + mBJ calculation.
[c] GW calculation.

spheres) which controls the size of the basis set in these calculations, was set to 7. The reciprocal space is sampled by a $5 \times 5 \times 5$ Monkhorst–Pack mesh [18] with sufficient 125 k-vectors in the irreducible Brillouin zone. The iteration process is repeated until the calculated total energy of the crystal converges to less than 10^{-5} Ry.

3. Results and discussion

3.1. Structural properties

To investigate the physical properties of pure and Er-doped ZnO, we performed the structural optimization by calculating the total energies for different volumes around the equilibrium cell volume V_0 of ZB structure. The equilibrium structural parameters were determined by fitting the total energy versus volume to Murnaghan's equation of states [19]. Our obtained results are summarized in Table 1 compared with the available experimental data and other theoretical results. Good agreement is achieved for pure ZnO in ZB structure with our recent [13] and other theoretical [20–26] results. This latter constitutes a good primary support to treat a hypothetical ZB Er-doped ZnO.

The calculated lattice constant for ZnO is a good agreement with the theoretical [21–35] and experimental [20] values. A ratio of 1.8% in found to be greater than the experimental value, indicating that the GGA scheme overestimates the lattice constant [27].

Our result of the bulk modulus B for ZB ZnO is in reasonable agreement with experimental results and previous theoretical studies [15,22], while for Er-doped ZnO, there are no experimental or theoretical values, to the best of our knowledge, for the structural properties in order to make the comparison.

The lattice parameter, bulk modulus and pressure derivative calculated both pure ZB ZnO and Er-doped ZnO are listed in Table 1.

3.2. Electronic properties

Electronic band structures obtained with GGA + mBJ approximation are shown in Fig. 2 for pure and Er-doped ZnO. It is clear that ZnO has a direct band gap semiconductor at Γ high symmetry point with a calculated value of 2.58 eV. This later is in good agreement with those of experimental and other sophistical calculations as seen in Table 2. Other principle features of the calculated band structures such as the upper valence bandwidth (UVBW), the total valence bandwidth (TVBW) and the splitting δd$_{Zn}$ and δf$_{Er}$ are given in the same table. For Er-doped ZnO, the estimated electronic energy gap (2.98 eV) is observed under Fermi level in the range from -1.74 eV to -4.72 eV. To illustrate the origin of this feature, we have calculated the total and partial densities of states DOS as given in Fig. 3. The valence band for pure ZnO mainly consists of the 2p, 2s states of O and 3d states of Zn. The upper valence band of the width 5.75 eV is dominated by 2p state of O, while its 2s state
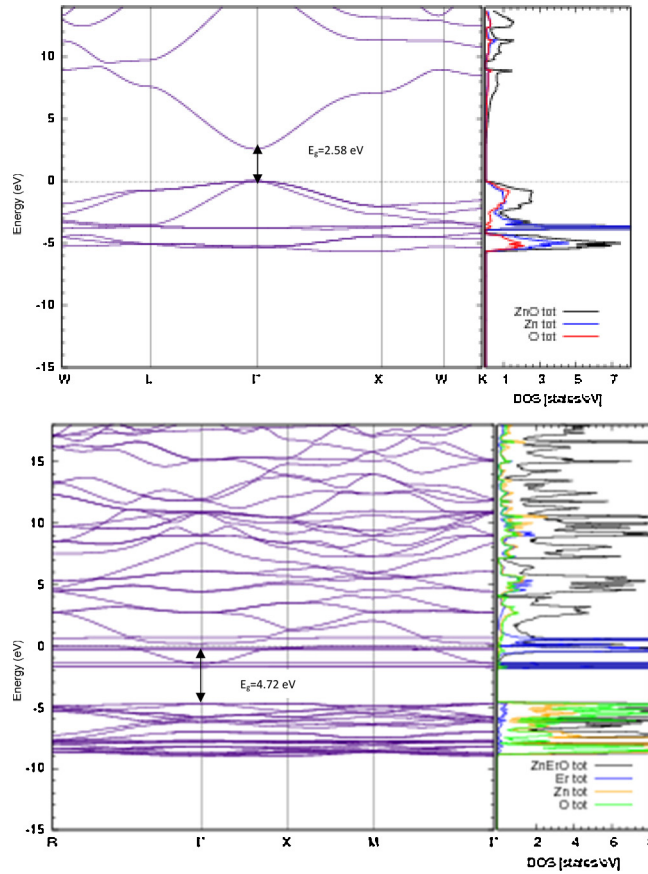
Fig. 2. Band structures and total DOS for: (a) pure ZnO and (b) Er-doped ZnO.

is localized in the lower level of VB at −18.64 eV. Below the valence band maximum (VBM), the 3d Zn states give rise in the same energy width of that of 2p O. As a result, the hybridization is formed between 2p O and 3d Zn states. It is worth noticing that the level position of 3d Zn is corrected via mBJ potential compared to the GGA one (see Table 2). This correction contributes to the enhanced energy band gap. Good agreement is achieved with other experimental and hybrid functional PBE0 values.

The lowest conduction band (CBM) is attributed to the Zn 4s states and O 2p states which is well compared to the experimental and theoretical data.

For Er doped ZnO, the position of 4f-Er is observed localizes around the Fermi level yielding to the movement of the upper valence band downward. The resulting value of the optical energy band gap is then 4.72 eV obtained by mBJ potential. Therefore, the Fermi level is shifted upward into the conduction band with the presence of 4f-Er state. Consequently, this later state acts as donor giving rise to the n-type metallic conductivity. The occupied states in the bottom of the conduction band, creates therefore an additional energy barrier, which help the electron to excite from the valence to the conduction bands. This barrier also causes the increasing of the optical band gap to 4.72 eV. The same conclusion is obtained by Wu et al. [9] for Ga doped ZnO in the wurtzite structure. We can notice from this feature that this significant effect of Er in ZnO had a strong modification in optoelectronic properties. Detailed information about the positions of several contributed states are summarized in Table 2 for pure and Er doped ZnO.

3.3. Optical properties

The optical properties are usually described by dielectric constant $\varepsilon(\omega)$, sometimes by refractive index $n(\omega)$, extinction coefficient $k(\omega)$ and absorption coefficient $\alpha(\omega)$. These features are very important to determine the optical and electronic properties of the crystal.

We have not used scissor operator since the mBJ potential is known to improve the band gap very closely to the experimental one as it is remarked for our pure ZnO (see Table 2). Therefore we expected that the calculated optical properties of pure and Er doped ZnO are more improved compared to GGA and LDA approximations.

Fig. 4 displays dielectric real part $\varepsilon_1(\omega)$ and dielectric imaginary part $\varepsilon_2(\omega)$ of pure and Er doped ZnO. The real part $\varepsilon_1(\omega)$ represents the dispersion of the incident photons by the materials, while the imaginary part $\varepsilon_2(\omega)$ of the dielectric function
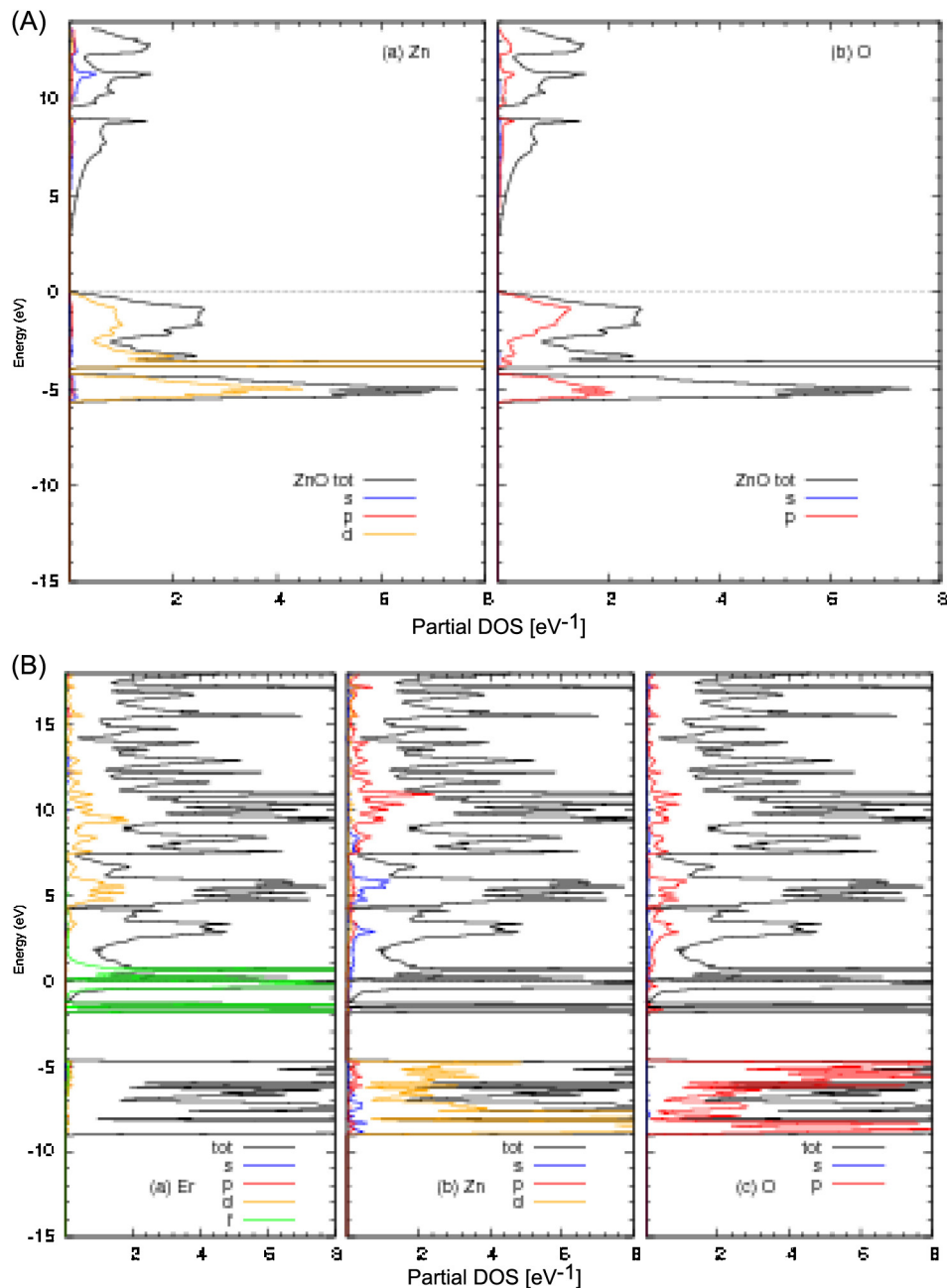
Fig. 3. Partial DOS for: (A) pure ZnO and (B) Er-doped ZnO.

of pure ZnO and Er-doped ZnO is important to determine the different transitions due to photons absorption in these two cases, from occupied to unoccupied states.

From 4(a), the calculated static dielectric function ε_1 (0) given at zero frequency is 2.26, 11.94 for ZnO and Er doped-ZnO respectively. The value of ZnO agree with the reported results, for instances, (LDA + U) [6] and (GGA + mBJ) [28]. The figure shows also a significant increase of the dielectric function under doping with Er. Fig. 4(b) shows the imaginary part ε_2 (ω) of the dielectric function. For pure ZnO, we found that the peak observed at 2.58 eV, which corresponds to the energy band gap value, corresponds to the transition from O 2p occupied sates at (VBM) to the Zn 4s unoccupied statesat (CBM). The others peaks viewed at high energies result from the transitions between various occupied to unoccupied states from the valence band to the conduction band. For Er doped ZnO, a new high peak is observed at low energy near 1.2 eV. This latter is due to the transition between Er 4f donor occupied states located around Fermi level and the Zn 4s and Zn 4p unoccupied states in the conduction band.
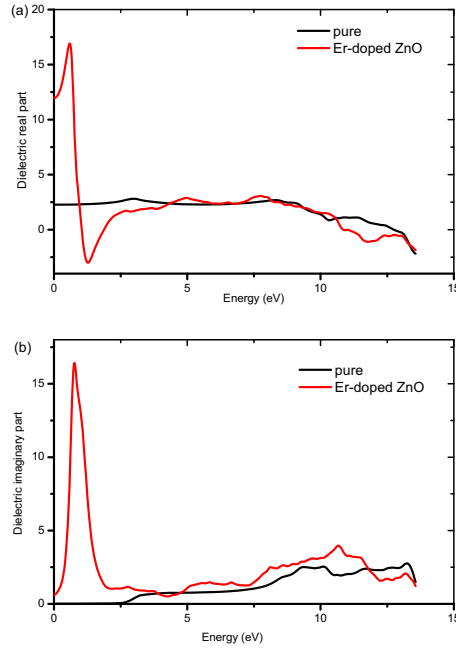
Fig. 4. The dielectric functions of pure and Er-doped ZnO: (a) Real part and (b) imaginary part.
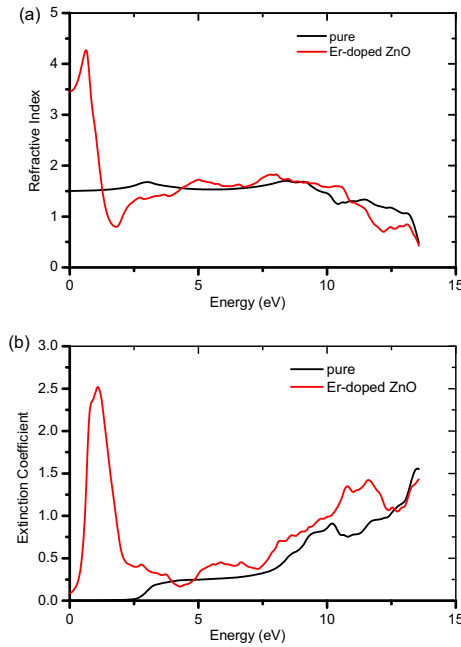

Fig. 5. (a) The refractive index and (b) the extinction coefficient, of pure and Er-doped ZnO.

Fig. 5 illustrates the calculated refractive index $n(\omega)$ and the extinction coefficient $k(\omega)$. The static refractive indices are deduced from Fig. 5(a) as 1.50 and 3.46 for pure and Er- doped ZnO respectively. Similar values were observed for pure ZnO compared to those reported in the literature [29]. Increasing behavior can be found with Er doping which consequently affects considerably the exciton energy (60 meV for ZnO).

The absorption coefficient is displayed in Fig. 6 for IR, Visible and UV regions. For pure ZnO, the absorption coefficient decreased of drastically from UV to visible regions finally vanished. We see that the Er doping has increased the coefficient absorption in all spectra regions unless in a small region in UV domain which can be neglected (as seen in the figure). Furthermore, red shift is also achieved under Er doping indicating the importance of its 4f donor occupied states.
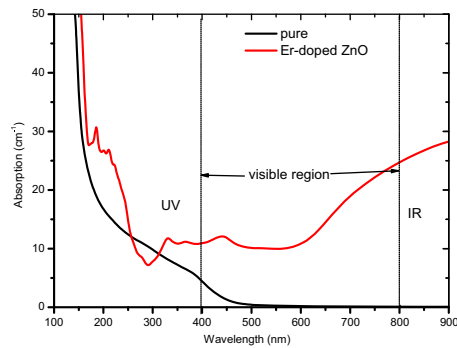
Fig. 6. The absorption coefficient of pure and Er-doped ZnO.

4. Conclusion

In summary, a theoretical investigation of the structural, electronic and optical properties of pure zinc blend ZnO and Er-doped ZnO has been reported. This study has been done using DFT with (GGA + mBJ) approximation. It is found that, the calculated energy band gap and the lattice parameter of pure ZnO are close to the experimental ones and in a good agreement with other theoretical calculations. The good agreement between our mBJ band gap with experimental one for pure ZnO supports our choice of no using the scissor operator for optical properties for both pure and Er-doped ZnO. It is also shown that, the incorporation of Er in ZnO affects considerably the electronic and optical properties compared with pure ZnO. For example, the optical energy gap has increased by 83% under Er doping. From imaginary dielectric function, we have established that red shift is also achieved under Er doping indicating the importance of its 4f donor occupied states.

Acknowledgements

References

 [1] C. Klingshirn, Phys. Status Solidi (B) 244 (2007) 3027.
 [2] D.K. Kim, H.B. Kim, J. Alloys Compd. 509 (2011) 421.
 [3] Ü. Özgür, Ya. I. Alivov, C. Liu, A. Teke, M.A. Reshchikov, S. Doğan, V. Avrutin, S.-J. Cho, H. Morkoç, J. App. Phys. 98 (2005) 041301.
 [4] D. Li, J.F. Huang, L.Y. Cao, L.I. Jia-Yin, H.B. OuYang, C.Y. Yao, Ceram. Int. 40 (2014) 2647.
 [5] G. Poongodi, R.M. Kumar, R. Jayavel, Ceram. Int. 41 (2015) 4169.
 [6] L. Honglin, L. Yingbo, L. Jinzhu, Y. Ke, J. Alloys Compd. 617 (2014) 102.
 [7] X.J. Zhang, W.B. Mi, X.C. Wang, H.L. Bai, J. Alloys Compd. 617 (2014) 828.
 [8] T. Gregorkiewicz, J.M. Langer, MRS Bull. 24 (1999) 27.
 [9] H.C. Wu, Y.C. Peng, C.C. Chen, Opt. Mater. 35 (2013) 509.
[10] G. Hautier, A. Miglio, G.M. Rignanese, X. Gonze, Nat. Commun. 4 (2013) 2292.
[11] F. Tran, P. Blaha, Phys. Rev. Lett. 102 (2009) 226401.
[12] H. Zaari, G. El Hachimi, A. Benyoussef, A. El Kenz, J. Magn. Magn. Mater. 393 (2015) 183.
[13] M.R. Boufatah, A.E. Merad, Mater. Sci. Semicond. Process. 19 (2014) 179.
[14] P. Blaha, K. Schwarz, G.K.H. Madsen, D. Kvasnicka, J. Luitz, J. wien2k, An augmented plane wave + local orbitals program for calculating crystal properties, Karlheinz Schwarz, Techn. Universität Wien, Austria (2001).
[15] G.K.H. Madsen, P. Blaha, K. Schwarz, E. Sjöstedt, L. Nordström, Phys. Rev. B 64 (2001) 195134.
[16] W. Kohn, L.J. Sham, Phys. Rev. A 140 (1965) 1133.
[17] J.P. Perdew, S. Burke, M. Ernzerhof, Phys. Rev. Lett. 77 (1996) 3865.
[18] H.J. Monkhorst, J.D. Pack, Phys. Rev. B 13 (1976) 5188.
[19] F.D. Murnaghan, Proc. Natl. Acad. Sci. 30 (1944) 244.
[20] A. Ashrafi, C. Jagadish, J. Appl. Phys. 102 (2007) 071101.
[21] H. Dixit, R. Saniz, D. Lamoen, B. Partoens, J. Phys.: Condens. Matter 22 (2010) 125505.
[22] S. Cui, W. Feng, H. Hu, Z. Feng, Y. Wang, J. Alloys Compd. 476 (2009) 306.
[23] B. Amrani, R. Ahmed, F. El Haj Hassan, Comput. Mater. Sci. 40 (2007) 66.
[24] A. JemmyCinthia, G. Sudhapriyanga, R. Rajeswarapalanichamy, M. Santhosh, Proc. Mater. Sci. 5 (2014) 1034.
[25] H. Liu, H. Mao, M. Somayazulu, Y. Ding, Y. Meng, D. Husermann, Phys. Rev. B 70 (2004) 094114.
[26] M. Kalay, H.H. Kart, S. Ö. Kart, T. Çağin, J. Alloys Compd. 484 (2007) 431.
[27] F. El Haj Hassan, B. Amrani, J. Phys. Condens. Matter 19 (2007) 386234.
[28] A. Slassi, Opt.—Int. J. Light Electron Opt. 126 (2015) 4751.
[29] G. Murtaza, I. Ahmad, B. Amin, A. Afaq, F. Ghafoor, A. Benamrani, Phys. B: Condens. Matter 406 (2011) 2632.

Abstract

In recent years, a large number of researches focused on study the physical properties of ZnO, because of its unique characteristics. These properties make ZnO suitable for a wide range of technological applications, for example in optoelectronic, solar cells, photocatalyst, light-emitting diodes and laser diodes. For this reason, ZnO presented an interesting subject for doping with various elements such as transition and noble metals. In our work, we investigated the effect of Erbium (Er), as a dopant element, on physical properties of ZnO. This study has been done using Density Functional Theory (DFT) with generalized gradient approximation (GGA) and modified Becke-Johnson exchange potential (mBJ). Our obtained results shown that, the incorporation of Er in ZnO affects considerably the structural, electronic and optical properties.

Keywords*: Er-dopedZnO; GGA; mBJ potential; Electronic structures; Optical properties.

Résumé

Au cours des dernières années, un grand nombre de recherches est porté sur l'étude des propriétés physiques du ZnO, du fait de ses caractéristiques propres. Ces propriétés rendent le ZnO un matériau qui convient à une large gamme d'applications technologiques, comme par exemple, les cellules solaires, le photo-catalyseur, les diodes émettrices de lumière optoélectroniques et les diodes laser. Pour cette raison, le ZnO a présenté un sujet intéressant pour le dopage avec divers éléments tels que les métaux de transition et les métaux nobles. Dans notre travail, nous avons étudié l'effet d'Erbium (Er), comme un élément dopant, sur les propriétés physiques du ZnO. Cette étude a été effectuée à l'aide de la théorie de la fonctionnelle de densité (DFT) avec l'approximation du gradient généralisé (GGA) et le potentiel d'échange du type Becke-Johnson modifié (mBJ). Les résultats obtenus montrent que l'incorporation du Er dans le ZnO affecte considérablement les propriétés structurales, électroniques et optiques.

Mots-clés : ZnO dopée Er ; GGA ; potentiel mBJ ; structures électroniques ; Propriétés optiques

ملخص

في السنوات الأخيرة، ركز عدد كبير من الباحثين على دراسة الخصائص الفيزيائية لأكسيد الزنك (ZnO)، بسبب خصائصه الفريدة .التي أهلته للاستخدام الواسع في التطبيقات التكنولوجية، مثل الخلايا الشمسية، الخلايا الكهروضوئية، الثنائيات الباعثة للضوء وثنائيات الليزر .لهذا السبب،ُقدمت دراسة أكسيد الزنك (ZnO) مع عناصر التطعيم (التشويب) مثل العناصر الانتقالية والعناصر النبيلة كموضوع مهم ومشوق .في عملنا هذا، قمنا بدراسة تأثير معدن الاربيوم (Er) على الخصائص الفيزيائية لأكسيد الزنك .وقد نفذت هذه الدراسة باستخدام نظرية الكثافة الوظيفية (DFT) بالاضافة الى تقريبي (GGA)و (mBJ).أظهرت النتائج المتحصل عليها أن معدن الاربيوم (Er) يؤثر بشكل كبير على الخصائص الهيكلية والالكترونية والبصريةلأكسيد الزنك.

كلمات البحث: تطعيم أكسيد الزنك (ZnO) بالاربيوم، تقريبي GGA و mBJ؛ الخصائص البلورية ؛ الخصائص الالكترونية ؛ الخصائص البصرية.